Insights into Mechanical Properties and Sustainability of Packing-Enhanced Recycled Aggregate Concrete

By

Yuan JIANG (20121263)

M.Eng

Department of Civil Engineering

University of Nottingham Ningbo China

A thesis submitted for the degree of

Doctor of Philosophy

2023

ABSTRACT

The use of recycled concrete aggregates (RCAs) and recycled concrete powder (RCP), produced by processing waste concrete, is a promising strategy to mitigate the depletion of natural aggregates and the environmental burden associated with disposing of construction and demolition wastes. However, the use of recycled aggregates generally has negative impacts on the properties of concrete, particularly for those with a high RCA amount. To mitigate the adverse impacts of using recycled materials, one of the effective methods is to improve concrete mix design through particle packing optimisation.

This study first focuses on understanding the role of aggregate packing enhancement in the properties of natural aggregate concrete (NAC) and recycled aggregate concrete (RAC). The results indicate that increasing the aggregate packing density can help to densify the granular skeleton of aggregates in concrete by reducing the voids around the aggregates and the cement paste film thickness, which subsequently enhances the mechanical properties of the concrete, including the compressive strength, flexural strength, and Young's modulus. This enhancement is higher for RAC than NAC, particularly for Young's modulus. Optimising the aggregate packing status can decrease the number of macropores in RAC, contributing to the enhancement in the mechanical properties of RAC.

This study subsequently investigates the effects of cement paste volume (CPV) and sand-to-aggregate volume ratio (Bs) on the properties of packing-optimised RAC, followed by a microstructure study to reveal their influencing mechanisms. The results indicate that the slump of RAC increases with the CPV at a growing rate, which is mainly attributed to the increased lubrication effect of fresh paste on the aggregates. However, increasing the Bs decreases the slump of RAC due to the reduced cement paste film thickness. Increasing the CPV decreases the macroporosity of RAC, as it reduces the amount of RCAs, thereby enhancing its

compressive strength and Young's modulus. However, excessive CPV increases the porosity and thickness of interfacial transition zones, which subsequently weakens the mechanical properties of RAC. The increase of Bs first enhances the granular skeleton by optimising the particle packing status, which is beneficial to RAC properties. However, excessive Bs can lead to an increase in macroporosity and mean pore size inside RAC, degrading its mechanical properties. Nonetheless, the flexural strength of the RAC is marginally influenced by the CPV or Bs.

This study further explores the use of RCP as a potential sand alternative by understanding its role in affecting the properties, particle packing density, hydration reaction, and microstructures of cement mortar. The results indicate that increasing the RCP content increases the water demand and decreases the dry bulk density of mortars due to the inferior characteristics of RCP. Replacing sand by 10-20% RCP has a negligible or slightly positive impact on the mechanical properties of mortars. This is mainly attributed to a decreased volume fraction of large capillary pores, air voids, and total porosity, which overcomes the negative effects induced by RCP. Specifically, incorporating RCP can reduce the fraction of large voids through its filling effect and slightly promote hydration in mortars. Besides, the drying shrinkage of mortars increases with the RCP replacement ratio due to the increased volume fraction of mesopores in the RCP mortars. However, an excessive amount of RCP increases the volume fraction of capillary pores and the total porosity of mortars due to the combined action of the decreased packing density and the high porousness of RCP particles, which subsequently decreases the mechanical properties of mortars and further increases the drying shrinkage of RCP mortars.

The environmental benefits of adopting packing-optimised RAC and using RCP as sand replacement are quantified via life cycle assessment (LCA). The environmental impacts of global warming, stratospheric ozone depletion, terrestrial acidification, freshwater eutrophication, land use, and non-renewable

energy consumption are evaluated. The results indicate that the adoption of packing-optimised RAC can decrease most environmental impacts, except for land use. However, using RCP as sand replacement can further decrease all the considered environmental impacts of packing-optimised RAC, particularly for land use. Replacing 20% river sand with RCP can decrease the land use of packing-optimised RAC by 12%. Overall, the findings of the LCA study can offer valuable guidance for optimising the mix design of RAC with respect to environmental protection.

PUBLICATIONS

Three journal papers have been published by the candidate based on the research work presented in this thesis.

1. **Jiang, Y.**, Liu, S., Li, B.*, He, J., & Hernandez, A. G. (2022). Effects of aggregate packing optimization and cement paste volume on the properties of natural and recycled aggregate concrete. *Structural Concrete*, *23*(4), 2260–2273.

2. **Jiang, Y.**, Li, B.*, He, J., & Garcia Hernandez, A. (2022). Properties and microstructure of packing-optimised recycled aggregate concrete with different cement paste or sand contents. *Construction and Building Materials*, *344*, 128178.

3. **Jiang, Y.**, Li, B.*, Liu, S., He, J., & Hernandez, A. G. (2022). Role of recycled concrete powder as sand replacement in the properties of cement mortar. *Journal of Cleaner Production*, *371*, 133424.

ACKNOWLEDGEMENTS

TABLE OF CONTENTS

LIST OF TABLES

LIST OF FIGURES

xiv

LIST OF ABBREVIATIONS

A/C	Aggregate-to-cement ratio
C&D	Construction and demolition
CPFT	Cement paste film thickness
CPM	Compressible packing model
CPV	Cement paste volume
CPV/V_V	Cement paste-to-voids volume ratio
CT	Computed tomography
DEM	Discrete element modelling
FA	Fly ash
FAs	Fine aggregates
GGBS	Ground granulated blast furnace slag
ITZ	Interfacial transition zone
LCI	Life cycle inventory
LCA	Life cycle assessment
LCIA	Life cycle impact assessment
MIP	Mercury intrusion porosimeter
NAC	Natural aggregate concrete
NCAs	Natural concrete aggregates
NS	Nano-silica
OD	Oven-dried
OPC	Ordinary Portland Cement
PPM	Particle packing method

PSD	Particle size distribution
RAC	Recycled aggregate concrete
RCAs	Recycled concrete aggregates
RCP	Recycled concrete powder
RCMP	Recycled cement mortar powder
RCPP	Recycled cement paste powder
RFAs	Recycled fine aggregates
SCC	Self-compacting concrete
SCM	Supplementary cementitious materials
SEM	Scanning electron microscope
SSA	Specific surface area
SSD	Saturated-surface-dry
TGA	Thermogravimetric analysis
TM	Traditional method
UHPC	Ultra-high-performance concrete
W/C	Water-to-cement ratio
XRD	X-ray diffraction
XRF	X-ray fluorescence

CHAPTER 1
INTRODUCTION

1.1 Background and Problem Statement

With the rapid urbanisation and industrialisation in China, a large amount of construction and demolition (C&D) wastes have been produced in the past decades, as shown in Fig. 1.1. However, the recycling rate of C&D wastes is only around 5% (Bao & Lu, 2020). The unrecycled C&D wastes are required to be disposed in licensed dumping sites. Due to the shortage of dumping spaces, some of the C&D wastes are disposed in unauthorised landfill sites, leading to a negative impact on the environment. Moreover, increasing demand for natural aggregates for new concrete production has also brought a tremendous pressure on the environment. In China, around 15 billion tons of aggregates, including coarse aggregates and sand, are consumed every year, which accounts for around 40% of the total demand worldwide (Ding *et al.*, 2016). For the sake of a balance between social development and the environment, recycling C&D wastes has attracted increasing attention in the past decades (Gálvez-Martos *et al.*, 2018). One of the commonly used methods is to recycle the aggregates from the C&D wastes (termed as recycled concrete aggregates, *i.e.,* RCAs) as the raw material for recycled aggregate concrete (RAC).

Fig. 1.1 Construction & demolition wastes

Different from natural aggregates, RCA can be regarded as a two-phase composite consisting of natural aggregate and adhered old mortar, as presented in Fig. 1.2. It has been found that the workability and mechanical properties of

RAC are not as good as those of natural aggregate concrete (NAC). For instance, Topçu and Şengel (2004) reported that the slump of fresh concrete decreased by around 20% when the natural concrete aggregates (NCAs) were fully replaced by RCAs. This could be caused by the porosity of the attached old mortar, which makes the RCA possess a higher water absorption, and therefore decreases the slump of fresh concrete (Duan & Poon, 2014). In terms of mechanical properties, most existing studies reported that the optimum replacement ratio of NCAs with RCAs can be up to 30% in RAC without compromising its mechanical properties (Tam *et al.*, 2005). A higher RCA replacement ratio generally decreases the mechanical properties of RAC. For example, Xiao *et al.* (2005) reported that using RCAs to fully replace NCAs decreases the compressive strength and Young's modulus of concrete by 26% and 45%, respectively. This can be attributed to that the old mortar attached on the aggregate weakens the interfacial transition zone (ITZ) between the RCA and the cement paste (Tam *et al.*, 2005). The existence of micro cracks in the old mortar could also weaken the mechanical properties of RAC (Kisku *et al.*, 2017).

Fig. 1.2 Recycled concrete aggregate

During the recycling process of RCAs, a large portion of waste concrete fines are produced. Liao and Yao (2022) reported that recycled concrete powder (RCP) with a particle size below 150 μm accounts for 10–20 wt.% of total concrete wastes. Thus, the rational utilisation of RCP is of great interest for sustainable construction and environmental protection. Many studies have explored the feasibility of using RCP as supplementary cementitious materials (SCM) to minimise the high carbon dioxide emissions and intensive energy consumption for cement production (Kim & Choi, 2012; Li *et al.*, 2021). These studies have

demonstrated that the use of RCP as SCM has a negative impact on the mechanical properties and microstructures of cementitious materials due to its low reactivity (Oksri-Nelfia *et al.*, 2016). Kaliyavaradhan *et al.* (2020) performed a statistical analysis of cement-based materials with RCP as cement replacement, and found that the compressive strength generally decreases with the RCP content. Liu *et al.* (2022), Sun *et al.* (2022), and Wu *et al.* (2022) also reported that the use of RCP as SCM degrades the compressive strength of cement mortar due to the reduced amount of hydration products and the increased porosity.

In general, the negative influence of incorporating high-volume recycled concrete aggregate or powder on the concrete properties involves a degradation in workability, mechanical properties (particularly compressive strength and Young's modulus), and microstructures. To mitigate these adverse impacts, extensive studies have been conducted to develop enhancement methods for reducing the RCA's porosity and increasing the RCP's reactivity. For example, Xuan *et al.* (2016) investigated the properties of RAC incorporated with carbonated RCAs, and found that the microhardness of cement paste in the old mortar and the new ITZs around the carbonated RCAs can be enhanced after the carbonation treatment. This in turn increases the compressive and flexural strengths of RAC by up to 23%. Moreover, Qian *et al.* (2020) investigated the effect of using high-temperature reactivated RCP as SCM on the properties of ultra-high performance concrete (UHPC), and found that the use of treated RCP has a negligible effect on the compressive strength of UHPC. Nevertheless, using treated RCP up to 25% can improve the durability and pore structure of UHPC. However, these treatments inevitably increase labour costs and environmental burdens, which are barriers for the large-scale manufacture of the concrete prepared with the treated materials. The improvement of the concrete mix design method is another effective strategy to tackle the problems of using RCA and RCP in concrete. This can be achieved by properly proportioning the constituents of concrete to compensate for the negative impacts brought by using RCA and RCP. This can also promote the wide application of high-performance sustainable concrete in the construction industry.

The concrete mix design method based on particle packing optimisation has

attracted increasing attention. It can be used to increase the particle packing density of granular materials to improve the properties of concrete. Nanthagopalan & Santhanam (2012) found that the optimisation of aggregate gradation can improve the packing density of aggregates, and thereby enhance the mechanical properties of concrete. Moini *et al.* (2015) also found that increasing the packing density by optimising aggregate gradation can enhance the compressive strength of concrete. Amario *et al.* (2017) adopted the compressible packing model to optimise the mix proportion of normal and high-strength RAC with an RCA replacement ratio of up to 60%, and the results showed that the optimised RAC mixtures can achieve the desired mechanical properties. Thus, particle packing optimisation is one of the most effective methods for improving RAC properties. However, the role of aggregate packing enhancement in affecting the properties and microstructure of RAC still requires a more in-depth study.

In addition to aggregate packing optimisation, cement paste volume (CPV) and sand-to-aggregate volume ratio (Bs) are important design parameters for developing high-performance packing-optimised RAC. For example, Chu (2019) reported that increasing the CPV by 6% could increase the slump of concrete by 150 mm but decrease the compressive strength by up to 7.2%. Similarly, Kolias & Georgiou (2005) and Piasta & Zarzycki (2017) reported that increasing the CPV can slightly decrease the compressive strength of concrete. However, Yurdakul *et al.* (2013) and Wang *et al.* (2015) stated that there exists an optimum CPV for concrete to achieve the maximum compressive strength. On the other hand, Lin (2020) pointed out that increasing the Bs negatively affects the compressive strength and microstructure of self-compacting concrete (SCC). Mohammed and Rahman (2016) found that increasing the Bs can improve the compressive strength and Young's modulus of concrete regardless of the aggregate type. Su *et al.* (2002) found that increasing the Bs can improve the flowability of SCC, but has a negligible influence on the elastic modulus when the total aggregate volume is kept constant. Therefore, there is still no consensus about the influence of CPV or Bs on the concrete properties. Moreover, there is lack of studies investigating the effect of CPV or Bs on the microstructure of RAC, particularly its pore structure and interfacial transition zone.

The RCP, as a by-product from C&D waste recycling, has also been used to replace sand in mortar or concrete. For example, Zhao *et al.* (2015) investigated the properties of mortars with RCP as a replacement of natural sand, and found that incorporating RCP decreases the slump and compressive strength of mortars by 55% and 29%, respectively. It has been recognised that the inferior properties of RCP mortar are mainly attributed to the high porosity and water absorption of RCP particles. Meanwhile, the incorporation of RCP as sand replacement can further broaden the particle size distribution and alter the packing density of aggregates under a dry packing condition (Mostofinejad & Reisi, 2012; Yu *et al.*, 1997). Therefore, the properties of RCP mortar might be improved through optimising the packing status of aggregates with the incorporation of RCP. This can be attributed to the refinement of pore structure with increased particle packing density. However, few investigations have been conducted to understand the role of RCP in affecting the particle packing density and the pore structure of RCP mortar.

In addition, it is crucial to evaluate the broader environmental impact of these materials. This requires a perspective that goes beyond the tangible properties of the construction materials and further considers the environmental implications associated with their production, use, and end-of-life management. This holistic perspective is facilitated by Life Cycle Assessment (LCA).

LCA is one of the environmental assessment techniques that can be used to effectively evaluate materials' sustainability. Numerous LCA studies have demonstrated that using recycled concrete aggregate has merit in reducing environmental burdens. For example, Blengini and Garbarino (2010) and Hossain *et al.* (2016) reported that the greenhouse gas emissions and energy consumption of recycled aggregate production are lower than those of the production of the same amount of natural aggregates. Weil *et al.* (2006) found that the use of RCAs in concrete can reduce the consumption of primary mineral resources. Zhao *et al.* (2020) found that replacing NCAs with RCAs in the production of concrete blocks can save the land use but gain limited refinement in global warming, acidification, and freshwater eutrophication. However, the environmental benefits of adopting packing-optimised RAC and using RCP as sand replacement have not been clearly demonstrated yet in the literature, which

necessitates an in-depth LCA study.

1.2 Research Questions

Although significant progress has been made on utilising C&D wastes for new concrete production, there are still several research questions that need to be tackled:

- Impact of aggregate packing enhancement on the properties of RAC: Incorporating a high volume of recycled aggregates generally has negative impacts on the concrete properties. One of the strategies to enhance the RAC's properties can be achieved via the improvement of concrete mix design based on aggregate packing enhancement. However, the role of aggregate packing enhancement in affecting the properties and microstructure of RAC remains unclear.

- Influence of design parameters CPV and Bs on the properties of RAC: Determining the optimal aggregate gradation and cement paste volume is important for developing high-performance packing-optimised RAC. There is still no consensus on effects of varying CPV and Bs on concrete properties in the literature. Furthermore, there is a lack of studies investigating the effect of CPV or Bs on the microstructure of RAC, particularly its pore structure and interfacial transition zone.

- Effect of using RCP as sand replacement on the properties of RAC: It has been recognised that the inferior properties of RCP mortar are mainly due to the high porosity and water absorption of RCP particles. Few investigations have been conducted to understand the role of RCP in affecting the particle packing density and pore structure of RCP mortar. Therefore, the potential improvement of RCP mortar properties through optimising the packing status of aggregates with the incorporation of RCP remains largely unexplored.

- Sustainability assessment: LCA has been increasingly used to evaluate the sustainability of construction materials. There is a lack of comprehensive LCA studies that fully account for the environmental benefits of adopting

packing-optimised RAC and using RCP as sand replacement.

These identified questions underline the need for further research and form the basis of this study's objectives in the subsequent section.

1.3 Research Objectives

The main aim of this study is to investigate the properties and sustainability of packing-enhanced concrete incorporating recycled concrete materials, specifically RCAs and RCP. In order to achieve this aim, the specific objectives of this research are as follows:

- To investigate the impact of aggregate packing enhancement on the improvement of RAC properties.

- To develop optimisation strategies for packing-optimised RAC through adjusting the mix design parameters of cement paste volume and sand-to-aggregate volume ratio.

- To reveal the role of using RCP as sand replacement in affecting the properties of mortar.

- To demonstrate the environmental benefits of adopting packing-optimised RAC and RCP as sand replacement via life cycle assessment.

1.4 Research Significance

The significance of this study lies in providing valuable insights into the practical implications of developing a high-performance RAC with enhanced particle packing. It can guide the industry in selecting the appropriate aggregate gradation and cement paste volume for enhancing the mechanical properties and sustainability of RAC. Moreover, the findings of this study can unveil the role of RCP in affecting the particle packing density and pore structure of mortar, which contributes to the knowledge of developing eco-friendly and high-performance RAC. The in-depth exploration of the micro-to-macro mechanisms in this study can further confirm the universal applicability of particle packing enhancement for developing high-performance RAC. This demonstrates its potential for contributing to the broader goal of sustainable and efficient

construction practices, particularly in the context of using recycled concrete materials.

1.5 Outline of the Thesis

The thesis is divided into seven chapters, and the outline of the thesis is presented in Fig. 1.3. The details of each chapter are summarised as follows.

Chapter 1 introduces the research background, motivations, research objectives, significance of the study, and outline of the thesis.

Chapter 2 provides a literature review on the characteristics of recycled concrete aggregate, concrete mix design method based on particle packing optimisation, the use of recycled concrete powder, and the environmental assessment of recycled aggregate concrete. Subsequently, the research gaps in the study are identified and presented.

Chapter 3 presents an experimental investigation into the effect of aggregate packing enhancement on the properties of natural and recycled aggregate concrete. The slump, compressive strength, flexural strength, and Young's modulus of concrete are first examined, followed by the characterisation of the macro-pore structure inside RAC. The role of aggregate packing enhancement in the properties of RAC is comprehensively discussed.

Chapter 4 presents an investigation of the influences of cement paste volume and sand ratio on the properties of packing-optimised RAC. The workability and mechanical properties of RAC are first examined, followed by the characterisation of the interfacial transition zones and the pore structure inside RAC to explain their impacts on macroscopic performance. Guidance on the determination of cement paste volume and sand ratio in the mix design of packing-optimised RAC is proposed.

Chapter 5 provides an investigation into the role of RCP as a sand replacement in the properties of cement mortar. The physical properties, mechanical properties, and drying shrinkage of RCP mortars are examined, followed by the characterisation of the crystalline phases and microstructures of RCP mortars. The filling effect of RCP and the hydration reaction promoted by RCP are quantified by measuring the particle packing density and hydration heat

evolution, respectively.

Chapter 6 provides a life cycle assessment for the packing-optimised RAC to evaluate its environmental benefits in terms of global warming and energy consumption. Moreover, the influence of using RCP as a potential sand replacement on environmental sustainability is also studied.

Chapter 7 summarises the main findings derived from this study, and provides recommendations for future research in the development of high-performance RAC.
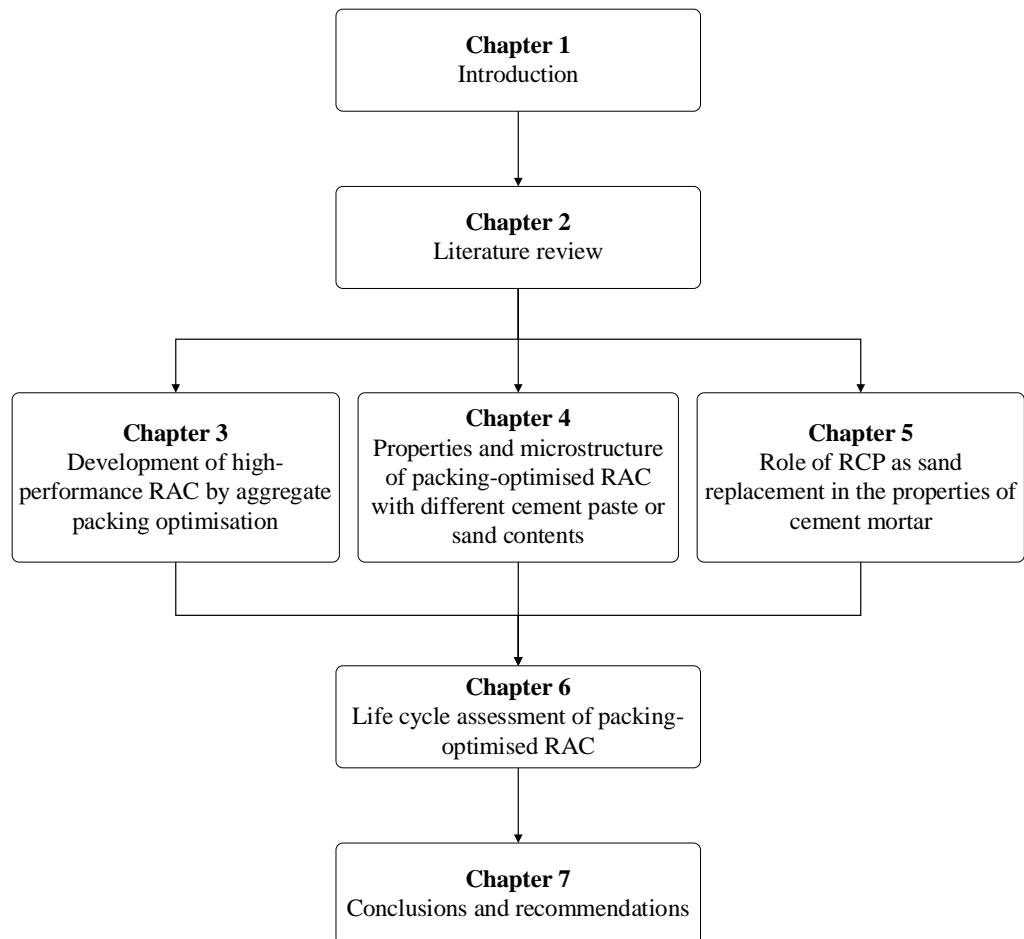
Fig. 1.3 Outline of the thesis

CHAPTER 2
LITERATURE REVIEW

2.1 Introduction

This chapter presents a literature review on the characteristics of recycled concrete aggregate and powder, the properties of concrete with recycled aggregate/powder, the concrete mix design method based on particle packing optimisation, and the environmental assessment of recycled aggregate concrete. The research gaps are subsequently identified and summarised.

2.2 Recycled concrete aggregate
2.2.1 Characteristics of recycled concrete aggregate

Recycled Concrete Aggregates (RCAs) generate from the recycling process of waste concrete elements. Inherently different from natural concrete aggregates (NCAs), RCAs' surfaces are attached by old mortars (Verian *et al.*, 2018). As schematically shown in Fig. 2.1, the presence of surface-attached old mortar causes increasing aggregate surface voids, interfacial transition zones (ITZs) and inner microcracks, eventually leading to a decreased density and increased water absorption as compared to NCAs (Behera *et al.*, 2014). The previous results are summarised in Table 2.1. These properties of RCAs mainly depend on the content of surface-attached old mortar. Generally, the content of the attached old mortar increases as the RCA size decreases, while it increases as the parent concrete strength increases (Kisku *et al.*, 2017). The former is mainly related to the current recycling process by continuously cumulating the paste debris into the finer RCAs (Gokce *et al.*, 2011), while the latter is attributed to the stronger bond between the aggregate and the attached old mortar for the RCAs obtained from the high-strength parent concrete (Padmini *et al.*, 2009).
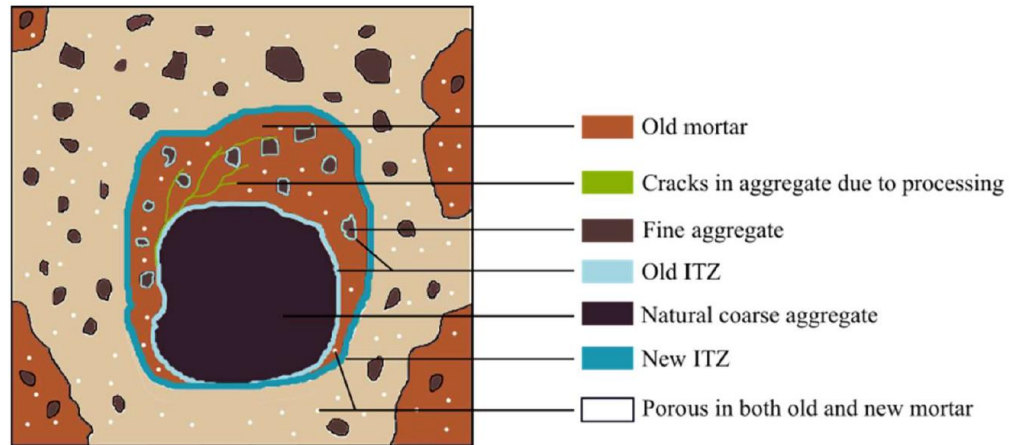
Fig. 2.1 Pictorial presentation of RCA characteristics (Wang *et al.*, 2021)

Table 2.1 Water absorptions and densities of RCAs and NCAs reported in the literature

Reference	Water absorption (%)		Specific density (g/cm³)	
	NCAs	RCAs	NCAs	RCAs
Poon *et al.* (2002)	1.25	4.19-7.60	2.57	2.31-2.47
Poon *et al.* (2004)	1.24–1.25	6.28–7.56	2.62	2.33-2.37
Xiao *et al.* (2005)	0.4	9.25	2.82	2.52
Kou *et al.* (2007)	1.11-1.12	3.52-4.26	2.62	2.49-2.57
Abbas *et al.* (2009)	0.34	3.30-5.40	2.73	2.64
Liu *et al.* (2011)	0.40	5.26-6.90	2.79	2.42-2.43
Duan & Poon (2014)	0.90-1.24	3.13-7.77	2.6	2.35-2.54
Pickel *et al.* (2017)	1.53	4.72-6.91	2.76	2.65-2.69
Duan *et al.* (2020)	1.00	6.53	2.61	2.59
Chen *et al.* (2022)	1.15	5.80	2.68	2.65

2.2.2 Characteristics of recycled concrete powder

Recycled Concrete Powder (RCP) is a by-product when processing RCAs. As seen in Table 2.4, the RCP is a very fine material normally with a particle size smaller or slightly larger than that of cement particles, possessing the specific density and specific surface area of 2.3~2.5 g/cm³ and 90~800 m²/kg, respectively. X-ray diffraction (XRD) analysis manifested that the mineral composition of RCP has common hydration products of cement clinker, such as

portlandite and calcite (Fig. 2.2). Moreover, the presence of alite or belite peak indicated that there exists a certain amount of unhydrated cement particles in the RCP. As seen in Fig. 2.3, Scanning Electron Microscope (SEM) illustrated that the RCP particles have more irregular shapes with rougher surface textures, more pores/voids and microcracks as compared to the cement particles. These RCP particles are usually coated with clustered hydrates. The chemical compositions of some RCPs were examined by X-Ray Fluorescence (XRF) test and listed in Table 2.2. They varied from case to case owing to different parent concretes and recycling techniques (Kaliyavaradhan *et al.*, 2020).

(a)

(b)
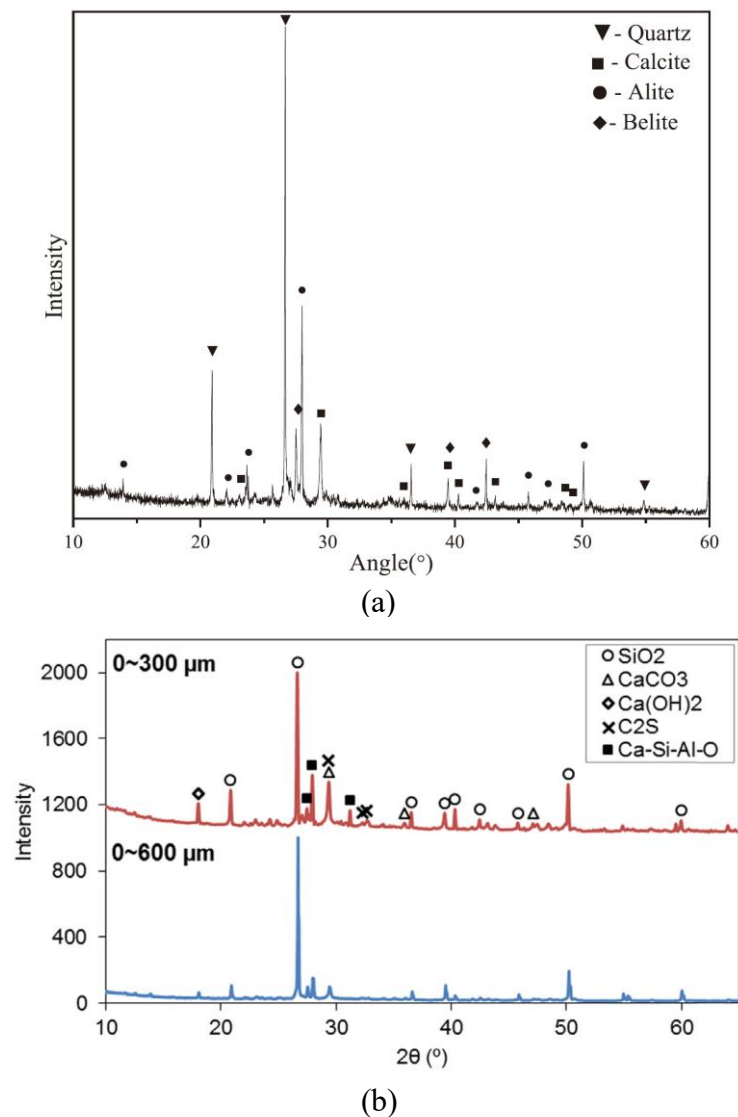
Fig. 2.2 Mineral composition of RCPs ((a) Ren *et al.*, 2020 and (b) Li & Yang, 2017)
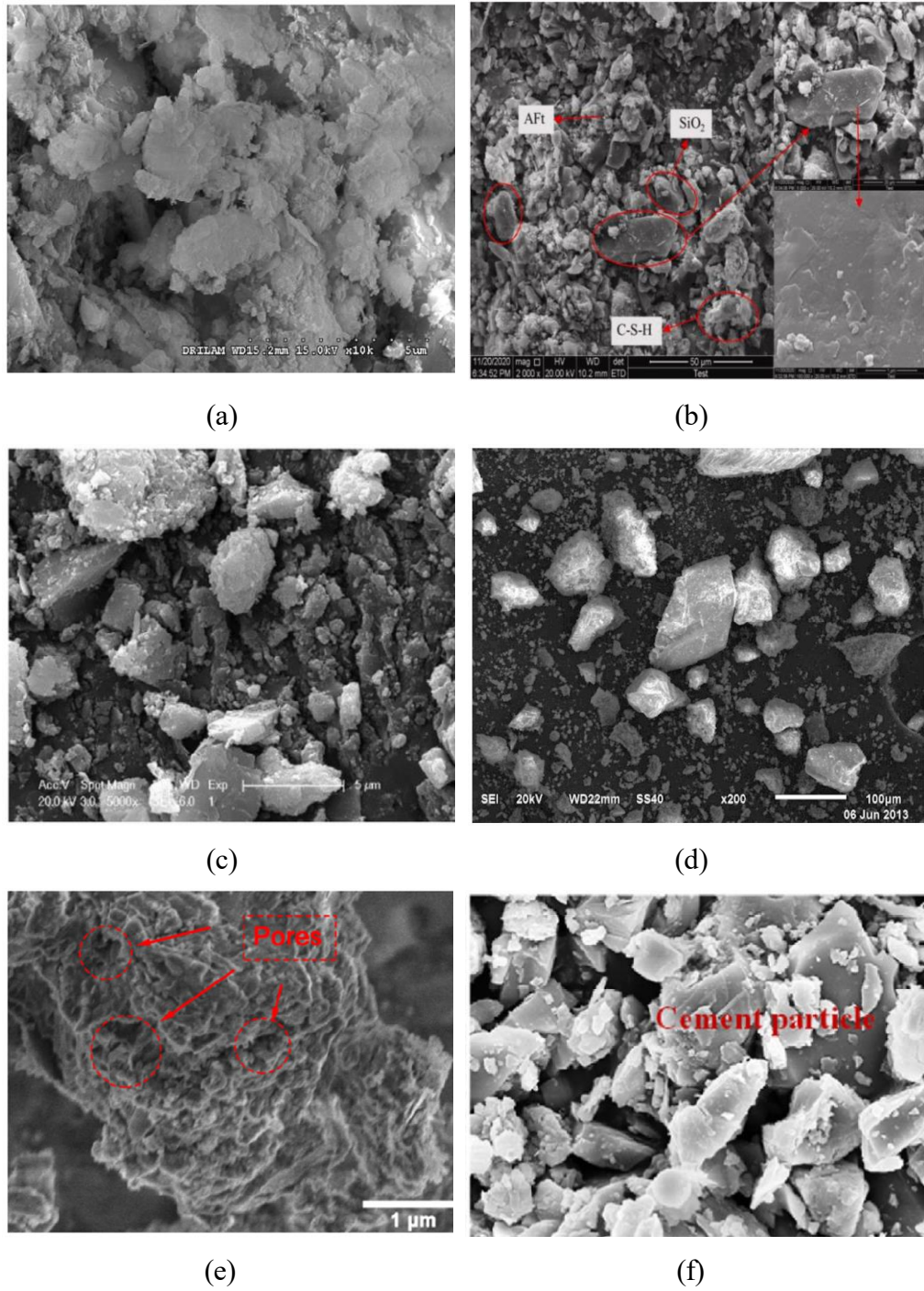
Fig. 2.3 Morphology of RCP particles ((a) Kim & Choi, 2012, (b) Liu *et al.*, 2022, (c) Duan *et al.*, 2020, (d) Liu *et al.*, 2016 and (e) Li *et al.*, 2021) and cement particles ((f) Wu *et al.*, 2022)

Table 2.2 Chemical compositions of RCPs from different studies (%)

Reference	SiO$_2$	CaO	Al$_2$O$_3$	Fe$_2$O$_3$	MgO
Kim & Choi (2012)	58.55	11.82	10.35	4.64	1.52
Duan *et al.* (2020)	57.01	21.30	10.93	3.45	1.82
Ren *et al.* (2020)	64.81	19.14	7.77	1.59	1.54
Li *et al.* (2021)	50.93	18.18	13.55	6.37	2.73
Wu *et al.* (2021)	31.00	54.90	3.40	1.90	5.60
Li *et al.* (2022)	60.30	17.40	10.40	3.00	3.40

2.2.3 Properties of fresh and hardened RAC

The properties of fresh and hardened RAC have been extensively investigated. Table 2.3 summarises the selected studies focusing on the use of various RCA contents in concrete and highlights their influences on the properties of workability (i.e., slump) and mechanical properties (i.e., compressive strength, flexural/tensile strength, and Young's modulus).

The most widely used method for evaluating the workability of fresh concrete is slump (flow) test. As seen in Table 2.3, the slump values of fresh RAC reported by Bairagi *et al.* (1993), Topçu & Şengel (2004), Yang *et al.* (2008) are generally lower than those of fresh NAC when a high RCA replacement rate is incorporated. This decrease in workability of fresh RAC can be caused by the increased water absorption as summarised in section 2.2.1. Moreover, the irregular shapes, roughness and grading of RCAs also significantly influence the RAC workability (Silva *et al.*, 2018). However, Poon *et al.* (2007) and Kou & Poon (2013) found that the slump of fresh RAC increases with the proportion of RCAs prepared with a saturated-surface-dry (SSD) condition. Mefteh *et al.* (2013) investigated the workability of RAC prepared with RCAs considering various moisture contents. In their study, they treated the RCAs into three different moisture states, *i.e.,* dry, pre-wetting and saturated-surface-dry (SSD) conditions. And they found that the RAC slump decreases with the dry RCA content, and a 100% replacing can decrease the slump by up to 83%. However, the RACs prepared with pre-wetting and SSD condition treated RCAs (termed as PW RAC and SSD RAC, respectively) exhibit higher slump than NACs, and the slumps increase with the treated RCA replacement rate. Similarly, Amario *et*

al. (2017) also found that the workability of fresh RAC incorporated with SSD RCAs is higher than that of NAC. Their research also indicated that the moisture condition of RCAs has a considerable impact on the workability of RAC.

As seen in Table 2.3, incorporating RCA up to 30% has a negligible effect on the mechanical properties of RAC, and a further increase of RCA replacement rate can render a considerably negative impact on the mechanical properties. Bairagi *et al.* (1993) investigated the mechanical properties of RAC with various RCA replacement ratios (25%, 50%, 75% and 100%). They found that the mechanical properties of RAC continuously decrease as the RCA replacement rate increases. An incorporation of 100% NCAs can decrease the compressive strength and Young's modulus by up to 13% and 29%, respectively. De Oliveira and Vazquez (1996) investigated the mechanical properties of RAC containing RCAs with various water saturation degrees (dry, semi-saturated and fully saturated). They found that the mechanical properties of RACs are inferior than those of NAC irrespective of the moisture degrees of RCAs. More specifically, the compressive and flexural strengths of RACs were around 10% lower than those of the NACs. However, the reduction in Young's modulus was more pronounced (up to 23%) as the incorporation of RCAs decreased. Kou and Poon (2013) investigated the long-term mechanical properties of RAC incorporated with a high replacement rate of RCAs. They found that the compressive strength and Young's modulus decrease by 22% and 25%, respectively when the NCA were completely replaced by RCAs. Kou and Poon (2015) also investigated the properties of RCAs obtained from various parent concretes. They found that the compressive strengths of RACs are lower than that of NAC. More specifically, the compressive strengths of RACs prepared with RCAs originated from 30 MPa, 45 MPa, 60 MPa, 80 MPa and 100 MPa parent concretes were 21.1%, 12.6%, 8.6%, 1.1% and 0.4% lower than that of NAC, respectively.

Many studies reported that these inferior properties of RAC are mainly caused by the change in their microstructures of interfacial transition zones (ITZs) and pore structure. Xiao *et. al.* (2005) found that the compressive strength and Young's modulus of concrete are reduced by 26% and 45%, respectively, when the NCAs were fully replaced by RCAs. They also pointed out that the presence of multi-ITZs induced by RCAs may increase the chance of micro-cracks

propagation, thereby leading to a higher strain increasing rate and lower Young's modulus. Moreover, Tam *et al.* (2005) investigated the microstructure of RACs by SEM. They found that using RCAs can induce more microcracks (Fig. 2.4(a)) and also weaken the ITZs between new cement paste and RCAs (Fig. 2.4(b)), thereby impairing the RAC properties.
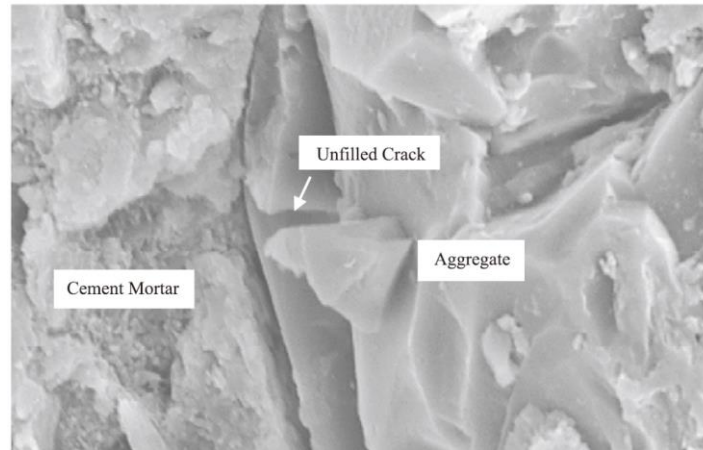
(a)
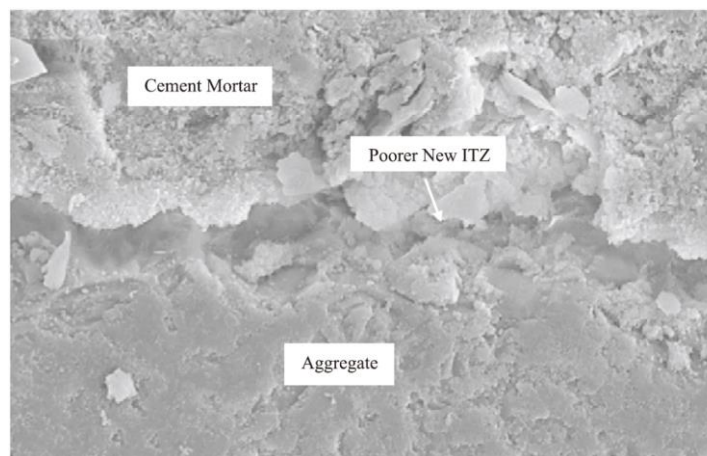
(b)

Fig. 2.4 (a) Microcracks in RCAs and (b) weakened ITZs between new cement paste and RCAs (Tam *et al.*, 2005)

Gómez-Soberón (2002) investigated the properties and microstructure of RACs with various RCA replacement rates (15%, 30%, 60% and 100%). They found that the mechanical properties of compressive strength and Young's modulus decrease with the increase of the RCA replacement ratio. Replacing 15%~100% NCAs with RCAs can decrease the compressive strength and Young's modulus of RACs by 1%~11% and 7%~19%, respectively. These decreasing trends in mechanical properties of RACs could be attributed to the increasing total

porosity as seen in Fig. 2.5, where 'r' indicate the replacing ratio.
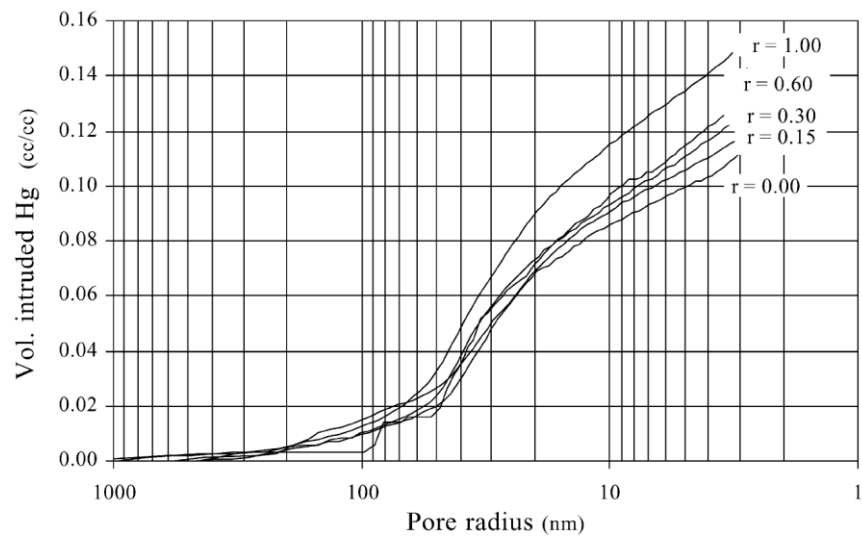
Fig. 2.5 Pore size distributions of RACs with various RCA replacement ratios
(Gómez-Soberón, 2002)

Table 2.3 Summary of the selected studies on investigating the properties of recycled aggregate concrete

Reference	Replacing rate (%)	Changing rate (%)			
		Slump (mm)	Compressive strength (MPa)	Flexural/Tensile strength (MPa)	Young's modulus (GPa)
Bairagi *et al.* (1993)	25	0	-2	-3	-7
	50	-17	-6	-10	-14
	75	-33	-9	-26	-21
	100	-33	-13	-35	-29
De Oliveira & Vazquez (1996)	100	N/A	-11	-10	-23
Topçu & Şengel (2004)	30	-7	-27	4	N/A
	50	-11	-31	0	N/A
	70	-21	-27	-4	N/A
	100	-16	-41	-8	N/A
Xiao *et al.* (2005)	30	-21	-5	N/A	-39
	50	-2	-18	N/A	-42
	70	-5	-16	N/A	-43
	100	5	-26	N/A	-45

Table 2.3 Summary of the selected studies on investigating the properties of recycled aggregate concrete (continued)

Reference	Replacing rate (%)	Changing rate (%)			
		Slump (mm)	Compressive strength (MPa)	Flexural/Tensile strength (MPa)	Young's modulus (GPa)
Tam *et al.* (2005)	10	N/A	6	N/A	N/A
	15	N/A	1	N/A	N/A
	20	N/A	-4	N/A	N/A
	25	N/A	-6	N/A	N/A
	30	N/A	4	N/A	N/A
Kou & Poon (2013)	50	13	-13	-5	-13
	100	30	-22	-8	-25
Mefteh *et al.* (2013)	20	-22	16	13	N/A
	40	-33	13	-3	N/A
	60	-67	-16	-15	N/A
	80	-78	-13	-13	N/A
	100	-83	-13	-12	N/A
Yang *et al.* (2008)	30	-3	-17	-20	-11
	50	-8	-23	-29	-18
	100	-10	-25	-36	-25

2.2.4 Properties of fresh and hardened RCP incorporated mortar or concrete

The properties of RCP incorporated mortar or concrete have been widely investigated previously. Table 2.4 summarises the previous studies on the use of the RCP as the supplementary cementitious material (SCM) in mortar or concrete. Their influences on the workability and mechanical properties are listed.

The workability (*i.e.,* flowability or slump flow) of mortar or concrete generally decreases with the increase of the RCP content. As seen in Table 2.4, the use of 15%~45% RCP can lead to a decrease in the slump flow of the fresh mortar/concrete by 15%-30%. Kim and Choi (2012) found that the mortars' slump flow decrease as the RCP replacement level increases. Replacing 15% and 45% of the cement with RCP would lower the slump flow by 14%~16% and 28%~30%, respectively. It indicates that more water or water reducer is required to compensate the high-water absorption of RCP particles due to their porous microstructure (*i.e.,* massive voids/microcracks). Duan *et al.* (2020) found that the mortar made with RCP needs more superplasticiser (around 70% higher) to achieve a comparable slump flow (*i.e.,* 180 mm) as reference to that without RCP. They explained that the lower flowability is attributed to the porous microstructures, rough surface and irregular shape of RCP particles. Nonetheless, Oksri-Nelfia *et al.* (2016) found that the slump flow of mortars made with RCP are higher than that of mortar without RCP. They considered that the addition of finer RCP can improve the particle packing density to release more free water (the water being in excess of that needed to fill with the voids) to lubricate the aggregate surface.

Mechanical properties of RCP incorporated mortar or concrete generally tend to decrease as the RCP content increases. As seen in Table 2.4, replacing 10%~75% of the cement with RCP can lead to a decrease in the compressive strength of the mortar/concrete by 11%~91%. Kim and Choi (2012) found that the mortars' compressive strengths decrease as the RCP replacement ratio increases. Replacing 15% and 45% of the cement with RCP can decrease the compressive strength by 28% and 73%, respectively. Similarly, Oksri-Nelfia *et al.* (2016) found that the compressive strengths of mortars made with RCP are lower than those of mortars without RCP. Replacing 25%, 50% and 75% of the cement with

RCP can decrease the compressive strength of mortar by 26%, 67% and 91%, respectively. Moreover, Duan *et al.* (2020) studied the properties of RCP from Construction and Building (C&D) wastes, and mortars prepared with that. They found that replacing 20% of the cement by RCP can decrease the hydration heat and compressive strength of the mortar by 23% and 27%, respectively. Duan *et al.* (2020) also investigated the properties of self-compacting concrete (SCC) with the incorporation of RCAs and RCP as the replacements of aggregate and fly ash, respectively. The results show that the concrete's mechanical properties and durability deteriorate. Therefore, the findings from the existing studies have demonstrated the relatively low reactivity of the RCP particles.

Moreover, many studies have reported that the use of RCP as SCM degrades the properties of mortar/concrete due to the weakened microstructures of ITZs and pore structure. Li *et al.* (2021) investigated the properties of the recycled powder from waste concrete, and its effects as SCM on the mortar properties. They found that the use of RCP considerably impairs the mortar's strength, and the incorporation of 30% RCP significantly decreased the compressive strength by up to 27%. This deterioration of the mechanical properties was mainly attributed to the impaired ITZs. As seen in Fig. 2.6, a porous ITZ can be observed between the cement paste and RCP particle, which mainly consists of microcracks, oriented flaky crystals, and fibrillar hydration products. Liu *et al.* (2022) investigated the properties of RCP mortars incorporated nano-silica (NS) as cement replacement. They found that replacing 30% of the cement with RCP dramatically decrease the compressive strength and flexural strength of the mortar by 29% and 17%, respectively. This was mainly attributed to the lower reactivity of RCP than that of cement, and thereby decreasing the amount of hydration products and resulting in larger pore size and total porosity. As seen in Fig. 2.7, it can be found that replacing 30% of the cement with RCP can increase the volume fraction of pores in harmful zone as well as the cumulative pore volume. However, the negative impacts of RCP incorporation could be mitigated by adding NS to refine the pore structure. Wu *et al.* (2022) investigated the properties of mortars that incorporated RCP as the cement replacement and recycled fine aggregates (RFAs) as the sand replacement synergistically. They found that replacing the sand with RFAs would decrease the mechanical

properties of the mortar, and the incorporation of RCP would further decrease their properties. Specifically, increasing the replacement ratio by 30% could decrease the compressive strength and flexural strength by 26.5% and 10.6%, respectively. Adding RCP as the replacement of the cement can reduce the hydration products of C-S-H gel and portlandite, as shown in Fig. 2.8 (TGA results) and Fig. 2.9 (XRD results). This tended to impair the pore structure of the mortar, and a replacement of 30% would increase the mean pore diameter and porosity by 16.4% and 35.9%, respectively. Similarly, Wu *et al.* (2021) investigated the properties and microstructures of the mortars with various RCP replacement rates. They found that the compressive strength decreases as the RCP replacement rate increases. This was mainly related to the increasing porosity as the RCP content increases as seen in Fig. 2.10.
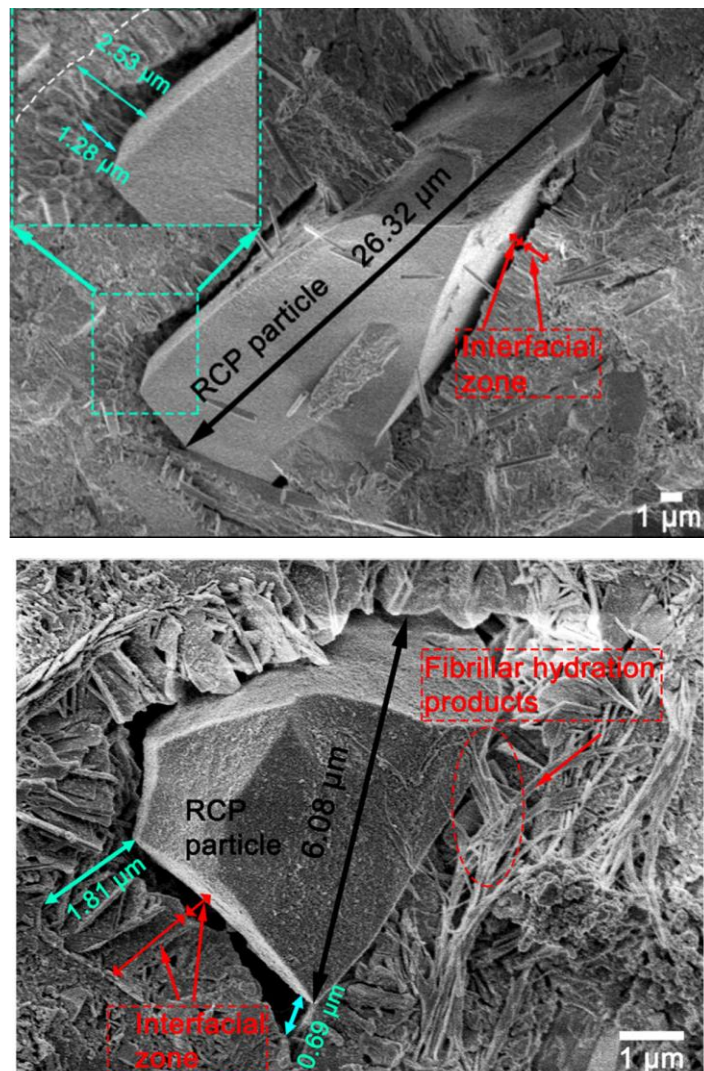
Fig. 2.6 ITZs between cement paste and RCP particle (Li *et al.*, 2021)

(a)   (b)
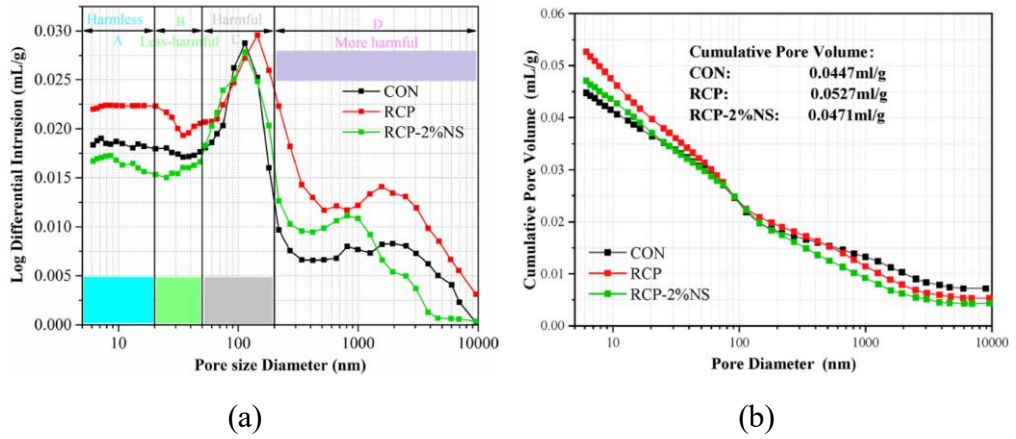
Fig. 2.7 Pore size distributions of RCP mortars (Liu *et al.*, 2022)

(a) Paste without RCP   (b) Paste with RCP
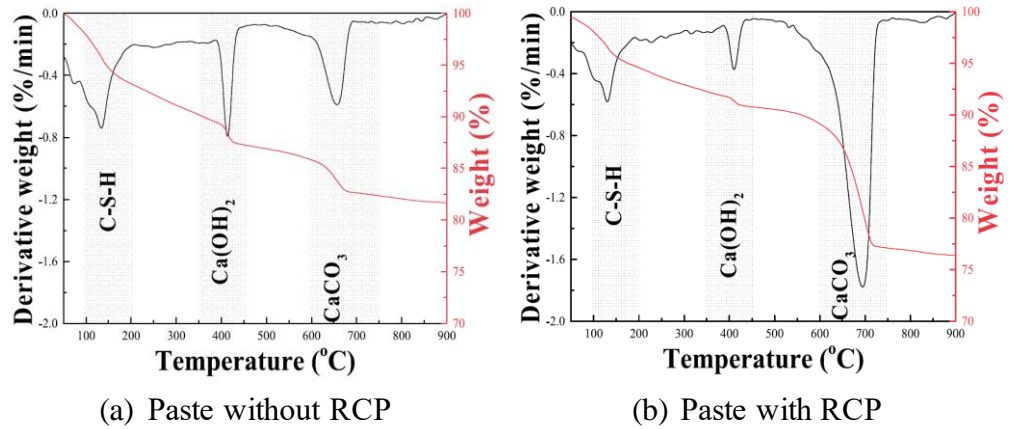
Fig. 2.8 TGA results of cement paste with or without RCP (Wu *et al.*, 2022)

(c) Paste without RCP   (d) Paste with RCP
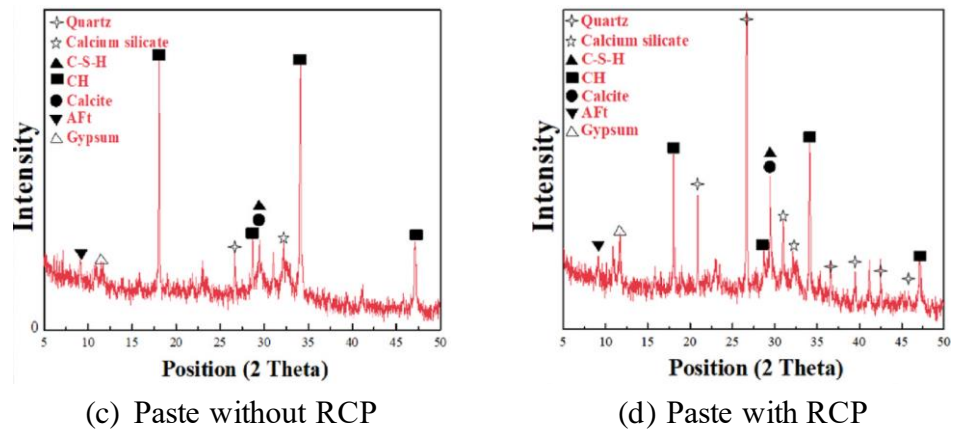
Fig. 2.9 XRD results of cement paste with or without RCP (Wu *et al.*, 2022)
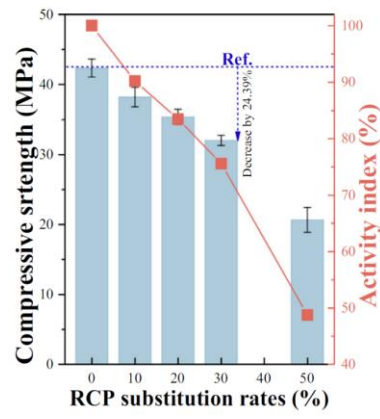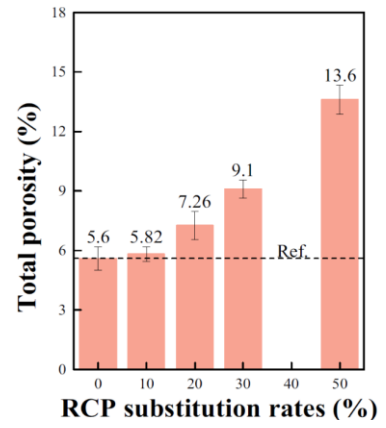
Fig. 2.10 (a) compressive strength and (b) porosity of RCP mortars (Wu *et al.*, 2021)

Table 2.4 Summary of previous studies on investigating the properties of mortar/concrete with RCP as SCM

Reference	Sample type	Particle size (μm)	Specific surface area (m^2/kg)	Density (g/cm^3)	Substitution (%)	Measured properties	Change rate (%)
Kim & Choi (2012)	Mortar	90.0	136.0	2.49	15, 45	Slump flow	-14, -28
						Compressive strength	-25, -64
		176.0	92.8	2.48	15, 45	Slump flow	-16, -30
						Compressive strength	-28, -73
Oksri-Nelfia *et al.* (2016)	Mortar	8.8	620.0	2.45	25, 50, 75	Slump flow	+39, +36, +31
						Compressive strength	- 26, -67, -91
Duan *et al.* (2020)	Mortar	48.2	N/A	N/A	20	Compressive strength	-27
Kim (2017)	Concrete	90.0	136.0	2.49	15, 30, 45	Slump flow	-2, -6, -10
						Compressive strength	-10, -30, -45
						Splitting tensile strength	-11, -21, -39
						Elastic moduli	-6, -14, -20
Ren *et al.* (2020)	Concrete	14.2	N/A	2.28	20, 40, 60	Compressive strength	+13, -9, -34

Table 2.4 Summary of previous studies on investigating the properties of mortar/concrete with RCP as SCM (continued)

Reference	Sample type	Particle size (μm)	Specific surface area (m²/kg)	Density (g/cm³)	Substitution (%)	Measured properties	Change rate (%)
Sun *et al.* (2022)	Mortar	15.0	N/A	N/A	30, 50	Compressive strength	-32, -46
						Flexural strength	+3, -20
Li *et al.* (2021)	Mortar	N/A	476.0	N/A	30	Slump flow	-15
						Compressive strength	-27
			821.0			Slump flow	-22
						Compressive strength	-23
Liu *et al.* (2022)	Mortar	52.3	575.0	2.40	30	Compressive strength	-29
						Flexural strength	-17
Wu *et al.* (2022)	Mortar	22.7	N/A	N/A	30	Compressive strength	-27
						Flexural strength	-11
Wu *et al.*	Mortar	22.7	N/A	N/A	10, 20, 30, 50	Compressive strength	-8, -18, -24, -53
Duan *et al.* (2020)	Concrete	90.0	N/A	N/A	10, 20	Slump flow	-1, -3
						Compressive strength	-1, -10
						Splitting tensile strength	0, -10

2.2.5 Performance enhancement of recycled concrete aggregate

Many enhancement methods have been proposed to improve the performance of RAC, as summarised in Fig. 2.11. There are two categories of methods that have been widely adopted to pre-treat the RCAs to mitigate their porosity, including removing the loose part of the attached old mortar and strengthening the attached old mortar.

Removing	Strengthening
• Ultrasonic cleaning • Pre-soaking in acid • Heat treatment • Mechanical grinding • Thermo-chemical treatment	• Carbonation treatment • Polymer emulsion coating • Cement slurry coating • Pozzolana slurry coating • Calcium carbonate biodepostion

Fig. 2.11 Enhancement treatments for RCAs

Katz (2004) ultrasonically removed the loose mortar attached on the RCAs surfaces to decrease their porosities. They found that the ultrasonic cleaning could increase the 28d compressive strengths of RACs by up to 7%. Ismail and Ramli (2013) utilised the acidic pre-soaking method and revealed the effect of the molarity of the acid solvent and soaking time on the properties of RCAs and the prepared RAC. They demonstrated that acidic pre-soaking could significantly reduce the water absorption of RCAs by up to 28%. Moreover, the strength of the RAC incorporated with 45% treated RCAs was comparable to that of the RAC incorporated with 15% untreated RCAs. It indicated that the acid pre-soaking treatment could increase the RCA replacement rate, mainly due to the enhanced surface contact between the newly formed cement paste and the treated RCAs. Wang *et al.* (2017) investigated the effect of RCAs treated by the acetic acid immersion on the properties of RAC. They found that the treated RCAs showed lower water absorptions and less attached old mortars, which enhanced the compressive strength of the RAC by up to 25%. Moreover, Ryu *et al.* (2018) treated the surface porosity of recycled fine aggregates (RFAs) by pre-soaking them into H_2SiF_6 Solution. They discovered that the mortar prepared with the treated RFAs exhibited better mechanical properties in compressive and

flexural strengths.

As for the enhancing manner, Kou and Poon (2010) investigated the properties of polyvinyl alcohol (PVA) impregnated RCAs and prepared RAC. They found that the water absorptions of PVA impregnated RCAs (1.6%) were lower than those of un-treated RCAs (6.2%) with a maximum particle size of 20 mm. Moreover, the compressive strength of RAC was comparable to that of NAC when the PVA impregnated RCAs were used to replace the NCAs. Xuan *et al.* (2016) investigated the properties of RAC incorporated with carbonated RCAs, where the water absorption was reduced by up to 17%. Moreover, they found that the microhardness of the cement pastes in the old mortar and the new ITZs around the carbonated RCAs were enhanced after carbonation treatment as seen in Fig. 2.12, thereby the compressive and flexural strengths of RAC can be improved by 23% in comparison with those prepared with 100% non-carbonated RCAs. Wang *et al.* (2017) investigated the properties of RAC with the RCAs treated by using bio-deposition. They found that the bacterial-produced carbonate precipitated into the pores/voids of old attached mortar, and decreased the water absorption of RCAs by up to 27%. Moreover, this bio-deposition treatment enhanced the elastic modulus by 33% and compressive strength by 40%.
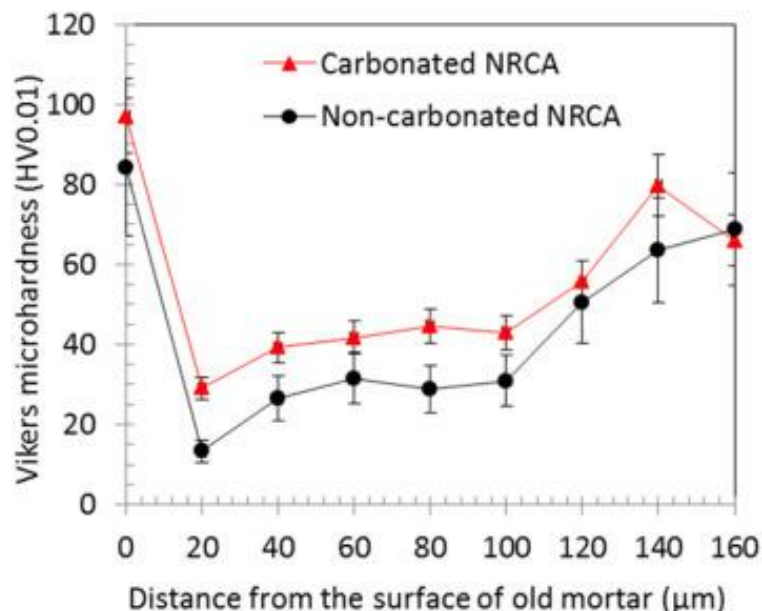
Fig. 2.12 ITZ microhardness distribution of RACs with or without carbonated RCAs (Xuan *et al.*, 2016)

Some researchers also compared the effects of various methods on enhancing the properties of RCAs and RAC. For instance, Kazmi *et al.* (2019) investigated the effects of five RCA treatment approaches (*i.e.,* carbonation, acetic acid immersion, acetic acid immersion with mechanical rubbing, acetic acid immersion with carbonation and lime immersion with carbonation) on the mechanical properties of RAC. It should be noted that the process of lime immersion with carbonation is performed by immersing the RCAs in lime saturated water for 24 hours, followed by drying at 25 °C and a relative humidity of 50% for three days to introduce some additional calcium into the pores of the old attached mortar artificially. Afterwards, the lime treated RCAs were carbonated by using the accelerated carbonation. They found that the physical properties (*i.e.,* water absorption, bulk density and crushing value) of the RCA were improved by these treatments. And the lime-carbonated RCAs could achieve the highest reduction rate in water absorption by up to 20%. The RACs with RCAs treated by acetic acid immersion with mechanical rubbing as well as that treated by lime immersion with carbonation exhibited better performances in the mechanical properties including compressive strength, split tensile strength and elasticity. Wang *et al.* (2020) investigated the effects of two RCA treatments methods (*i.e.,* carbonation treatment and cement slurry coating) on the properties of RCAs and the RAC. They found that both of the carbonation treatment and cement slurry coating can decrease the water absorption of the RCAs and further improve the mechanical properties of the RAC. These methods increased the compressive strength of RACs by up to 10.7% and 7.8% in comparison with those without treated RCAs, respectively. It indicates that the carbonation treatment is more effective than the cement slurry coating method in terms of compressive strength. Micro-hardness analyses showed that the carbonation treatment exhibited better performance in strengthening the old ITZ within RCAs than cement slurry coating method.

2.3 Concrete design based on particle packing optimisation

2.3.1 Factors affecting the particle packing density

Many existing studies demonstrate that the properties, engineering behaviours and performance of concrete are highly related to their particle packing status. The particle packing status of granular solids can be characterised by particle packing density, which is defined as the ratio of the absolute volume to the bulk volume of solid particles. Generally, particle size distribution (PSD) has a significant influence on the particle packing density. Wang *et al.* (1999) investigated the influence of particle size distribution on the packing density of cement. And they found that a wider PSD is beneficial for increasing the particle packing density and can result in an increase of 30% in packing density. Mehdipour and Khayat (2017) investigated the effect of particle size distributions on the packing density of binder particles with various compositions (Fig. 2.13). They pointed out that a wider PSD with a higher content of fine particles can lead to a higher packing density of the binder. For instance, the reference pure cement mixture with the largest distribution modulus (q) of 0.286 exhibits the lowest packing density of 0.58, and the highest packing density of 0.73 was achieved for the ternary binder with a relatively lower q of 0.21. However, a further decrease of q from 0.21 to 0.18 would result in a reduction in the packing density of the binder. Therefore, it suggests that an optimum PSD is a prerequisite for a granular mixture to achieve a higher particle packing density.
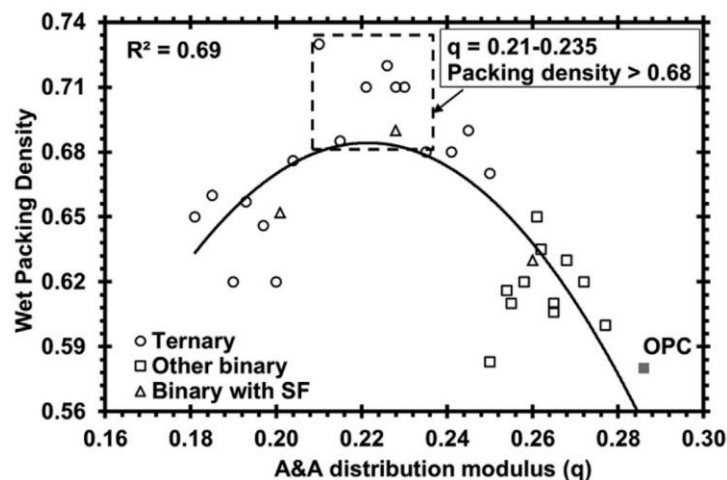
Fig. 2.13 Relationship between the packing density and A&A distribution modulus of various binders (Mehdipour & Khayat, 2017)

In addition, particle morphology also plays an important role in affecting the particle packing density. Cho *et al.* (2006) investigated the effects of particle shape, including sphericity and roundness, on the packing density. They found that the difference between maximum and minimum packing density increased as the sphericity and roundness decreased. They explained that the extreme irregularity of particles hindered the particle mobility to attain a denser particle packing. Mostofinejad and Reisi (2012) also pointed out that the shape and texture of aggregates can inevitably influence the particle packing density, and suggested that the particle shapes can be quantified by the friction coefficient in the discrete element modelling. Hafid *et al.* (2016) investigated the particle morphological parameters of aspect ratio and convexity on the packing densities of various types of sand grains. Each type of sand grain was sieved into three grain size ranges of 160 μm~200 μm, 315 μm~400 μm and 800 μm~1000 μm to minimise the induced effect of particle size distribution. They found that the dense and loose packing densities generally decrease with the aspect ratio, and slightly increase with the convexity, as seen in Fig. 2.14. It indicated that the shape of particles (*i.e.,* the aspect ratio) is an essential morphological parameter influencing the particle packing density.
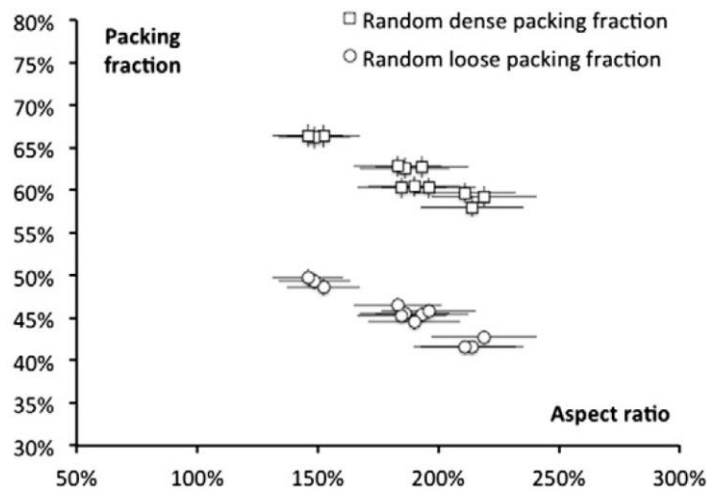
(a)
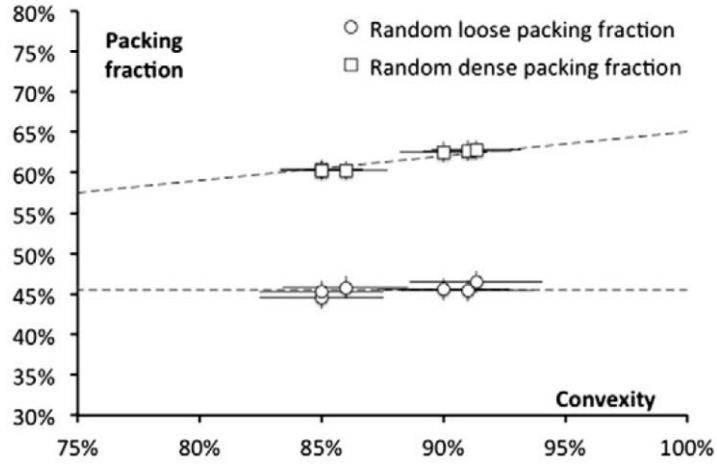
(b)

Fig. 2.14 Dense packing density and loose packing density versus (a) aspect
ratio and (b) convexity (Hafid *et al.*, 2016)

2.3.2 Particle packing density determination

2.3.2.1 Experimental packing methods

Packing density can be directly measured through experiments with solids in
either a dry or wet state. Dry packing method involved the following procedures.
First, the aggregates in different size classes were blended in portion thoroughly.
The dry aggregate mixture was then poured into a container with a known
volume in three equal portions and compacted densely layer-by-layer.
Afterwards, the covered container was vibrated for 30 seconds to densely pack
the grains, followed by weighing the total aggregates to obtain the bulk density
of aggregates (ρ_{bulk}). Finally, the particle packing density (ϕ) of aggregates could
be calculated by Equation (2.1).

$$\phi = \frac{\rho_{bulk}}{\rho_{aggregate}} \qquad (2.1)$$

where ρ_{bulk} and $\rho_{aggregate}$ are the bulk density and absolute density of
aggregates, respectively.

The packing density of solid particles under a wet condition can be determined
as follows. First, the mixture of solid particles was prepared with a
predetermined amount of water with or without superplasticizer. Then, the fresh
sample was filled into a container with a known volume. During the filling

32

process, compaction/vibration was applied on the infilled sample by steel rod and vibrating table. Finally, the bulk density of the sample was measured to evaluate the packing density of solid particles (ϕ). The optimum water content for achieving a maximum packing density was determined for each material mix design corresponding to its water-to-solid ratio. The maximum ϕ was considered as the wet packing density. The void ratio (u) and packing density (ϕ) of each mixture were calculated according to the equations (2.2)-(2.4).

$$V_S = \frac{M}{\rho_w u_w + \sum_{i=1}^{n} \rho_i R_i} \tag{2.2}$$

$$u = \frac{V-V_s}{V_s} \tag{2.3}$$

$$\phi = \frac{V_s}{V} \tag{2.4}$$

where V_S is the absolute volume of solids in the freshly mixed sample; M is bulk weight of fresh sample filling the container; V is the volume of the container; ρ_w and ρ_i are the densities of water and material i; R_i is the volumetric ratio of the material i to the total solid materials, and u_w is the water-to-solid volumetric ratio.

2.3.2.2 Particle packing models

Particle packing optimisation is the process of enhancing the packing density by selecting the proper size ranges and amounts of particles to sequentially fill up the voids among larger particles with smaller particles. The developed methods for particle packing optimisation can be classified into three categories as follows.

(a) Continuous packing model-based optimisation

The packing density could be optimised based on continuous packing models with continuous particle size distributions.

The first continuous packing model (Equation (2.5)) was proposed by Fuller and Thompson (1907), by using which a gradation curve for the greatest particle packing density could be obtained.

$$CPFT = 100(\frac{d}{D})^n \tag{2.5}$$

where *CPFT* represents the cumulative percentage of the particles finer than d, d represents a particle size, D represents the maximum particle size, and n is an index equal to 1/2.

Andreasen and Andersen (1930) followed the previous research done by Fuller and Thompson and proposed an equation to model the densest particle packing status based on the ideal continuous particle size distribution. In their model, they assumed that the smallest particles would be infinitesimally small. The Andreasen and Andersen (A&A) model is shown in Equation (2.6) as follows.

$$P(D) = (\frac{D}{D_{max}})^q \tag{2.6}$$

where q is the size distribution coefficient or exponent in the range of 1/3 to 1/2, $P(D)$ is the fraction that can pass the sieve with an opening size of D, and D_{max} is the maximum particle size.

Funk and Dinger (1994) reported that the smallest particle should have a size limit in real particle grading. As a result, the A&A model was modified into the Equation (2.7) by introducing the minimum particle size (D_{min}).

$$P(D) = \frac{D^q - D_{min}{}^q}{D_{max}{}^q - D_{min}{}^q} \tag{2.7}$$

where the size distribution coefficient, q, may vary from 0.21 to 0.37, which is highly dependent on the workability of the fresh concrete. In general, the lower q means that the fresh concrete behaves more flowable.

It should be noted that these continuous packing models do not take into account the effects of particle shapes; thereby the outputs of these models may not lead to a mixture with the highest packing density.

(b) Discrete packing model-based optimisation

Discrete packing models have been developed to predict the particle packing density based on the assumption that particles can be packed to achieve the maximum packing density in all the predefined size classes. Furnas (1931) firstly proposed the Binary packing model (e.g., Equation (2.8)) and considered that the maximum packing density of spherical binary particle blends can be fulfilled by

introducing the fine particles into interstices of coarse packed particles without disturbing their packing status. Later and Powers (1968) considered the loosening effect in their packing model to achieve the minimum void ratio of the binary particle mixture. Aïm and Goff (1968) suggested a geometrical model considering the wall effect with a correction factor to interpret the packing density variation in binary mixtures of spherical grains.

$$PE_{max} = PE_c + (1 - PE_c)PE_f \tag{2.8}$$

where PE_{max} is the theoretical maximum packing density of a mixture of coarse and fine particles, PE_c and PE_f are the packing density of the coarse and fine particle fractions, respectively.

Toufar *et al.* (1976) extended the binary packing model to be capable of calculating the packing density of ternary grain classes. They assumed that smaller particles with diameter d_1 will be sufficiently situated within the interstices of larger particles with diameter d_2 when $d_1/d_2 < 0.22$, hence the packing density could be obtained from the sum of packing densities of large and small particles. For a ternary mixture, each of two grain classes could form a binary mixture combined with another grain class. Then the packing density for the ternary mixture could be calculated by summing the contributions of all the binary mixtures. The proposed model is described by Equations (2.9)-(2.12) as follows.

$$\phi_t = \frac{1}{\frac{y_1}{\phi_1} + \frac{y_2}{\phi_2} - y_2\left(\frac{1}{\phi_2} - 1\right)k_d k_s} \tag{2.9}$$

$$k_d = \frac{d_2 - d_1}{d_2 + d_1} \tag{2.10}$$

$$k_s = 1 - \frac{1 + 4x}{(1+x)^4} \tag{2.11}$$

$$x = \frac{y_1}{y_2} \frac{\phi_2}{\phi_1(1-\phi_2)} \tag{2.12}$$

where ϕ_t is the predicted total packing density, ϕ_1 and ϕ_2 are the packing density of fine and coarse aggregates, y_1 and y_2 are the particle volume fraction of fine and coarse aggregates, k_d and k_s are characteristic diameter factor and

statistical factor, respectively.

Stovall *et al.* (1986) proposed a linear packing density model to predict the packing density of multi-sized grains by taking into account their geometrical interactions of wall effect and loosening effect. The loosening effect happens when smaller particles are too large to be inserted into the interstices of dominant large grains; the wall effect happens when some isolated larger grains are immersed into the agglomerated finer grains. The loosening effect and wall effect of particle interactions are schematically illustrated in Fig. 2.15. The linear packing density model is described by Equation (2.13) as follows.

$$\phi_t = \min\left(\frac{\phi_i}{1-(1-\phi_i)\sum_{j=1}^{i-1} g(j,i)\eta_j - \sum_{j=i+1}^{n} f(i,j)\eta_j}\right) \tag{2.13}$$

where ϕ_t is the predicted packing density, $f(i,j)$ is the formula considering the loosening effect of size class j on the dominant size class i, $g(j,i)$ is the formula considering the wall effect of size class j on the dominant size class i, and η_j is the volume fraction of size class j.

De Larrard (1999) developed the Compressible Packing Model (CPM) on the basis of linear packing model, which allows to predict the packing density of polydisperse granular sets. He considered the packing density of granular particles as a function of interactions between the grain classes and the applied compaction method via adopting three parameters, *i.e.,* wall effect coefficient, loosening effect coefficient and compaction index. The CPM considered the calculation of virtual packing density for each grain class (γ_i) using Equation (2.14), and the virtual packing density is the maximum packing density of an orderly packed grains. The loosening effect coefficient (a_{ij}) and wall effect coefficient (b_{ij}) were obtained through Equations (2.15) and (2.16), respectively. Based on the mix proportion, the actual packing density of a granular mixture (ϕ) could be obtained by performing a back-analysis according to Equation (2.17), where the compaction energy applied to the solid mixture was considered via the compaction index (K).

$$\gamma_i = \frac{\beta_i}{1-\sum_{j=1}^{i-1} y_j\left(1-\beta_i+\beta_i b_{ij}\left(1-\frac{1}{\beta_j}\right)\right)-\sum_{j=i+1}^{n} y_j\left(1-a_{ij}\frac{\beta_i}{\beta_j}\right)} \tag{2.14}$$

$$a_{ij}=\sqrt{1-\left(1-\frac{d_j}{d_i}\right)^{1.02}} \tag{2.15}$$

$$b_{ij}=1-\left(1-\frac{d_i}{d_j}\right)^{1.5} \tag{2.16}$$

$$K = \sum_{i=1}^{n} K_i = \sum_{i=1}^{n} \frac{\frac{y_i}{\beta_i}}{\frac{1}{\phi}-\frac{1}{\gamma_i}} \tag{2.17}$$

Where d_i is the particle size of grain class i, β_i is the experimentally obtained packing density of grain class i, and y_i is the mutual volume fraction of grain class i.

(a)

(b)
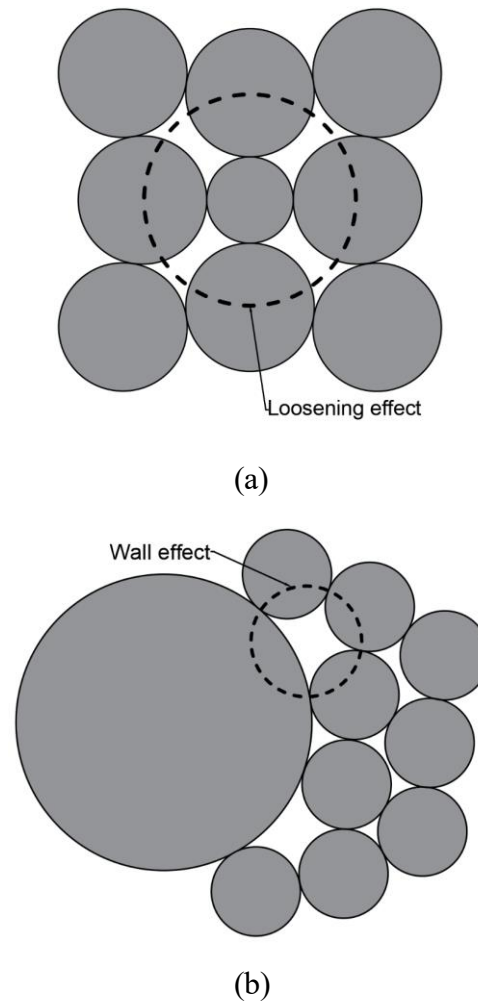
Fig. 2.15 Schematic illustration of particle interactions (a) loosening effect, and (b) wall effect

(c) Discrete element modelling-based optimisation

Discrete Element Modelling (DEM), as a numerical simulating method, can also be used to identify the particle packing status. Yu and Shen (2011) investigated the effect of particle size distribution on the packing density of aggregates. They found that the aggregate contact degree and interlocking were associated with the aggregate size. Moreover, the mean contact force was deemed as an indication of the stability of aggregate skeleton. Majidi *et al.* (2014) investigated the effects of particle shape and inter-particle friction coefficient on the particle packing characteristics. In this study, the shapes of particles were captured by 3D image processing followed by simulating them in DEM. They found that the particle packing density decreased as the friction coefficient increased, and this effect tended to be more pronounced for the particles with lower sphericity. Reisi *et al.* (2018) used the DEM to predict the packing density of graded aggregates in concrete as shown in Fig. 2.16 In their study, each graded aggregates with specific shapes, particle size distribution and packing density were modelled by equivalent mono-sized spherical aggregates with a certain friction coefficient. The friction coefficient of each graded aggregates was calibrated by packing density tests. They found that the differences in terms of packing densities between experimental results and DEM results are less than 1%.
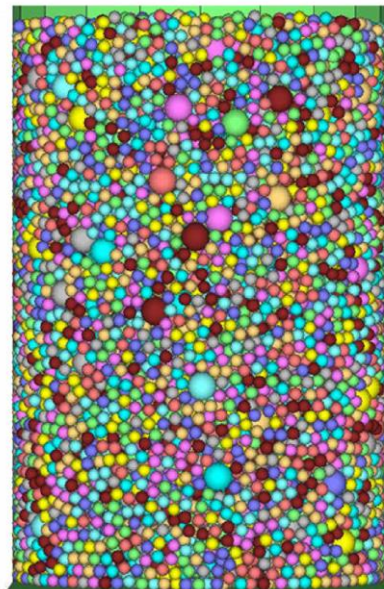
Fig. 2.16 Discrete element modelling for packing of concrete aggregates (Reisi *et al.*, 2018)

2.3.3 Effects of particle packing on properties of fresh concrete

Particle packing density significantly influences the workability of fresh concrete. Powers (1968) proposed that a concrete mixture can be considered as a mixture consisting of cement paste and aggregates. He suggested that the increase of the aggregate packing density can improve the workability of fresh concrete since the excessive paste (the paste being in excess of that needed to fill with the voids) would lubricate the aggregate surface. Nanthagopalan and Santhanam (2012) found that the slump flow of self-compacting concrete could be improved from 420 mm to 615 mm as the aggregate packing density increased by 6.25%. They also noticed that the concretes with similar aggregate packing densities would exhibit different flowabilities due to change of the aggregate gradations. For instance, the slump flow varied from 445 mm to 720 mm for concretes with a constant packing density of 0.68. This pronounced variation in slump flow was mainly related to the decrease in the surface area of the aggregates due to the decreasing content of the fine aggregates in the total aggregates. Hanzic and Ho (2017) investigated the workability of fresh concrete with multi-sized fillers. In their study, limestone powder with a similar particle size to the cement and foundry sand coarser than the cement particles were used to partially replace the cement and aggregates, respectively. They found that the ratio of the slump flow to the superplasticizer dosage (SF/D_{sp}) decreases by up to 6.1% with the increase of the particle packing density by 2.2%. It indicated that more superplasticizer was required for a concrete with fillers to achieve a similar slump flow to that without fillers, as the addition of fillers increased the yield stress of the fresh mixture due to the increased total surface area. Therefore, it implied that both effects of particle packing density and particle size distribution should be taken into account for a proper design of high-performance concrete with relatively low cement paste volume and desired workability.

It should be noted that the empirical slump flow test is not capable of fully quantifying the workability of all types of concrete, *e.g.,* high-performance concretes. These high-performance concretes with a similar slump flow may behave differently during the placement process. It indicates that the concrete workability cannot be only defined by a single parameter of slump or slump flow

value. The more accurate method for quantifying the workability of concrete is with the adoption of two-parameter workability tests (rheological tests) to study the rheological properties of fresh concrete regarding to its yield stress and plastic viscosity. The yield stress is the minimum stress for fresh concrete initiating to flow, and the plastic viscosity is the proportional coefficient of shear stress to shear rate under a state of steady shear motion. The yield stress (τ_c) and plastic viscosity (η_c) of fresh concrete can be estimated by the Farris model (Farris, 1968) and Chateau–Ovarlez–Trung model (Chateau *et al.*, 2008) as follows, respectively.

$$\frac{\tau_c(\phi)}{\tau_c(0)} = \sqrt{\frac{1-\phi}{(1-\frac{\phi}{\phi_m})^{2.5\phi_m}}} \tag{2.18}$$

where $\tau_c(\phi)$ and $\tau_c(0)$ are the yield stress of concrete and cement paste, respectively; and ϕ and ϕ_m are the solid volume fraction and maximum packing density, respectively.

Considering the fresh concrete as a suspension with fine and coarse aggregates in the fresh cement paste, the Farris model (Noor & Uomoto, 2004) can be expressed as:

$$\eta_c = \eta_p (1 - \frac{S}{S_{lim}})^{-[\eta^{FA}]S_{lim}} (1 - \frac{G}{G_{lim}})^{-[\eta^{CA}]G_{lim}} \tag{2.19}$$

where S and S_{lim} are the sand volume fraction and maximum sand packing density, respectively; G and G_{lim} are the gravel volume fraction and maximum gravel packing density; $[\eta^{FA}]$ and $[\eta^{CA}]$ are the intrinsic viscosities of fine and coarse aggregates, respectively; and η_p and η_c are the plastic viscosities of fresh paste and concrete, respectively.

Based on the aforementioned relations from Equations. (2.18) and (2.19), it is concluded that the rheological properties of fresh concretes are strongly influenced by the solid volume fraction ϕ and the maximum packing density ϕ_m. And the maximum packing density of granular mixture is highly related to the PSD and morphology of particles as mentioned in the subsection 2.3.1.

Many studies have attempted to correlate the rheological properties with the

slump or slump flow of fresh concrete. For example, Wallevik (2006) suggested that the relationship between the yield stress and slump of fresh concrete mainly depends on the volume fraction of cement paste, *i.e.,* the slump and yield stress varied with the cement paste volumes in concrete mixture proportions. He also proposed an empirical equation to predict the slump of fresh concrete with a given yield stress by considering the volume and the lubrication degree of the cement paste, as shown in Equation (2.20). The results showed that the predicted slumps by this equation were in good agreements with the measured slumps with a correlation coefficient (R^2) of 0.86 as seen in Fig. 2.17. However, there was a low correlation between the plastic viscosity and slump.

$$s = 300\text{-}0.416\frac{(\tau_0+394)}{\rho_{sg}} + \alpha(\tau_0 - \tau_0{}^{ref})(V_m - V_m{}^{ref}) \tag{2.20}$$

where s is the slump or slump flow, τ_0 is the yield stress, ρ_{sg} is the specific density of concrete, V_m is the cement paste volume, and the term of $\alpha(\tau_0 - \tau_0{}^{ref})(V_m - V_m{}^{ref})$ is related to the lubrication effect and volume fraction of the cement paste in the designed concrete mix.
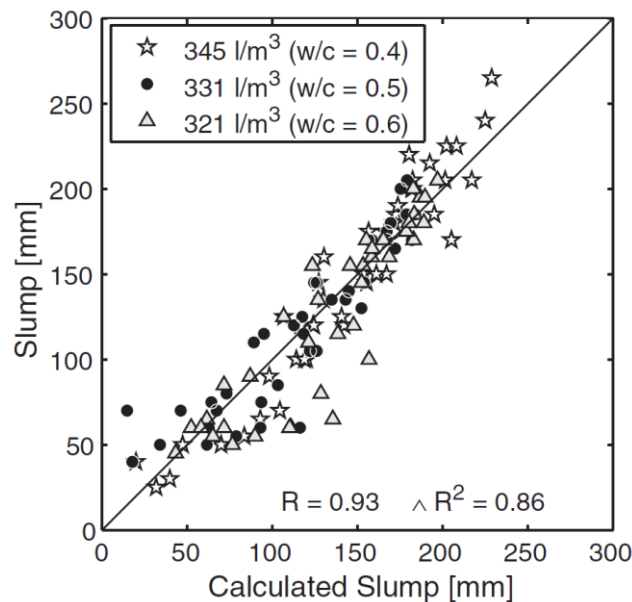
Fig. 2.17 Comparison of the measured slump against calculated slump by Equation (2.20) (Wallevik, 2006)

41

2.3.4 Effects of particle packing on properties of hardened concrete

Influences of packing density on the mechanical properties of various concretes have been widely investigated in previous studies as summarised in Table. 2.5. For a concrete with a fixed water-to-binder ratio and proper workability, the compressive strength and Young's modulus generally increase with the packing density. Moini *et al.* (2015) investigated the effect of aggregate packing on the concrete strength. They found that the use of 10% intermediate-sized aggregates could increase the packing density and result in an increment in the strength by up to 37%. Soliman *et al.* (2017) investigated the properties of Ultra-High-Performance Concrete (UHPC) that incorporated glass sands partially or completely as the replacements of quartz sands. The compressive packing model (CPM) was employed to predict the particle packing density of each mixture, and three ideal grading curves approaching to the maximum packing density were selected for the mix design of the UHPC. They found that the compressive strength of UHPC that incorporated glass sands increased with the particle packing density. The UHPC with the highest packing density could achieve the maximum compressive strength, which was 23.6% higher than that of the mixture with lowest packing density. Li *et al.* (2017) investigated the effect of packing density on the compressive strength and elastic modulus of RAC. In this study, the wet packing method was extended to measure the particle packing density. They found that the compressive strength and elastic modulus of RAC increased with the packing density. Wang *et al.* (2019) applied a D-optimal statistical model to maximise the particle packing density of UHPC. They found that increasing the packing density by 4.8% could increase the compressive strength of UHPC by 11.3%. The pore structure of UHPC mixture was also further investigated by using X-ray Computed Tomography (CT), and they found that the UHPC with a high packing density presented a denser structure with fewer air voids. Klein *et al.* (2020) investigated the effect of aggregate packing density on the elastic modulus of concrete with a design strength of 25 MPa or 40 MPa. In this study, the gradation of aggregates was optimised for the maximum packing density. They found that increasing of the packing density by 7.6% and 9.9% could increase the 28-day elastic modulus by 7.9% and 8.8% for 25 MPa and 40 MPa concretes, respectively.

Table 2.5 Summary of previous studies on investigating the effects of packing density on mechanical properties of various concretes

Reference	Concrete type	Packing density Determination	Water-to-binder ratio	Packing density increase rate (%)	Properties	Enhancement rate (%)
Nanthagopalan & Santhanam (2012)	Self-compacting concrete	Experimental packing method	0.37	6.3	Compressive strength	12.6
Moini *et al.* (2015)	Traditional concrete with low cement content	Experimental packing method	0.60	3.5	Compressive strength	37.3
Soliman & Tagnit-Hamou (2017)	UHPC with glass sand	CPM	0.19	4.0	Compressive strength	23.6
Soliman & Tagnit-Hamou (2017b)	UHPC (normal curing)	CPM	0.20	8.0	Compressive strength	26.5
	UHPC (heat curing)	CPM	0.20	8.0	Compressive strength	34.8

Table 2.5 Summary of previous studies on investigating the effects of packing density on mechanical properties of various concretes (continued)

Reference	Concrete type	Packing density determination	Water-to-binder ratio	Packing density increase rate (%)	Properties	Enhancement rate (%)
Wang *et al.* (2019)	UHPC	Experimental packing method & statistical model	0.16	4.8	Compressive strength	11.3
Li *et al.* (2017)	Recycled aggregate concrete	Experimental packing method	0.20	2.44	Compressive strength	9.2
					Young's modulus	12.3
			0.30		Compressive strength	11.0
					Young's modulus	6.2
			0.40		Compressive strength	4.5
					Young's modulus	10.6
			0.50		Compressive strength	14.9
					Young's modulus	22.7
Klein *et al.* (2020)	Traditional concrete	Experimental packing method and CPM	0.41	9.9	Young's modulus	8.8

2.3.5 Effects of cement paste volume on the properties of packing-optimised concrete

Cement Paste Volume (CPV) is a volumetric parameter used to quantify the cement content in a given bulk volume of concrete with a constant water-to-cement (W/C) ratio. The statements in terms of the influence of CPV on the concrete properties have not yet reached a consensus. For example, Kolias and Georgiou (2005) investigated the effect of CPV on the concrete strength. They found that the concrete strength decreased as the designed CPV increased and this negative influence is more pronounced for concrete with a lower W/C ratio. They explained that the concrete with higher paste volume would provide a short route for the cracks to circle around the aggregate particles with less energy consumption for cracking failure. Similarly, Piasta and Zarzycki (2017) found that the compressive strength of the concrete with a proper workability was negatively correlated with the CPV. They explained that the reduced strength was attributed to the increase in actual W/C ratio with the decreased aggregate surface area. Chu (2019) also investigated the workability and mechanical properties of concrete mixes with various CPV at different W/C ratios. He found that increasing the CPV by 6% can increase the slump of concrete by 150 mm, but decrease the compressive strength by up to 7.2%. This might be caused by that the excessive cement paste thickened the mortar film around the aggregates. Nevertheless, some studies mentioned that there exists an optimum CPV for concrete to achieve the maximum compressive strength. For example, Yurdakul *et al.* (2013) attempted to investigate the minimum CPV for designing the concrete with required workability and strength. They discovered that about 1.5 times more CPV than the void volume among the aggregates was required to obtain a minimum workability. And they also pointed out that an optimum CPV for maximising the compressive strength is about twice the void volume among aggregates and a further increase of CPV would not significantly improve the compressive strength. Similarly, Wang *et al.* (2015) studied the properties of self-consolidating concrete with various paste-to-voids volume ratios (CPV/V_V). In their study, the concrete mixtures were made with different aggregate types and sizes. They found that the slump flow increased with CPV/V_V at a given viscosity. Moreover, the concrete strength increased with the CPV/V_V up to a point, and

then the strength tends to be independent of the CPV/V$_V$ or even slightly decreased as the CPV/V$_V$ further increased. They explained this downtrend in strength was mainly attributed to the impaired crack tortuosity with the increasing CPV.

2.4 Environmental assessment of recycled aggregate concrete

2.4.1 Definitions and frameworks of life cycle assessment

Life cycle assessment (LCA) is one of the environmental assessment techniques to evaluate the environmental performance and associated impacts on the product or service by quantifying the environmental inputs of material and energy and the outputs of waste throughout the whole lifecycle (Hossain *et al.*, 2016). The main purpose to conduct LCA is to emphasise the importance of resource efficiency and to increase the sustainability claims and credibility of the products (Blengini *et al.*, 2012). According to ISO 14040: 2006 (ISO, 2006a) and ISO 14044: 2006 (ISO, 2006b), LCA includes four steps as shown in Fig. 2.18: goal and scope definition, Life Cycle Inventory (LCI) analysis, Life Cycle Impact Assessment (LCIA) calculation, and results interpretation.
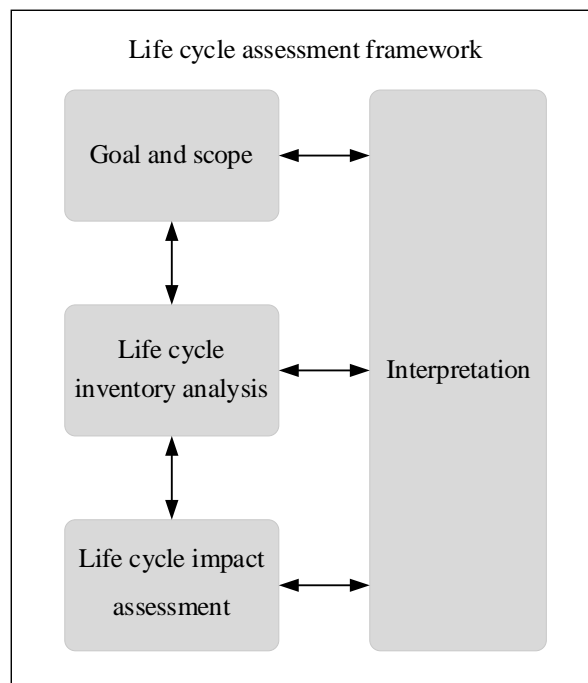
Fig. 2.18 Life cycle assessment framework

2.4.1.1 Goal and scope

The 'goal and scope' defines the overall objectives, system boundary, LCI data sources, and the functional unit of the analysis (Blengini, 2009). Defining the functional unit is an essential step of LCA, which provides a reference to the selection of inputs and outputs, and to allow for LCA results comparisons between different products under the equivalent function unit (Xing *et al.*, 2022). Take RAC as an example, the choice of function unit should properly reflect all the necessary function aspects including strength and durability/service life (Van Den Heede & De Belie, 2012). The system boundary defines the unit processes to be included in the system, which is normally described by the flow diagram as shown in Fig. 2.20. LCA could be performed at different boundary levels, *i.e.*, cradle-to-gate, cradle-to-grave, and cradle-to-cradle. Most existing LCA studies on environmental impacts of RAC selected the system boundary of the model from cradle to gate by considering the impacts of raw material extraction, transportation and concrete production until the delivery of final product. The impacts of construction, use, maintenance, and end-of-life phases were assumed to be identical and can be omitted (Xing *et al.*, 2022).

2.4.1.2 Life cycle inventory (LCI)

The main objective of LCI analysis is to quantify the environmental inputs and outputs of the system by means of balancing the mass and energy (La Rosa *et al.*, 2013). The process of LCI data collection is to quantify the elementary flows based on the defined system boundary through considering the function unit, and the specified LCI data can be applied into the subsequent LCIA stage. LCI consists of all environmental inputs of the materials, energy and fuels, and the outputs of emissions to the air, water and land within the system boundary (Kurda *et al.*, 2018). Therefore, establishing a LCI based on data with higher specificity is important for a reliable LCA. Nevertheless, the use of existing LCA databases (e.g., Ecoinvent database) is more practical due to the time-saving (Xing *et al.*, 2022).

2.4.1.3 Life cycle impact assessment (LCIA)

LCIA phase tends to evaluate the level and significance of all the environmental impacts obtained from LCI phase. There are three mandatory steps as shown in Fig. 2.19, *i.e.,* selection of the impact categories, classification of the assigning LCI results to the corresponding impact categories, and characterisation by aggregating the LCI results into an indicator. The optional normalisation, weighting and grouping can be further applied for the LCIA results analysis (Marinković *et al.*, 2010). The LCIA methodology should be in line with the defined goal and scope. It can be generally divided into two approaches, *i.e.*, problem-oriented (midpoint-oriented) approach and damage-oriented (endpoint-oriented) approach (Ortiz *et al.*, 2009). The problem-oriented approach considers the environmental impacts related to the real phenomena, such as climate change, acidification, and so on. The damage-oriented approach evaluates the environmental impacts of a product by identifying its potential damages those may cause to human health, ecosystem, and resources.

Mandatory elements

Selection of impact categories, category indicators and characterisation models (selection)

Assignment of LCI results (classification)

Calculation of category indicator results (characterisation)

Impact category indicator results (LCIA profile)

Optional elements

Calculating the magnitude of category indicator results relative to reference data (normalisation)

Sorting and ranking of the impact categories (grouping)

Conversion of category indicator results by using the value-based factors (weighting)

Fig. 2.19 Life cycle impact assessment elements

2.4.2 Life cycle assessment of recycled aggregate concrete

Many studies have performed the LCA for assessing and comparing the environmental impacts of the production of NAC and RAC. Based on the functional unit and system boundary considered in these studies as depicted in Fig. 2.20, it can be found that the production of raw materials (e.g., cement, natural, recycled aggregates, etc.) and their amounts used in the mix design have significant influences on the environmental performance of concrete.
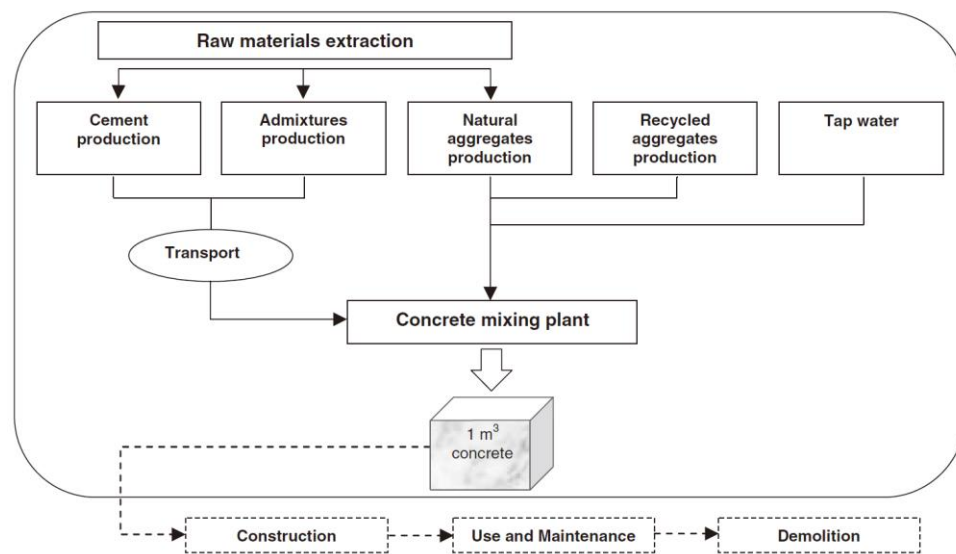
Fig. 2.20 Cradle-to-gate system boundary of the concrete production (Jiménez *et al.*, 2015)

The statements on the environmental friendliness of using RCAs in concrete have not yet to reach a consensus, however, the extensive LCA studies have reported that replacing natural aggregates by recycled aggregates is beneficial for the sustainable development of concrete. Simion *et al.* (2013) compared the environmental impacts of productions made with natural and recycled aggregates. Life cycle assessment methods of Eco-Indicator 99, EDIP/UMIP and Cumulative Energy Demand were used. They found that the environmental impacts of global warming potential and energy consumption of recycled aggregates from C&D wastes were all around 85% lower than those of natural aggregate extraction. Hossain *et al.* (2016) assessed the environmental impacts of aggregate production from C&D wastes and natural sources by using LCA. In their study, the LCIA approach of IMPACT 2002+ was adopted for assessing both problem-oriented and damage-oriented indicators, and the China Light and

Power (CLP) and the Chinese Life Cycle Database (CLCD) were used as the LCI data sources. They found that the environmental impacts of the recycled aggregates made production were lower than the natural stone made production. More specifically, the production of RCAs could reduce the greenhouse gases emission by 65%, the land occupation by 20%, and the non-renewable energy consumption by 58%. Estanqueiro *et al.* (2016) reported the LCA results of aggregates productions obtained under three procurement scenarios (*i.e.,* NCA extraction, recycling aggregates from waste concrete using a fixed plant and that using a mobile plant) by means of Ecoindicator 99, CML Baseline and cumulative energy demand method. They found that the environmental impact of land use for RCA production was lower than that for NCA production due to the decreased quarry exploitation. Kleijer *et al.* (2017) used the LCA to assess the global warming potential and cumulative energy demand of the natural and recycled aggregate concrete with designed strength class. They found that the environmental impacts of RAC prepared with 28% RCAs were slightly lower than those of NAC. They also explained that these differences were mainly due to the relatively lower impacts of the RCA production process, considering that the same cement type and amount was adopted for both concretes. Braga *et al.* (2017) also found that the environmental impacts in terms of global warming potential, ozone depletion, acidification, eutrophication potential, photochemical ozone creation potential, and primary energy consumption of concrete generally decreased as the RCA content increases for each designed strength class. More specifically, replacing 100% NCAs with RCAs could decrease the impact of global warming potential by 19%, 11% and 9% for the concretes with design strength classes of C20/25, C25/30 and C30/35, respectively. Differently, Weil *et al.* (2006) assessed the environmental impacts of the concretes produced with natural and recycled aggregates. The transportation distances of the natural and recycled aggregates were assumed to be identical. They found that the higher energy consumption was needed for crushing and intensive cleaning during the producing of the high-quality recycled aggregates than the natural aggregate extraction. As a result, the cumulated energy demand and global warming potential of RAC with 50% volume fraction of RCAs are slightly higher than those of the concrete prepared with gravels, when the cement content kept the same.

Traditional mix designs of RAC normally replace a certain percentage of NCAs with RCAs based on the equivalent volume or mass replacement rule. More cement content is generally required to compensate for the negative impacts induced by the RCA incorporation, thereby increasing the environmental impacts. Several previous studies investigated the effect of cement content through LCA. For instance, Marinkovic′ et al. (2010) stated that an additional 5% cement was required for RAC to achieve the similar compressive strength as NAC. Based on the data collected from local manufacturers and reliable sources regarding the specific geographical location, they summarised that the increased cement content for RAC design could lead to higher environmental impacts than those of NAC. More specifically, it caused the increments in environmental impacts of RAC in terms of the energy use by 4.6%, the global warming by 4.7%, the eutrophication by 4.5%, the acidification by 4.4%, and the photochemical oxidant creation by 4.7%. Knoeri et al. (2013) also demonstrated that the additional cement content in RAC significantly influences its environmental performance. They found that replacing 45% NCAs with RCAs decreased the global warming potential of RAC by 14%, but this impact of RAC would be comparable to that of NAC when an additional 14% cement was considered in the mix design.

Moreover, some novel mix design methods, such as methods developed based on equivalent mortar volume, were adopted for the design of high-performance RAC. It has been found that these novel design methods also significantly influence the environmental impacts of RAC. Jiménez et al. (2015) investigated the environmental impacts of NAC and RAC designed by various mix design methods (i.e., American Concrete Institute (ACI) method, Bolomey method, and Equivalent Mortar Volume (EMV) method, etc.). In their study, the Bolomey method was the conventional method for designing the NAC, and the ACI method was used to develop the RAC design based on the equivalent aggregate volume rule. As for the EMV method, it was applied to optimise the mix proportioning of RAC by taking into account the surface-attached old mortar of RCAs as a part of the total mortar content in concrete, so that the EMV designed RAC would have an equivalent mortar volume as the NAC. LCA results comparisons were conducted within designed concretes possessing the similar

properties, in terms of workability, strength, and durability. The results show that the concretes designed by the EMV method exhibit better environmental performances in terms of abiotic depletion, global warming potential, ozone layer depletion, terrestrial ecotoxicity, acidification, and eutrophication than that designed based on the other two methods. Notably, the use of EMV method could decrease the environmental impact of global warming potential by 21%.

2.5 Summary

Based on the literature review, the following points can be highlighted.

- The properties of fresh and hardened RAC generally decrease as the RCA content increases. Extensive studies explained that these inferior properties of RAC are mainly attributed to the higher porosity of RCAs, the weakened ITZs between RCAs and cement paste, as well as the existence of microcracks in the old mortar of RCAs. Hence, many methods have been proposed to improve the RAC performance, and most of them mainly focus on mitigating the porosity of RCAs. However, these treatments inevitably increase the labour costs and environmental burdens to hinder their large-scale application. Less attention has been paid on optimising the packing density of the total aggregates, which would reduce the voids among aggregates and improve performance of RAC. It would be of great significance to develop a novel design method to improve the performance of RAC from the perspective of particle packing optimisation, especially for RAC with high RCA contents.

- Maximising the particle packing density could enhance the mechanical properties of various concretes. Nonetheless, adding excessive fine particles tends to decrease the workability of fresh RAC and negatively influences the properties and microstructures of RAC. The negative effect would be more evident for high-performance RAC. To better understand the property-enhancing mechanisms, a detailed study would be expected to investigate the biphasic effect of packing density optimisation on the properties and microstructures of RAC.

- CPV can be regarded as an important parameter that significantly influence the concrete performance. Few studies focused on investigating the

influence of CPV on the properties and microstructure of RAC, particularly on the pore structure and interfacial transition zone. For the mix design of RAC based on particle packing optimisation method, the effect of CPV on the performance needs to be investigated and the influencing mechanism is required to be studied from the microscopic perspectives.

- The use of RCP would negatively influence the properties of mortar or concrete. Current studies explained these inferior properties are mainly related to the lower reactivity and higher porosity of RCP. However, a proper use of RCP as sand replacement might improve the properties and microstructure of mortar due to the enhanced particle packing density and promoted hydration reaction. Few investigations have been conducted to understand the biphasic role of the RCP.

- The use of LCA is considered to be effective in assessing the environmental impact of RAC. For RAC design based on a novel design method, such as the particle packing optimisation method proposed in the present study, LCA is required to evaluate its environmental performance. Comparisons with the LCA of RAC designed by the conventional mix design methods are also required. The findings would be valuable in guiding the optimisation of the mix design of RAC regarding environmental protection.

CHAPTER 3

EFFECTS OF AGGREGATE PACKING ENHANCEMENT ON THE PROPERTIES OF NATURAL AND RECYCLED AGGREGATE CONCRETE

3.1 Introduction

The packing optimisation of aggregates has been recognised as an effective strategy to enhance the properties of concrete, as this can reduce the void volume among the aggregates to densify the structure of concrete. However, the effect of particle packing enhancement on the properties and microstructure of recycled aggregate concrete (RAC) has been not well understood. Therefore, this chapter presents an experimental study on investigating the influence of aggregate packing enhancement on the properties of both natural aggregate concrete (NAC) and RAC. Four groups of concretes containing natural concrete aggregates (NCAs) or recycled concrete aggregates (RCAs) were prepared with different design methods. A comparison on the properties of NAC and RAC designed by different methods is conducted. Moreover, the microstructures of RACs are characterised by the X-ray computed tomography (CT) analysis with a focus on their macropore structures, which helps to understand the role of aggregate packing optimisation in enhancing the properties of RAC.

3.2 Experimental programme

3.2.1 Raw materials

The type 42.5N ordinary Portland cement was employed in this study and the density of cement is 3100 kg/m^3. Local crushed limestone aggregates with a particle size ranging from 5 to 20 mm were adopted as the NCAs. RCAs with the same size range were collected from a C&D wastes recycling plant in Ningbo, China. All the NCAs and RCAs were washed and stored in air-tight containers after oven drying. For fine aggregates (FAs), natural river sand with a medium grade and a fineness modulus of 2.62 was selected. The gradation curve of FA is shown in Fig. 3.1. The other properties such as the particle density on oven-dried

(OD) basis, particle density on saturated surface dry (SSD) basis, apparent particle density and water absorption of NCAs, RCAs and FAs were measured according to BS 812-2:1995 (BSI, 1999) and are tabulated in Table 3-1.
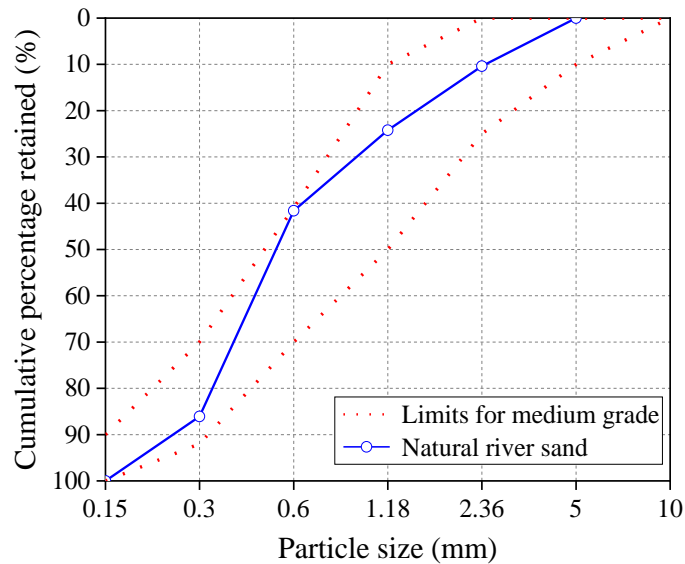
Fig. 3.1 Particle size distribution of FA

Table 3.1 Physical properties of NCAs, RCAs and FAs

Type	Size range (mm)	Size group name	Particle density on OD basis (kg/m^3)	Particle density on SSD basis (kg/m^3)	Apparent particle density (kg/m^3)	Water absorption (%)
	5-10	R$_3$	2530	2558	2601	1.08
NCAs	10-16	R$_2$	2595	2609	2631	0.52
	16-20	R$_1$	2610	2620	2635	0.36
	5-10	R$_3$	2167	2300	2499	6.13
RCAs	10-16	R$_2$	2230	2321	2454	4.11
	16-20	R$_1$	2258	2337	2452	3.50
FA	0.15-5	R$_4$	2550	2557	2567	0.26

3.2.2 Aggregate packing enhancement

Two methods were used in the present study for the selection of aggregates. One is the particle packing method (PPM), which can enhance the packing density of aggregates to the greatest extent possible under a certain compaction energy. By using PPM, the particles (including both coarse and fine aggregates) were

divided into several groups according to the particle size, termed as R_n (n=1,2,3,4...). In this study, the particles have been divided into four groups as shown in Table 1. R_1 and R_2 were first mixed in proportion until a maximum packing density was obtained. A further addition of smaller particles R_3 can fill the voids and make the compacted mixture denser. A maximum packing density therefore can be obtained when an optimum proportion of R_3 was added. Similarly, the optimum proportion of R_4 of aggregates can be subsequently determined. In the PPM design based on BS 812-2:1995 (BSI, 1999), aggregates in different particle sizes were blended in proportion based on the design scheme. The mixture was poured into a 10L steel container in three equal portions and compacted densely layer-by-layer by a steel rod. Packing density of the aggregate, therefore, could be calculated when the bulk weight and bulk volume of the packed aggregates were obtained. The other aggregate design method is the traditional method (TM), where the particle packing was not optimized. The mass fractions of fine aggregate and coarse aggregate were determined according to JGJ55-2011 (Standards China, 2011).

3.2.3 Concrete mix proportion

The absolute volume method was employed in the concrete mix design in this study. The cement paste volume (CPV) is defined as the absolute volume of cement paste in 1 m^3 bulk volume of concrete. The NAC with a slump of 75 mm was first prepared based on the traditional method, and the CPV of the mixture was found to be 39%. This medium level slump was designed to facilitate the preparation of concrete samples. Another NAC mixture was designed with packing-optimised aggregates as determined in section 3.2.2. Afterwards, the traditional RAC was designed through fully replacing the NCAs with RCAs in volume. Another RAC mixture was also designed with packing-optimised aggregates as determined in section 3.2.2. All the RACs were prepared with a constant CPV (i.e. 39%) as same as the NAC mixtures. The mix formulations in 1 m^3 bulk volume of concrete are tabulated in Table 3.2. The W/C ratio is fixed at 0.42 for all the mixtures. The type of the concrete (*i.e.* NAC or RAC), and the aggregate design method (*i.e.* TM or PPM) are included in the mixture name.

Table 3.2 Mix proportions of NAC and RAC designed by TM and PPM

Mixture ID	Design method	CPV (%)	Water (kg/m³)	Cement (kg/m³)	Aggregate proportions (kg/m³)			
					R_1	R_2	R_3	R_4
NAC-TM	TM	39	230	548	539		539	545
RAC-TM	TM	39	230	548	463		463	545
NAC-PPM	PPM	39	230	548	476	118	385	646
RAC-PPM	PPM	39	230	548	300	198	206	808

3.2.4 Concrete sample preparation and curing

The RCAs were first pre-wetted by a certain amount of water which is the sum of products of the fraction in mass and the water absorption for each particle group. The pre-wetted RCAs were then mixed in a 120L pan mixer for 3 mins. Afterwards, the cement and sand were added into the mixer for another 1 min mixing. The mixing water was added and mixed for another 3 minutes. Cubes with a length of 100 mm and cylinders with a height of 200 mm and a diameter of 100 mm were prepared for the compressive strength and Young's modulus tests, respectively. Three $100\times100\times400$ mm prisms were prepared for four-point bending test. All the samples were demoulded 24 hours after casting and then placed into a water tank for curing. The samples for compressive tests were cured by 3, 7 or 28 days, while the samples for flexural tests and Young's modulus tests were cured for 28 days. The preparation process of NAC is similar to that of RAC, but the pre-wetting process was omitted.

3.2.5 Workability and mechanical properties tests

The workability of fresh concrete was evaluated by the slump of concrete. The slump test was conducted in accordance with BS EN 12350-2:2009 (BSI, 2009a). The compressive strength of concrete was tested in accordance with BS EN 12390-3:2009 (BSI, 2009b) considering a curing age of 3 days, 7 days and 28 days. Young's modulus and flexural strength of concrete were determined according to BS EN 12390-13:2013 (BSI, 2019) and BS EN 12390-5:2009 (BSI, 2009c), respectively. Three samples were used in each test, and an averaged strength or Young's modulus was calculated.

3.2.6 Theoretical cement paste film thickness

The amount of excess CPV remaining after filling the voids among the aggregates could be determined by the volume of cement paste and packing density of total aggregates. The excess paste forms the paste film coating the aggregate particles and its average thickness is dependent on the solid surface area of aggregates. Thus, the application of PPM would change the cement paste film thickness (CPFT) of concrete. In other words, the average spacing between adjacent aggregates is varied by changing the packing density of aggregates. The CPFT can be calculated as follows.

The void volume (V_V) of aggregates in 1 m³ bulk volume of concrete could be calculated according to Equation (3.1).

$$V_V = \frac{1-\phi}{\phi}(1-CPV) \tag{3.1}$$

where ϕ indicates the packing density of total aggregates. The aggregate can be idealized as octahedron, and the specific surface area (SSA) can be calculated by Equation (3.2) (Ghasemi *et al.*, 2018).

$$SSA_{R_i} = \frac{7.348}{d_{R_i}} \tag{3.2}$$

where d_{Ri} is the arithmetic mean diameter of the particles within the lower size bound d_{lower} and the upper size bound d_{upper} for a particle size group R_i (i = 1,2,3,4 ...,n). For an aggregate distribution with several particle size groups, the total surface area (SA) of the aggregates can be calculated by Equation (3.3).

$$SA = sum(SSA_{R_i} \times V_{R_i}) \times (1-CPV) \quad i = 1, 2, 3..., n \tag{3.3}$$

where V_{Ri} is the volume fraction of the ith particle size group. For the particle size groups given in Table 3-1, the d_{Ri} and SSA_{Ri} of each particle size group are listed in Table 3.3. Based on this, the CPFT formed due to the excessive cement paste can be subsequently calculated as Equation (3.4).

$$CPFT = \frac{CPV - V_V}{SA} = \frac{CPV_{exc}}{SA} \tag{3.4}$$

Table 3.3 Summary of d_{Ri} and SSA_{Ri} values for different particle size groups

Size group	R_1	R_2	R_3	R_4
d_{Ri} (mm)	18.0	13.0	7.5	1.0
SSA_{Ri} (m^2/m^3)	408	565	980	14026

3.2.7 X-ray computed tomography

The X-ray computed tomography (CT) was used to characterize the macropore structure in RAC samples. The sample size was determined based on the largest heterogeneity in RAC (*i.e.* RCA with a maximum size of 20 mm). A desired spatial resolution for identifying the smallest heterogeneity (*i.e.* the smallest macro-pore with a size around 100 μm) was also considered. The RAC samples with a diameter of 50 mm and a height of 100 mm were selected for CT scanning and were cored from RAC cylinders after 28 days' curing. The phase identification in CT scanning is based on the physical density difference of phases due to their variable energy attenuation of X-ray. The qualitatively visual 3D macro-pore structure of RAC can be rendered and reconstructed by processing the tomographic images. The reconstructed 3D macro-pore structure model enables to provide a quantitative analysis for macro-pore characteristics, including diameter, volume, surface area, position in X-Y-Z axis, sphericity, number of pores, etc. Statistical analysis such as the distribution of sphericity and number of macro pores was performed in this study.

3.3 Results and discussion

3.3.1 Packing density of aggregates

Fig. 3.2 shows the packing densities of NCAs and RCAs with the usage of a combination of different particle size groups (*i.e.* R_1 to R_4). Here, the bulk volume of the aggregates keeps at constant. It is readily seen that increasing the volume fraction of small-size aggregates can increase the packing density of aggregates until an optimum volume fraction is reached. Further increasing the volume fraction of small-size aggregates decreases the packing density as the volume of the small-size aggregates exceeds the volume of the voids formed by the large-size aggregate skeleton, and the packing state of the aggregate skeleton

would be consequently loosened. Fig. 3.2(a) shows the packing density of aggregates within the ranges of R_1 and R_2. The results show that more aggregates within the range of R_2 are required by RCAs than NCAs to optimize the packing density. The addition of R_3 can significantly increase the packing density of RCAs as shown in Fig. 3.2(b). This can be attributed to the unique morphology of grain class, R3, could have led to a more favourable size distribution, resulting in a higher packing density. Since the surface roughness of river sand is much smaller than that of RCA, the addition of R_4 (*i.e.* river sand) could compensate the surface roughness of RCAs and further narrows the difference of the maximum packing density between RCAs and NCAs as seen in Fig. 3.2(c). A volume proportion of 40% to 50% can be recommended for the fine aggregates (*i.e.* R_4) to improve the packing density of aggregates in concrete, which agrees with the finding reported by Moini *et al.* (2015). Furthermore, it can be known from Fig. 2 that the optimum mix proportions of R_1:R_2:R_3:R_4 in volume are 2.88:0.72:2.4:4 and 2.1:1.4:1.5:5 for NAC and RAC, respectively. This indicates that less coarse particles (*i.e.* R_1) and more fine particles (*i.e.* R_4) are needed to achieve an optimized packing density for the RAC. In other words, more small-size particles are required to fill into the large voids among the coarse RCAs due to their irregular shapes and rough surfaces.
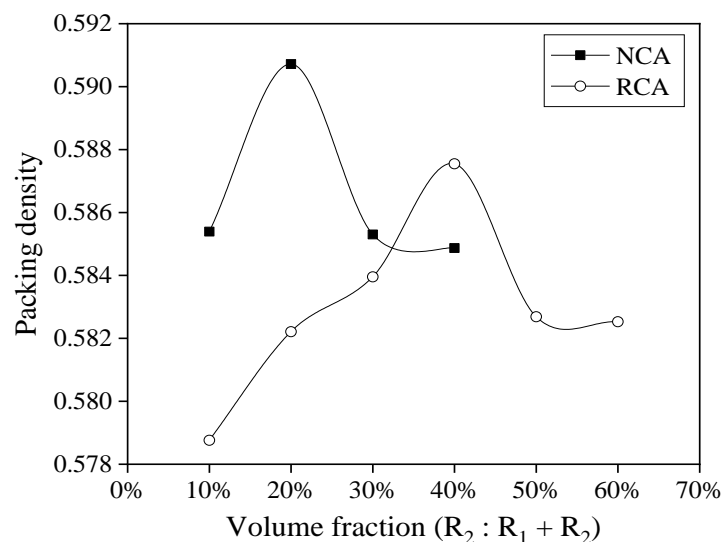
(a)
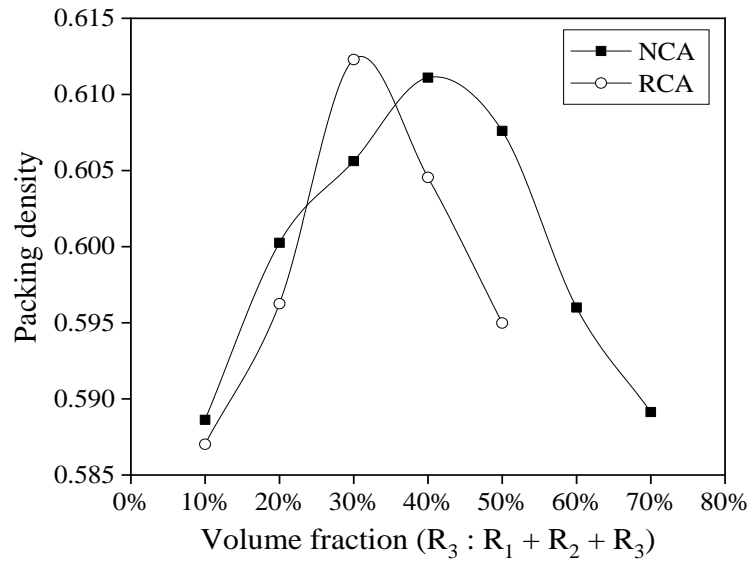
(b)
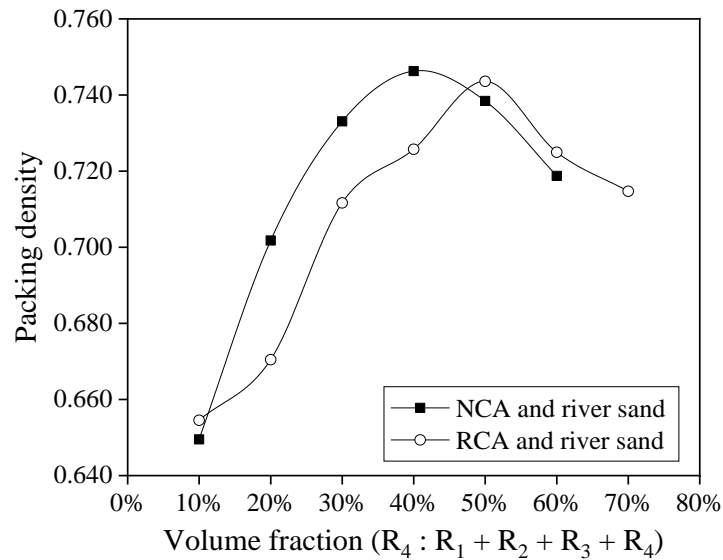
(c)

Fig. 3.2 Packing densities versus volume fraction of aggregates with various size classes: (a) R_1 - R_2, (b) R_1 - R_3, and (c) R_1- R_4.

3.3.2 Void volume and cement paste film thickness

Fig. 3.3 compares the cement paste file thickness and the void volume among the aggregates in each mix designed by the TM and the PPM. When the CPV is constant, void volume in 1 m^3 concrete mainly depends on the packing density of the aggregates. The mixtures designed by the PPM exhibit lower void volumes as compared with those designed by the TM, indicating that the PPM can effectively increase the compaction degree of aggregates in concrete. For

instance, the use of PPM decreases the void volumes among the aggregates by 4.5% and 12.4% for NAC and RAC, respectively. Besides, the CPFTs for NAC and RAC were decreased by 8.3% and 14.3% after the aggregate packing enhancement, respectively. The higher reduction rates of the void volume and CPFT for RAC indicate that the PPM is more effective in decreasing the void volumes and CPFTs for the RAC than the NAC. Both decreasing void volume and CPFT could contribute to densify the granular skeleton of aggregates in concrete.
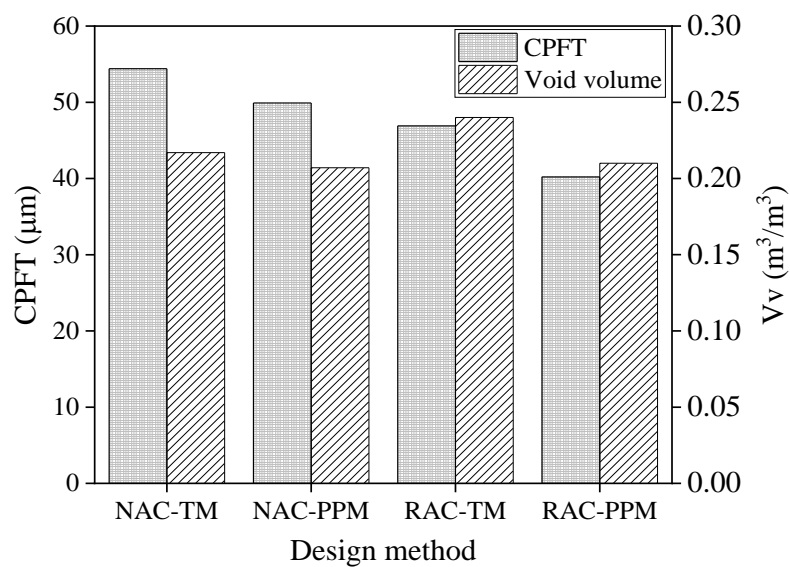
Fig. 3.3 Cement paste film thickness and void volume of concretes

3.3.3 Slump of fresh concrete

Fig. 3.4 shows the slump of fresh RAC and NAC designed by different methods. The slump values of RAC are lower than those of NAC regardless of the mix design method. This might be caused by the angularity and high surface roughness of RCAs, which results in a higher yield stress and subsequently decreases the slump of the fresh RAC (Silva *et al.*, 2018). Besides, the slumps of the PPM designed concrete are higher than those of TM designed concrete as seen in Fig. 3.4. For instance, the use of PPM enhances the slumps of NAC and RAC by 16% and 25%, respectively. It also indicates that the particle packing optimization by PPM is more effective in improving the workability for RAC than NAC. This could be related to the change of the void volume among the

aggregates. When the CPV and W/C ratio are constant, the smaller void volume leads to more excessive cement paste, which can enhance the workability of concrete through lubricating the aggregates and mitigating the inter-particle friction (Schwartzentruber *et al.*, 2006).
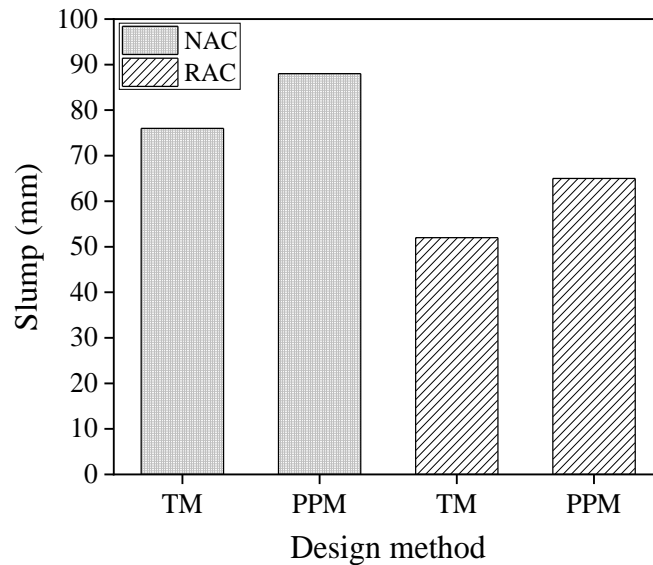
Fig. 3.4 Slump of fresh concrete

3.3.4 Compressive strength

Fig. 3.5 shows the compressive strength of NAC and RAC prepared with a constant CPV of 39%. When the CPV and the W/C ratio are constant, the PPM designed concrete shows higher compressive strengths than those designed by the TM. For instance, the adoption of PPM in concrete mix design increases the 28-day compressive strengths of NAC and RAC by 13.4% and 6.6%, respectively. Since the application of PPM decreases the void volume and the CPFT of aggregates, it facilitates the formation of a denser aggregate skeleton for resisting a higher compressive stress. It could also be caused by the increased adhesive behaviour between the mortar and the coarse aggregates when more fine aggregates are used by the PPM (Braga *et al.*, 2014). Furthermore, it can be found that the 3-day compressive strengths of the RAC are higher than those of the NAC. This could be caused by the reduced CPFT of RAC as shown in Fig. 3.3. At the early curing stage, the strength of cement paste is relatively lower so

that the crack could be more easily initiated around the coarse aggregates and then passing into the surrounding cement paste. The length of crack path consequently increases inside RAC, which increases the absorbed strain energy and enhances the compressive strength (Chidiac *et al.*, 2013). However, the 28-day compressive strengths of RAC are lower than those of NAC. This is mainly caused by the higher porosity of the RAC and the weaker ITZs between RCAs and the cement paste.
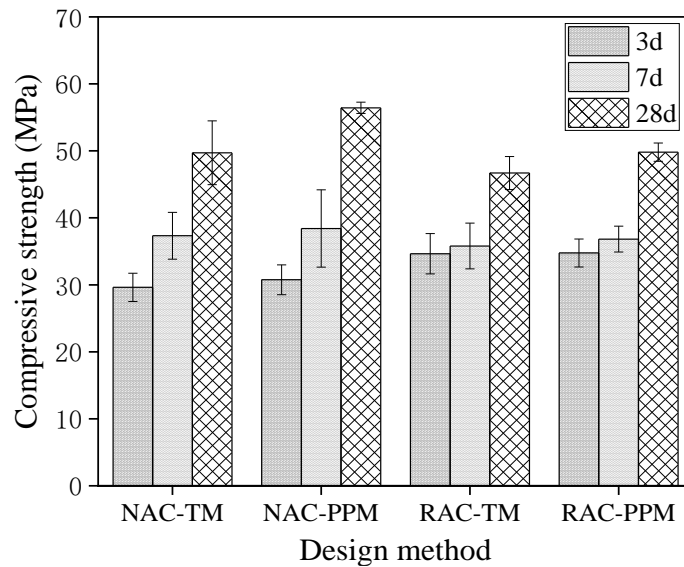
Fig. 3.5 Compressive strength of concretes

3.3.5 Flexural strength

Fig. 3.6 presents the flexural strengths of NAC and RAC with the same CPV of 39%. Both the type and the packing status of the aggregates have marginal impacts on the flexural strength of concrete. It indicates that the flexural strength of concrete is not sensitive to the packing status of aggregates. This could be mainly attributed to that the flexural strength of concrete depends more on the properties of cement paste than the aggregates. The slight increase of flexural strength by replacing the TM by PPM could be attributed to the higher fraction of fine aggregates in the concrete. Similar to the compressive strength, the PPM is more effective in enhancing the flexural strength of RAC in comparison with that for NAC.
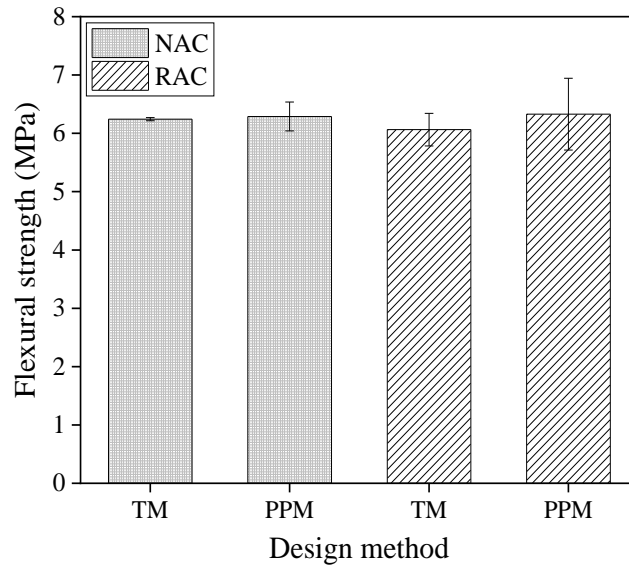
Fig. 3.6 Flexural strength of concretes

3.3.6 Young's modulus

Fig. 3.7 shows the Young's modulus of concrete designed by the PPM and TM. The application of PPM can efficiently increase the Young's modulus of both NAC and RAC, since the void volume among the aggregates is decreased due to the increase of packing density. Specifically, the adoption of PPM enhances the Young's modulus of NAC and RAC by 13.5% and 27.7%, respectively. It demonstrates that the optimization of aggregate packing is more effective in increasing the Young's modulus of RAC than NAC. The PPM designed NAC and RAC are able to achieve similar Young's modulus.
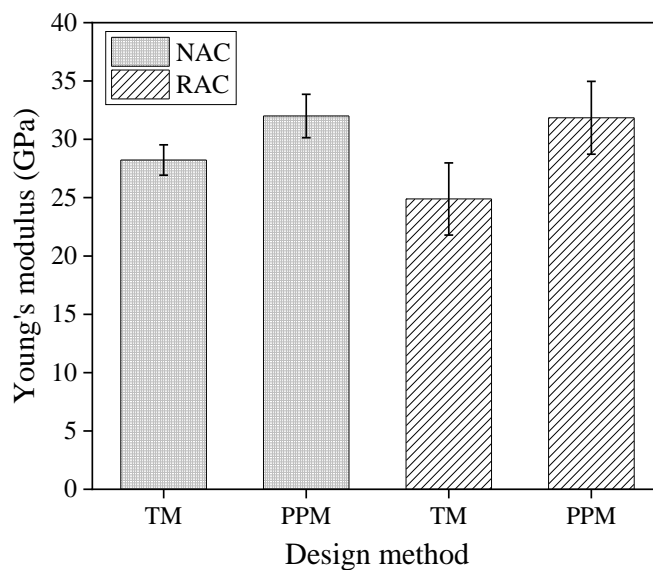
Fig. 3.7 Young's modulus of concretes

3.3.7 Microstructural analysis by X-ray CT

The pore structure inside RAC has a significant impact on the properties of hardened concrete, especially for the macro pores with a size larger than 100 μm (Gong *et al.*, 2014). The macropore structures of RACs with various packing methods were characterized and compared. Fig. 3.8 shows the sphericity distribution of macro pores in the RACs. The macro pores in each mix tend to have a sphericity between 0.4 and 0.8, indicating most voids inside RACs are macro pores instead of cracks (Sidiq e*t al.*, 2019, 2020). This can be also seen in the 3D macro-pore space distribution in RAC samples with different packing methods in Fig. 3.9.

Fig. 3.10 shows the macro-pore size distribution inside the RAC samples. For the RAC with the same CPV, the number of macro pores within each size range is decreased after the aggregate packing enhancement. The total macro-pore number in PPM designed RAC is around 30% lower than that of TM designed RAC. This is mainly attributed to the reduction of macro pore number in the hardened cement paste after the aggregate packing enhancement in RAC as seen in Figs. 3.11(a) and 3.11(b). This indicates that the densification of aggregate skeleton with a higher volume proportion of large-sized RCAs and river sand can optimise the pore structure of RAC through decreasing its macro pore number, which subsequently enhances the mechanical properties of PPM designed RAC.
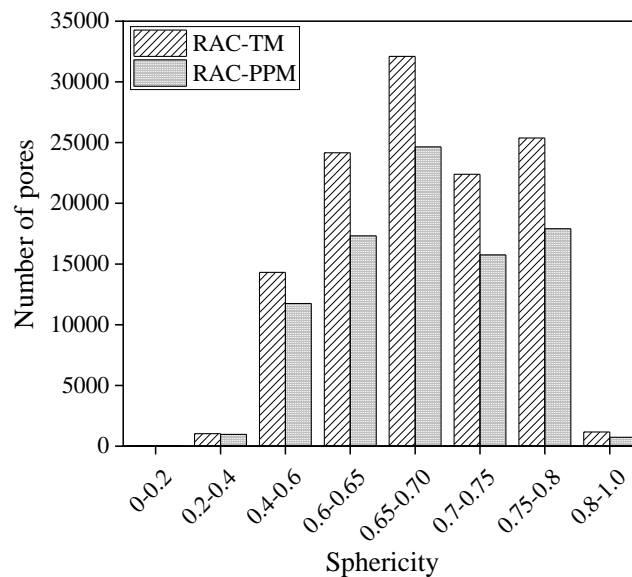
Fig. 3.8 Sphericity of macro pores inside RAC

66

(a)   (b)
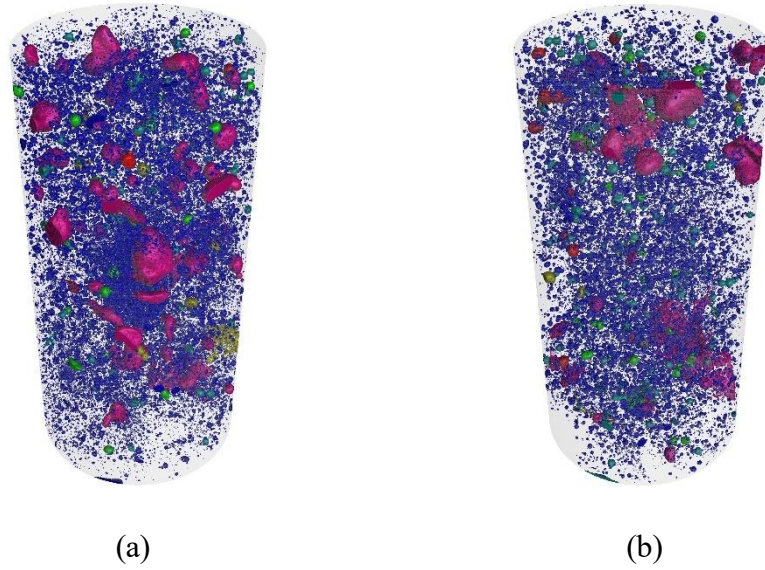
Fig. 3.9 3D macropore space distribution in different RAC samples (a) RAC-

TM, and (b) RAC-PPM
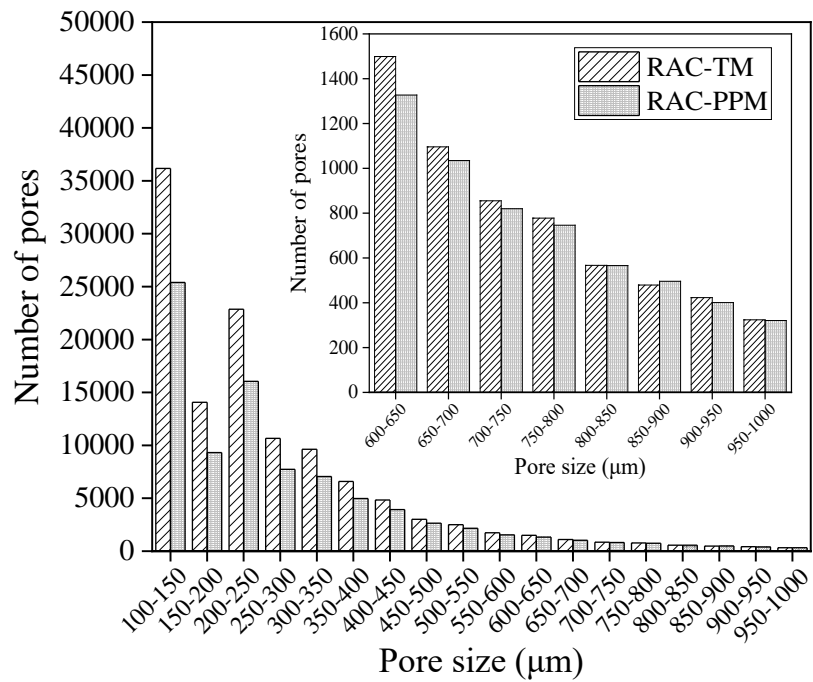
Fig. 3.10 Distribution of macropores in different RAC samples with various

packing methods
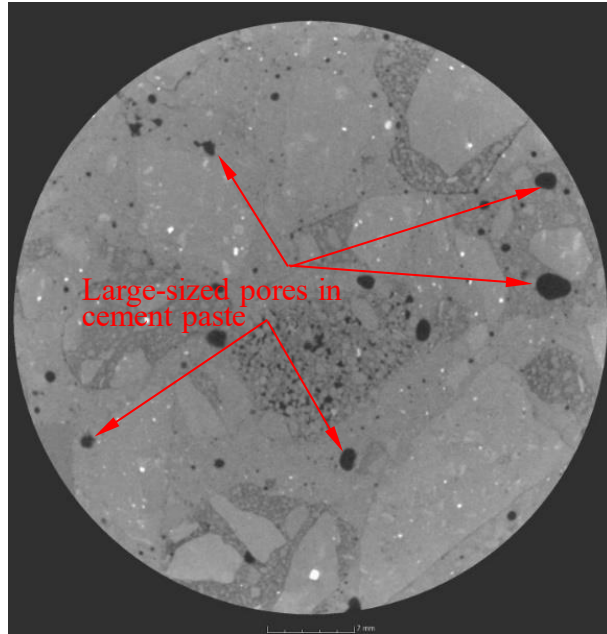
(a)
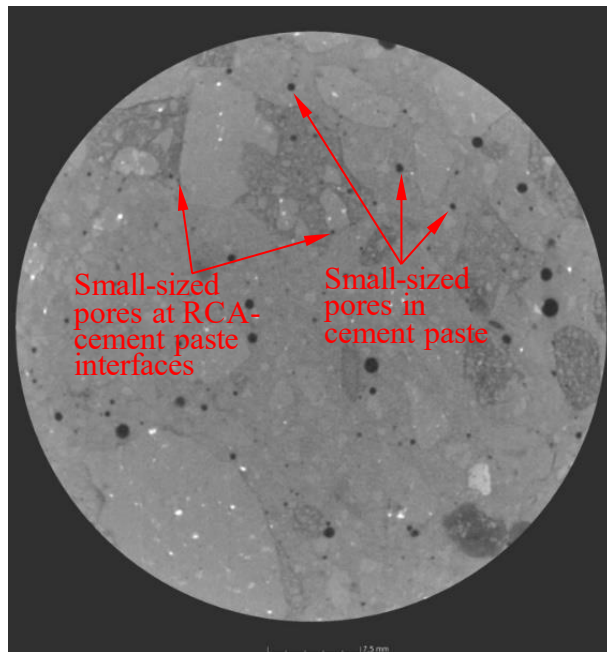
(b)

Fig. 3.11 Distribution of macro pores in RAC samples (a) RAC-TM, and (b) RAC-PPM

3.4 Summary

This chapter investigated the effects of aggregate packing enhancement on the workability and mechanical properties of both NAC and RAC. The macropore structure of RAC was also characterised by the X-ray CT. Based on the test results and the discussion, the following conclusions can be drawn.

- The packing density of RCAs with various amounts of small-size aggregates (i.e. river sand) is smaller than that of NCAs, which is mainly attributed to larger voids created by heterogeneous RCAs with irregular shapes and rough surfaces. However, it can be increased by filling with more small-size aggregates to compensate the drawbacks of RCAs. The RCAs could consequently achieve a comparable maximum packing density as NCAs.

- The adoption of PPM can enhance the workability of NAC and RAC with the same W/C ratio and CPV, particularly for RAC. The PPM can increase the slump of RAC by 25%. This is mainly attributed to the enhanced lubrication effect of excess cement paste on the mixture of RCAs. The use of PPM significantly enhances the particle packing density in RAC, leading to a more efficient use of cement paste to fill voids among aggregates. This optimised packing status, in turn, amplifies the lubrication effect of the excess cement paste on the RCAs, thereby enhancing the workability of the RAC.

- The aggregate packing enhancement can increase the compressive strength and Young's modulus of RAC by 7% and 28%, respectively, through creating a dense and stable aggregate skeleton inside concrete by decreasing the void among the aggregates and the CPFT. In addition, the refinement of pore structure through decreasing the number of macro pores in the PPM-design RAC also contributes to the enhancement in its compressive strength and Young's modulus.

CHAPTER 4

PROPERTIES AND MICROSTRUCTURE OF PACKING-OPTIMISED RECYCLED AGGREGATE CONCRETE WITH DIFFERENT CEMENT PASTE OR SAND CONTENTS

4.1 Introduction

The cement paste volume (CPV) and sand-to-aggregate volume ratio (Bs) are the key parameters affecting the performance of packing-optimised recycled aggregate concrete (RAC). However, the impact of varying CPV or Bs on the properties and microstructure of RAC has not been fully understood. Therefore, this chapter presents an experimental investigation on the properties and microstructure of packing-optimised RAC with different cement paste or sand contents. The workability and mechanical properties of RAC with four levels of CPV and three contents of Bs were evaluated. Moreover, the interfacial transition zones and pore structure inside RAC were also characterised using microhardness test and X-ray computed tomography, respectively. The relationship between the macro properties and microstructure was analysed and discussed. The results obtained in this chapter can guide the selection of CPV and Bs in the mix design of packing-optimised RAC to refine its microstructure and mechanical properties.

4.2 Experimental programme

4.2.1 Materials

Materials adopted for preparing the RAC include the ordinary Portland cement (OPC), recycled concrete aggregate (RCA), river sand, and water. The grade 42.5N OPC with a density of 3100 kg/m³ was used. The RCAs collected from the local C&D wastes recycling plant in Ningbo, China were used as the coarse aggregates. The RCAs were washed, dried, sieved and stored with three size classes, including 5 to 10 mm, 10 to 16 mm, and 16 to 20 mm. The particle size distribution of river sand is given in Fig. 4.1. According to GB/T 14684-2011 (Standards China, 2011), the sand is classified as medium grade and has a

fineness modulus of 2.62. The densities and water absorption of aggregates were characterised according to BS 812-2:1995 (BSI, 1999). The physical properties of the aggregates are summarised in Table 4.1.
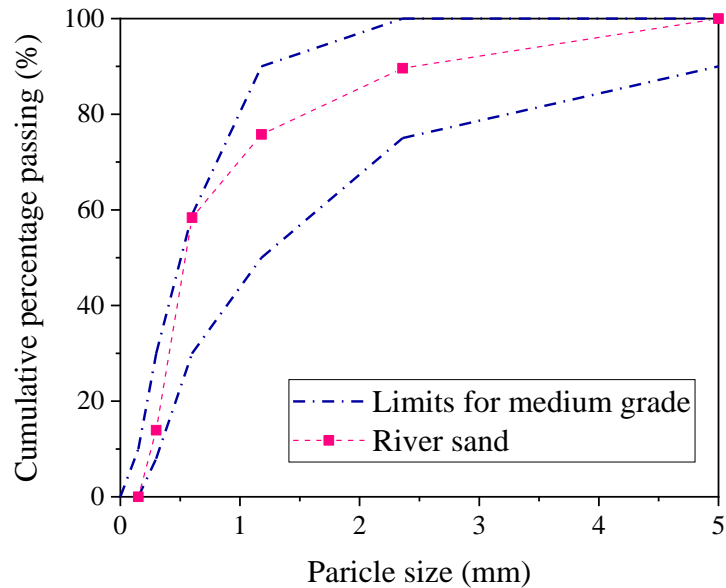
Fig. 4.1 Particle size distribution of river sand

Table 4.1 Physical properties of RCAs and river sand

Type	Size range (mm)	Oven-dried density (kg/m^3)	Saturated-surface-dried density (kg/m^3)	Apparent density (kg/m^3)	Water absorption (%)
RCAs	5-10	2167	2300	2499	6.13
	10-16	2230	2321	2454	4.11
	16-20	2258	2337	2452	3.50
River sand	0.15-5	2550	2557	2567	0.26

4.2.2 Particle packing optimisation

Particle packing optimisation was performed to achieve the minimum void volume among RCAs for all the mixtures referring to Li *et al.* (2017). Packing density of aggregates under dry condition was determined based on the method reported by Li *et al.* (2014). The aggregates in different size classes were blended in portion thoroughly. The dry aggregate mixture was then poured into a container in three equal portions and compacted densely layer-by-layer. Afterwards, the covered container was vibrated for 30 seconds to closely pack

the grains, followed by weighing the total aggregates to obtain the bulk density of aggregates (ρ_{bulk}). Finally, the particle packing density (ϕ) of aggregates can be calculated by Equation (4.1).

$$\phi = \frac{\rho_{bulk}}{\rho_{aggregate}} \qquad (4.1)$$

where ρ_{bulk} and $\rho_{aggregate}$ are the bulk density and absolute density of aggregates, respectively.

In this study, an experimental procedure was adopted to optimise the volume proportion of RCAs with three size classes, *i.e.* 16 to 20 mm, 10 to 16 mm and 5 to 10 mm. Two coarser RCAs were first proportioned into various combinations. The proportion between these two classes of RCAs with maximum packing density was kept constant for further mixing with finer RCAs. Afterwards, the finer RCAs were added into the aggregate combination with three size classes in different volume fractions. As seen in Fig. 4.2, the packing density of aggregates first increases with the volume fraction of small-sized aggregates, followed by a reduction as it further increases. This phenomenon can be regarded as the filling and loosening effects of finer aggregates on the packing state of coarse aggregates (Roquier, 2016). The maximum packing density of RCAs reaches 0.612 when the volume proportion of 16 to 20 mm, 10 to 16 mm and 5 to 10 mm sized RCAs is equal to 4.2: 2.8: 3.
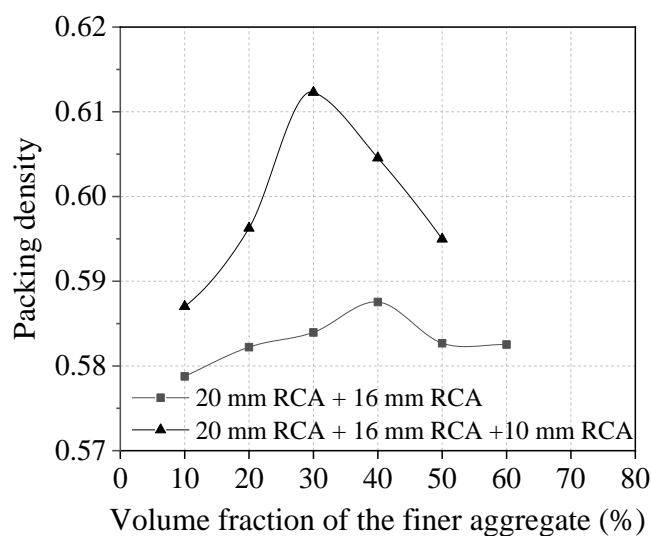
Fig. 4.2 Packing density of different RCA proportions

4.2.3 Concrete mix design

The volume proportion of RCAs in all the mixtures was optimised to achieve the maximum packing density as determined in section 4.2.2. By accounting for the water absorption of aggregates, the effective W/C ratio for each mixture was finally controlled as 0.5. Cement paste volume (CPV) in the mixtures varied from 33% to 42% with an increment of 3%. The values of cement paste volume were designed in a broad range to achieve different packing statuses of aggregates, including closely pack aggregates and suspended aggregates floating in the fresh paste. Sand-to-aggregate volume ratio (Bs) varied from 30% to 70% with an increment of 20%. This aims to alter the granular mixture from dominant coarse grains of RCAs to dominant fine grains of sands. The mix formulations of all the RACs are tabulated in Table 4.2. Each concrete mix is named as RAC-X-Y, where X and Y denote the values of Bs and CPV, respectively.

In this study, the theoretical cement paste film thickness (CPFT) was calculated for each RAC mixture (Kwan & Li, 2014). Based on the calculation method for the CPFT in the literature (Rangaraju *et al.*, 2010; Jiang *et al.*, 2021), the packing density of total aggregates (φ) and specific surface area (SSA) of the blended aggregates were pre-determined, which can be used to calculate the CPFT. The determined φ and SSA for each RAC mixture are shown in Table 4.2. As explained in section 4.2.2, increasing the Bs improves the packing density of total aggregates due to the filling effect of sand. However, a further increase of Bs from 50% to 70% decreases the packing density as the finer sand loosens the packing status of RCAs. Moreover, it also shows that the CPFT increases with the CPV but decreases with the Bs.

Table 4.2 Mixture proportion of RACs

Mix	Water (kg/m³)	Cement (kg/m³)	River Sand (kg/m³)	RCAs		Packing density	SSA (m²/m³)	CPFT (μm)
				Size class (mm)	(kg/m³)			
RAC-50%-33%	215	358	854	5-10	218	0.744	4908	20.2
				10-16	209			
				16-20	318			
RAC-50%-36%	234	390	816	5-10	208	0.744	4688	29.7
				10-16	200			
				16-20	303			
RAC-50%-39%	254	423	778	5-10	198	0.744	4468	40.2
				10-16	190			
				16-20	289			
RAC-50%-42%	273	455	740	5-10	189	0.744	4248	51.8
				10-16	181			
				16-20	275			
RAC-30%-39%	254	423	467	5-10	278	0.712	2833	50.4
				10-16	267			
				16-20	405			
RAC-70%-39%	254	423	1089	5-10	119	0.715	6103	24.0
				10-16	114			
				16-20	174			

Notes: (1) SSA denotes the specific surface area of the blended aggregates; and (2) CPFT denotes the theoretical cement paste film thickness.

4.2.4 Sample preparation and test methods

4.2.4.1 Casting and curing methods

The preparation of RAC consists of two steps. Firstly, river sand, RCAs and cement were added to the mixer and mixed for 2 minutes under the dry condition. Secondly, the water was added gradually and mixed for another 3 minutes. Afterwards, a portion of fresh concrete was taken out for the slump test. The fresh RAC was remixed and used to cast the 100 mm cubes and $\Phi 100 \times 200$ mm cylinders for the compressive strength and Young's modulus tests, respectively. Three $100 \times 100 \times 400$ mm prisms were also prepared for four-point bending tests. All the prepared samples were demoulded 24h after casting and then cured in a water tank until testing.

4.2.4.2 Workability and mechanical properties

The slump test was conducted using the standard slump cone per BS EN 12350-2:2009 (BSI, 2009a). Compressive strengths of concrete at 7 and 28 days were measured as per BS EN 12390-3:2009 (BSI, 2009b). Young's moduli of RAC samples were measured following the BS EN 12390-13:2013 (BSI, 2019). Four-point bending tests determined the flexural strength of concrete according to BS EN 12390-5:2009 (BSI, 2009c). The results of three specimens for each test were averaged to obtain the final test result.

4.2.4.3 Microhardness test

Vickers microhardness test was conducted to characterise the interfacial transition zone (ITZ) between the aggregates and cement paste. The RAC samples for the microhardness test were prepared according to the procedure adopted by Li *et al.* (2021). The RAC samples with a diameter of 20 mm and a height of 10 mm were cored from the centre of 100 mm cubic samples after curing for 28 days. The samples were then immersed into absolute ethyl alcohol for more than 24h to terminate the cement hydration and vacuum oven-dried at 60°C for 24h. Afterwards, the selected samples were impregnated with epoxy resin and moulded in a $\Phi 25 \times 20$ mm rubber mould. The moulded sample surfaces were ground and polished using a Buehler AutoMet 250 polishing equipment with grits of P180, P400, P600, P1200 and MetaDi supreme diamond of 9 μm, 3 μm, 0.5 μm. Fig. 4.3 shows the typical RAC samples for the microhardness test.
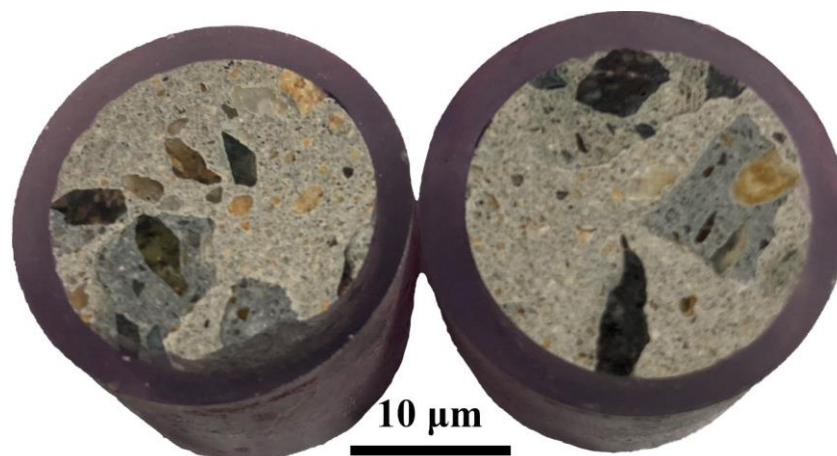
Fig. 4.3 Typical RAC samples for microhardness test

A digital Vickers microhardness tester was used in this study. A 10g load and 10s dwelling time were applied for each indentation. For each RAC sample, 50 points were randomly indented to characterise the microhardness of bulk-paste far away from the interfacial transition zone (ITZ). The quantitative method given in the literature (Qiu *et al.*, 2021) was performed by plotting the statistical box diagram to characterise the standard microhardness dispersion of the mortar. The area with a microhardness value below this standard dispersion is considered as the ITZ. An indentation zone including the RCA, ITZ and bulk-paste was selected for characterising the ITZ. In this test, an 11 × 6 grid area with a dimension of 300 × 250 μm² was characterised as shown in Fig. 4.4. The 2-D microhardness distribution cloud maps within the indentation zone were subsequently rendered to evaluate the ITZ thickness based on the method adopted by (Zhao *et al.*, 2021).
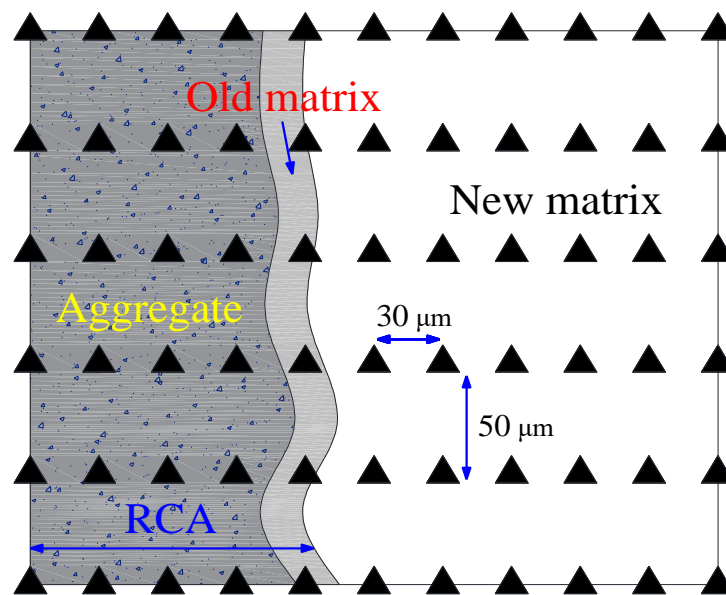
Fig. 4.4 Designed grid area for microhardness test

4.2.4.4 X-ray computed tomography

The macropore structure in RAC was characterised by using X-ray CT. The basic principle for X-ray CT to identify each phase in samples was based on the physical density difference in phases due to their different energy attenuation of X-ray. Considering the RCA size, RAC cylindrical samples with a diameter of

50 mm and a height of 100 mm were cored from the RAC cylinders cured for 28 days. The X-Ray CT used in this study can identify the smallest macropore with a size around 100 μm. The CT images were processed to reconstruct the 3-D macropore structure in RAC. This model could provide quantitative analysis for macropore characteristics, including diameter, volume, surface area, position on the X-Y-Z axis, or sphericity.

4.3   Experimental results and discussion

4.3.1 Slump

Fig. 4.5 shows the slump of fresh RAC with varying cement paste volume (CPV) and sand-to-aggregate volume ratio (Bs). The cement paste film thickness (CPFT) in each mix is also included in Fig. 4.5. The slump of fresh RAC increases with the CPV, as seen in Fig. 4.5(a). For instance, the slump of fresh RAC increases by 11 mm and 33 mm when the CPV increases from 33% to 36% and from 36% to 39%, respectively. More pressingly, the slump of fresh RAC increases by 84 mm when the CPV increases from 39% to 42%. It indicates that the slump of RAC increases at a growing rate as the CPV increases. This is mainly attributed to the lubrication effect of fresh cement paste on the mixture of aggregates (Choi *et al.*, 2013). This is evidenced by that the slump of fresh RAC increases with the CPFT, indicating that more cement paste is available for coating the aggregates and separating them to reduce the inter-particle friction for the fresh RAC with a thicker cement paste film (Kwan & Li, 2012). It is also worth noting that no segregation occurs in all the RAC mixtures with various CPVs, indicating that all the RAC mixtures have a good cohesiveness. Moreover, the slump of fresh RAC decreases with the Bs, as shown in Fig. 4.5(b). For instance, the slump of RAC decreases by 64.5% as the Bs increases from 50% to 70%, while it decreases by 36.8% when the Bs increases from 30% to 50%. It indicates that increasing the Bs decreases the slump of fresh RAC with constant CPV and W/C ratio. Similarly, this is mainly caused by the reduced CPFT in the fresh RAC with a higher Bs, which weakens the lubrication effect of fresh paste on the aggregates.
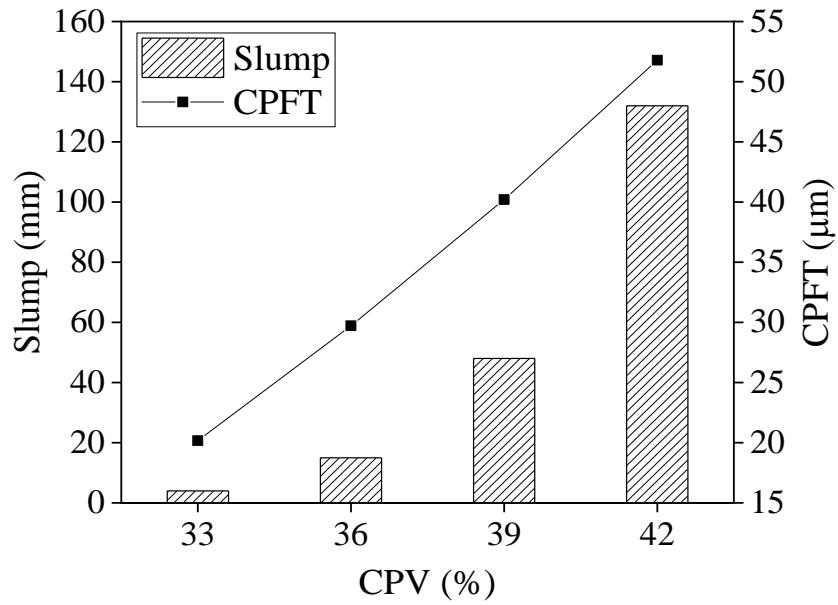
(a)
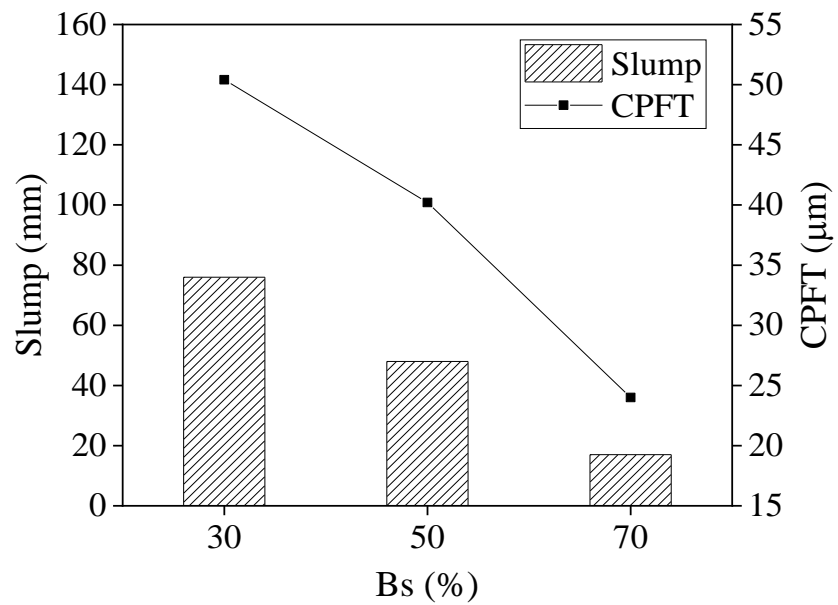
(b)

Fig. 4.5 Slump and CPFT of fresh RAC with varying (a) CPV and (b) Bs

4.3.2 Compressive strength

Fig. 4.6(a) shows the compressive strength of RAC with varying cement paste volume (CPV). The early compressive strength of RAC first increases with the CPV up to 39%. Specifically, the 7-day compressive strength of RAC increases by 15.6% as the CPV increases from 36% to 39%. However, further increasing

the CPV to 42% slightly decreases the compressive strength of RAC as the cement paste content tends to dominate the strength of RAC. The 28-day compressive strength of RAC increases as the CPV from 33% to 36%, followed by a gradual reduction as the CPV further increases to 42%. For instance, the compressive strength of RAC is dramatically increased by 37.6% when the CPV increases from 33% to 36%. This is mainly attributed to the refinement in the macro-pore structure of RAC by decreasing its porosity and macropore number as the CPV increases from 33% to 36%, which is confirmed by the X-ray CT results. Unlike the 7-day compressive strength, the maximum 28-day compressive strength of RAC is attained at a CPV of 36%. This can be attributed to the enhanced interfacial transition zones (ITZs) as the cement paste hardens, forming a stronger skeleton inside the RAC. The 28-day compressive strength of RAC decreases by 4.1% as the CPV increases from 36% to 42%. This is mainly attributed to the increased porosity and thickness of ITZs around RCAs, as evidenced by the X-ray CT and microhardness test.

Fig. 4.6(b) shows the compressive strength of RAC with various sand-to-aggregate volume ratios (Bs). Both 7-day and 28-day compressive strengths of RAC increase and then decrease with the Bs. The RAC with a Bs of 50% achieves the highest compressive strengths at the ages of 7 and 28 days, which are slightly higher than that with a Bs of 30%. This is mainly because the RAC with a Bs of 50% possesses the highest packing density of total aggregates, as seen in Table 4.2. It indicates that an optimum Bs can enhance the compressive strength of RAC, which is consistent with the findings reported by Mohammed and Rahman (2016) . However, excessive Bs (e.g., 70%) is detrimental to the compressive strength of RAC. For instance, as the Bs increases from 50% to 70%, the 7-day and 28-day compressive strengths of RAC decrease by 23.8% and 25.0%, respectively. With the lack of coarse aggregates, the contribution of aggregate skeleton to the compressive strength of concrete is limited due to the weaker interlocking between the aggregates (Shen *et al.*, 2021). Besides, an excessive Bs leads to an increase of macroporosity and mean pore size of cement mortar around RCAs, which is also detrimental to the compressive strength of RAC. As a result, the RAC with a Bs of 70% exhibits the lowest 7-day and 28-day compressive strengths. Therefore, it is recommended that the sand content

in RAC needs to be controlled to achieve a high packing density of total aggregates. This not only minimises the voids among aggregates but also creates strong granular skeleton of the aggregates, which is beneficial to the mechanical properties of RAC.
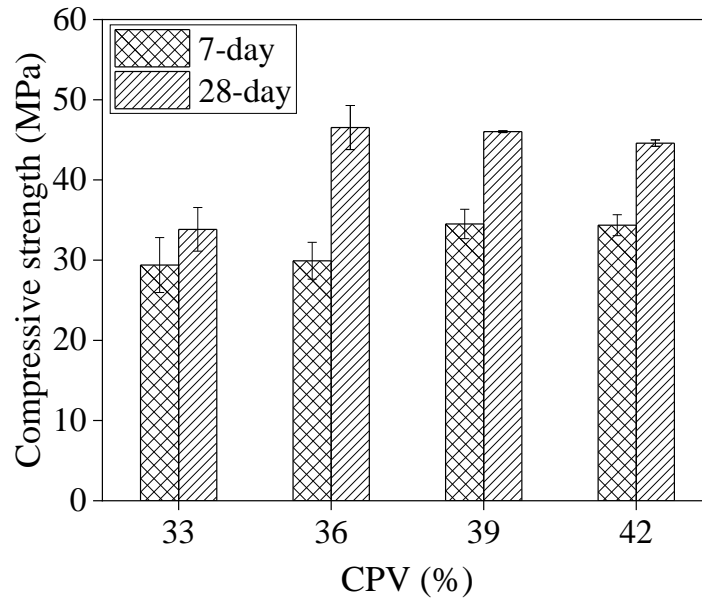
(a)
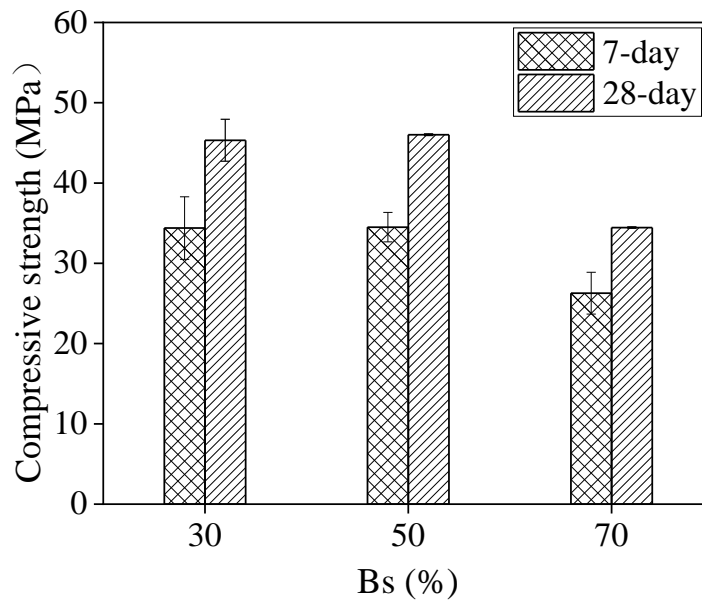
(b)

Fig. 4.6 Compressive strength of RAC with varying (a) CPV and (b) Bs

4.3.3 Flexural strength

Fig. 4.7 shows the flexural strength of RAC with varying cement paste volume (CPV) and sand-to-aggregate volume ratio (Bs). The flexural strength of RAC is around 5 MPa and varies marginally with the CPV and Bs. Specifically, the flexural strength of RAC increases by 7.0% when the CPV increases from 33% to 36%. However, the flexural strength of RAC decreases by 8.6% as the CPV further increases to 42%. Therefore, the influence of CPV on the flexural strength of RAC is negligible. Under a given W/C ratio and CPV, the flexural strength of RAC gradually decreases with the Bs. For instance, the flexural strength of RAC with a Bs of 30% is 3.2% and 3.9% higher than that for RAC with Bs of 50% and 70%, respectively. This slight increase could be attributed to a better interfacial bond between the RCA and the surrounding cement matrix due to RCAs' rough surface and angular characteristics (Helal *et al.*, 2015; Li *et al.*, 2019). This indicates that a high sand content in the RAC mixture is not beneficial to the flexural strength of RAC. In summary, the flexural strength of RAC is marginally affected by the factors of CPV and Bs as it highly depends on the effective W/C ratio which has been controlled as constant for each mixture.
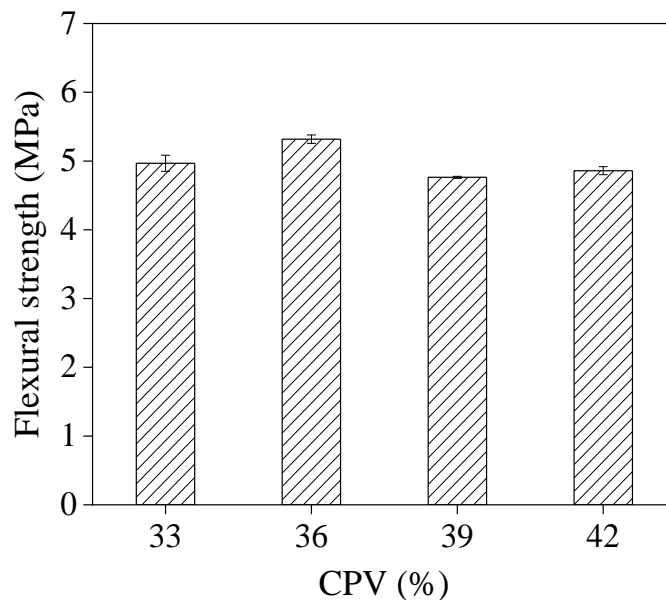
(a)
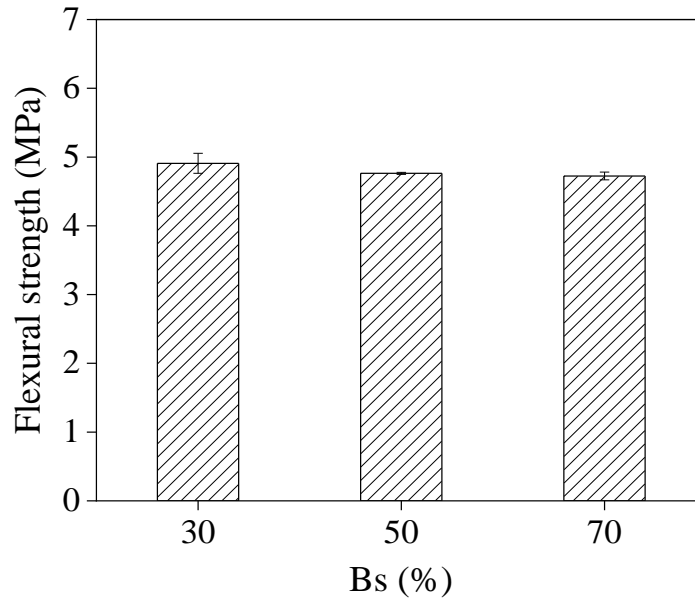
(b)

Fig. 4.7 Flexural strength of RAC with varying (a) CPV and (b) Bs

4.3.4 Young's modulus

Fig. 4.8 shows the 28-day Young's modulus of RAC with varying cement paste volume (CPV) and sand-to-aggregate volume ratio (Bs). The Young's modulus of RAC slightly increases with the CPV up to 36%, followed by a decrease as the CPV further increases to 42%. Specifically, the Young's modulus of RAC increases by 4.2% as the CPV increases from 33% to 36%. As explained in compressive strength, this is mainly attributed to the refinement in macropore structure of RAC. Nonetheless, increasing the CPV from 36% to 42% decreases the Young's modulus of RAC by 16.7%, which is related to the elastic properties and volume fraction of the cement paste, fine aggregates and coarse aggregates (Su *et al.*, 2002). Increasing the CPV would decrease the overall modulus of concrete due to its relatively lower elasticity. Moreover, the increase of thickness and porosity at the interfacial transition zones with the CPV also negatively influences the elasticity of RAC. For the RAC with constant CPV, increasing the Bs first increases and then decreases the Young's modulus of RAC. The RAC with a Bs of 50% shows the highest Young's modulus, which is 9.4% and 8.9% higher than that of RAC with Bs of 30% and 70%, respectively. Similarly, this is mainly related to the mixture's highest packing density of total aggregates.

Therefore, an appropriate increase of Bs helps to enhance the Young's modulus of RAC.
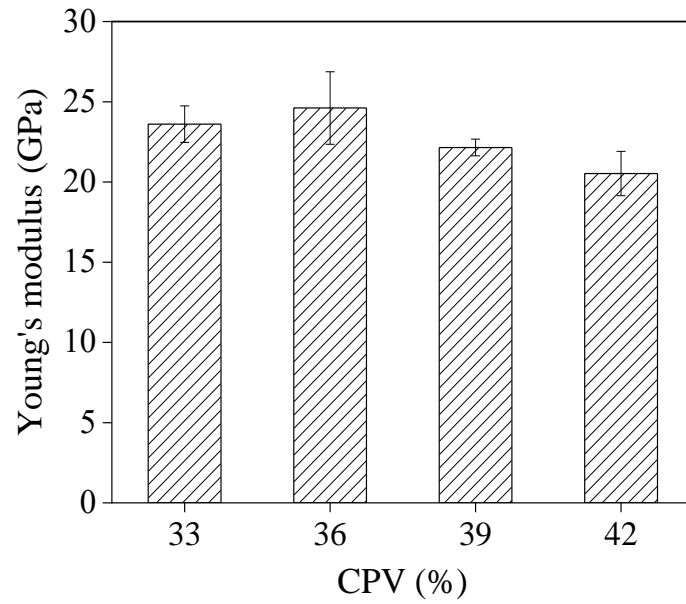
(a)
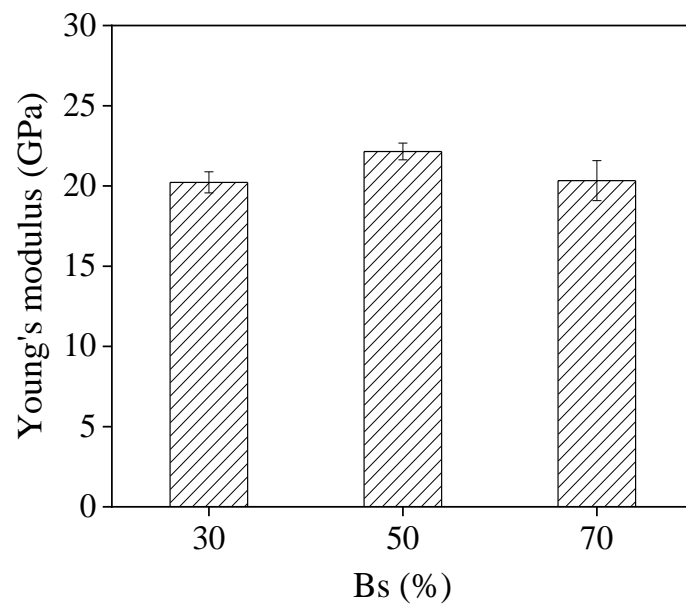
(b)

Fig. 4.8 Young's modulus of RAC with varying (a) CPV and (b) Bs

4.3.5 Microhardness analysis

Fig. 4.9 shows the box diagram of microhardness distribution of cement mortar far away from interfacial transition zones (ITZs) between recycled concrete aggregate (RCA) and cement paste in RACs. It can be found that the microhardness of mortar ranges from 35 to 50 HV, and the mean and median values of mortar microhardness vary marginally among the RACs. It indicates that the microstructure compactness of mortar far away from the ITZs in RACs is insensitive to the variations of cement paste volume (CPV) and sand-to-aggregate volume ratio (Bs), which is dominated by the effective W/C ratio in bulk cement paste.
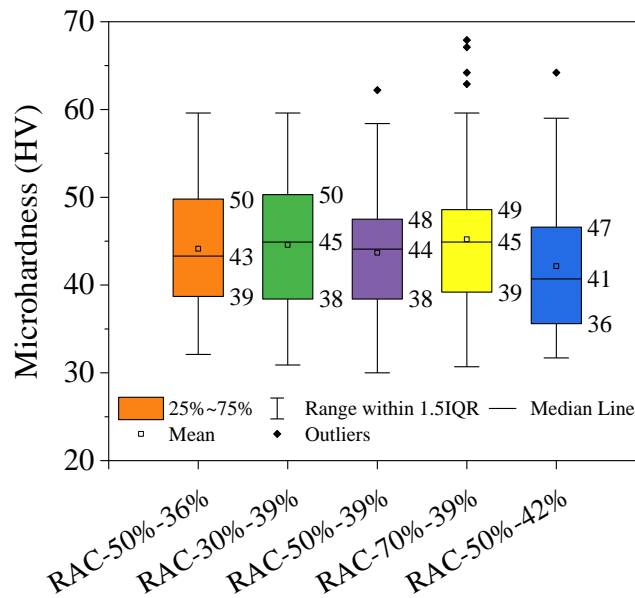
Fig. 4.9 Statistical analysis of microhardness distribution of mortar far away ITZ in RACs

(a) RAC-50%-36%   (b) RAC-30%-39%

(c) RAC-50%-39%   (d) RAC-70%-39%

(e) RAC-50%-42%
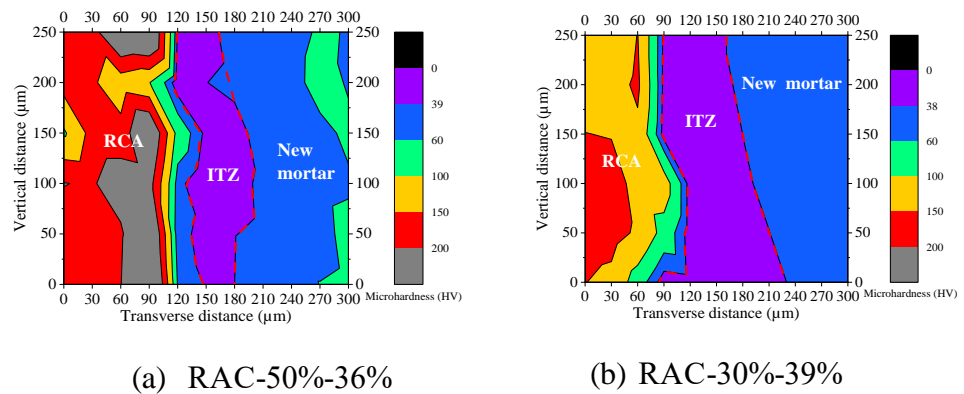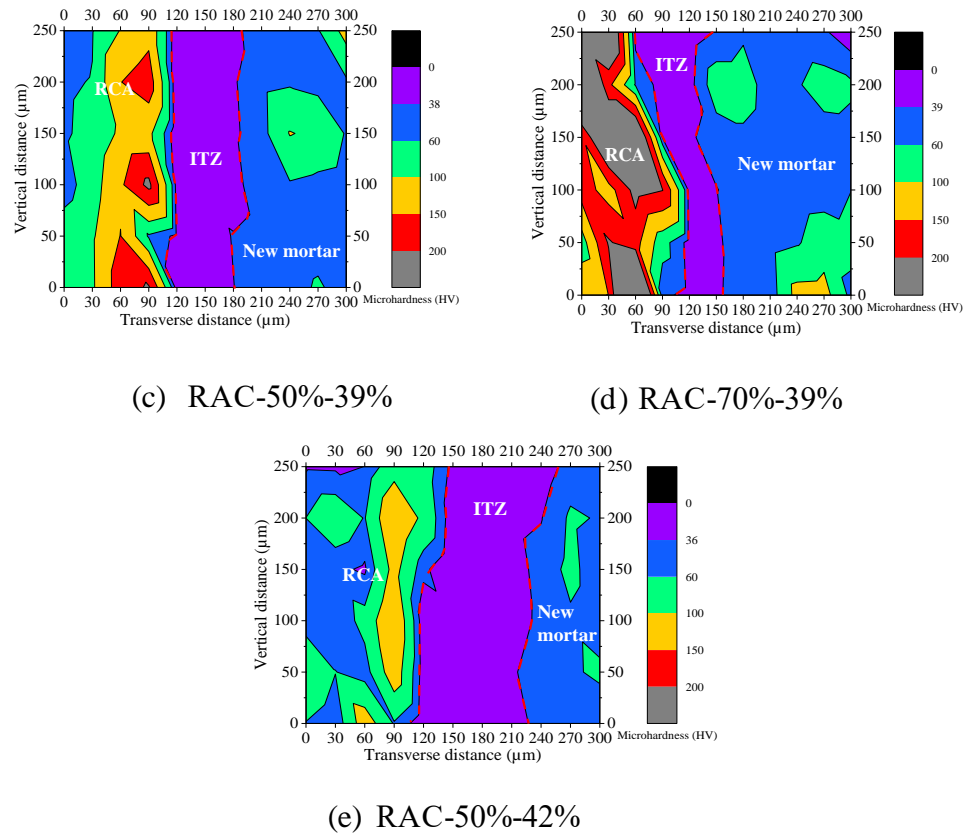
Fig. 4.10 ITZ microhardness distribution of RACs

Fig. 4.10 shows the microhardness distribution around the interfacial transition zones (ITZs) in the RACs. The area with a microhardness lower than that of the old matrix in RCAs and the newly formed bulk matrix is recognized as the ITZs. The average ITZ thickness in each RAC can be subsequently calculated through dividing the ITZ area by its vertical distance, and then plotted against CPV or Bs in Fig. 4.11. It shows that increasing the CPV or decreasing the Bs increases the ITZ thickness. For instance, the ITZ thickness increases by 38% and 69% when the CPV increases from 39% to 42% and the Bs decreases from 70% to 50%, respectively. Consequently, the mechanical properties of RAC with an excessive CPV deteriorate due to the increased ITZ thickness (Vargas *et al.*, 2017). However, a larger Bs tends to decrease the ITZ thickness but negatively influences the pore structure of RAC, which eventually weakens the mechanical properties of RAC. For example, mixture RAC-70%-39% possesses the narrowest ITZ but the lowest compressive strength. This discrepancy between the macro and micro performance also indicates that RAC properties are simultaneously affected by the ITZ and pore structure. The macropore structure

85

of cement mortar around RCAs will be discussed in section 4.3.6.
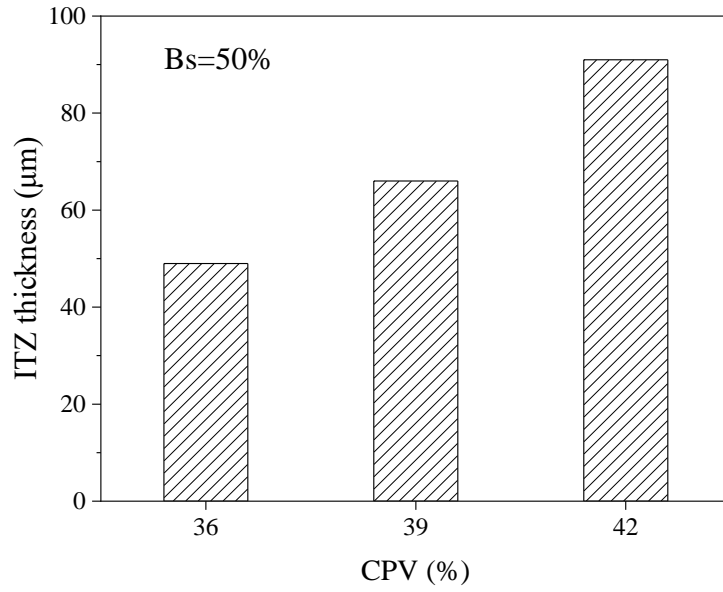
(a)
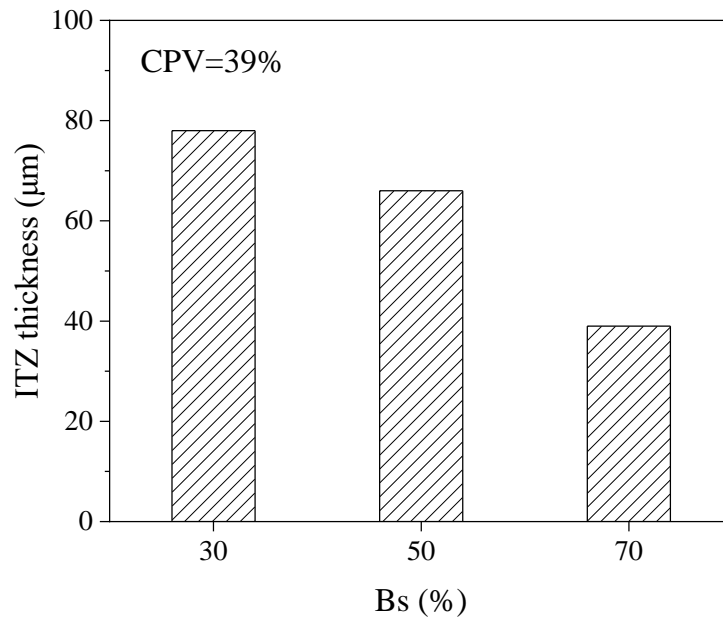
(b)

Fig. 4.11 Thickness of ITZ in RAC with varying (a) CPV and (b) Bs

4.3.6 Microstructural analysis by X-ray CT

Fig. 4.12 shows the sphericity distribution of macropores in RACs. The sphericity of macropore is an indicator of the macropore shape and is equal to 1.0 when it is a perfect sphere (Sidiq *et al.*, 2020). It can be found that the sphericity of most macropores is within the range of 0.2–0.8. As the sphericity of microcracks tends to be zero (Sidiq *et al.*, 2020), most large voids inside the

RACs represent the macropores. Therefore, it indicates that the variation of CPV or Bs does not induce more cracks into RAC. Table 4.3 summarises the statistical analysis of macropores in RACs. Fig. 4.13 shows the macropore size distribution in all the RAC mixtures. It is readily seen that there are more macropores within each size range in mixture RAC-50%-33% as compared with other mixtures. The total macropore number in the RAC, with a cement paste volume (CPV) of 33% is almost two times that in the RAC, with a CPV of 36% or 42%. Correspondingly, mixture RAC-50-33% exhibits the largest macroporosity among all the RAC mixtures. These macropores mainly exist in the hardened cement paste. As seen in Figs. 4.14(a) and (b), there are more large-sized pores in the RAC with a CPV of 33% than that with a CPV of 42%, which is mainly caused by its lower compactness and higher amount of RCAs. This also explains the poor mechanical properties of RAC with a CPV of 33%. However, Table 4.3 shows that the macroporosity mitigates continuously with the increasing CPV. As seen in Fig. 4.13, increasing the CPV from 36% to 42% brings about more macropores smaller than 250 μm in RAC. It also demonstrates that the mean pore size decreases as the CPV increases in RAC. As confirmed in Fig. 4.14(b), these small-sized macropores mainly distribute at the interfaces between RCAs and cement matrix. Gao *et al.* (2014) reported that the interfacial transition zone (ITZ) capillary porosity is increased due to the increased CPV. Therefore, excessive CPV could be detrimental to the RAC properties due to the increased porosity at the ITZs between RCAs and cement matrix.

Moreover, it can be found that mixture RAC-70%-39% has a larger mean macropore size than mixture RAC-30%-39%, as seen in Table 4.3. Particularly, the macropore size distribution demonstrates that the number of pores larger than 250 μm increases as the sand-to-aggregate volume ratio (Bs) increases from 30% to 70%. Correspondingly, the macroporosity also increases with the Bs. Hence, incorporating a high sand volume in total aggregates leads to a loose microstructure of cement mortar around RCAs. It is evidenced by the occurrence of massive macropores with a size closing to sand and sporadically distributed RCAs in the cement mortar of mixture RAC-70%-39% as seen in Figs. 4.14(c) and 4-14(d). Similar finding is also reported for self-compacting concrete with various Bs by Lin (2020). For the RAC with a high Bs, the external load can be

mainly supported by the cement mortar rather than the granular skeleton of coarse aggregate. Consequently, this loose microstructure of cement mortar around RCAs potentially increases the chance for microcracks initiating in RAC. It explains the low performance in mechanical properties of RAC with a high Bs, *i.e.* mixture RAC-70%-39%.
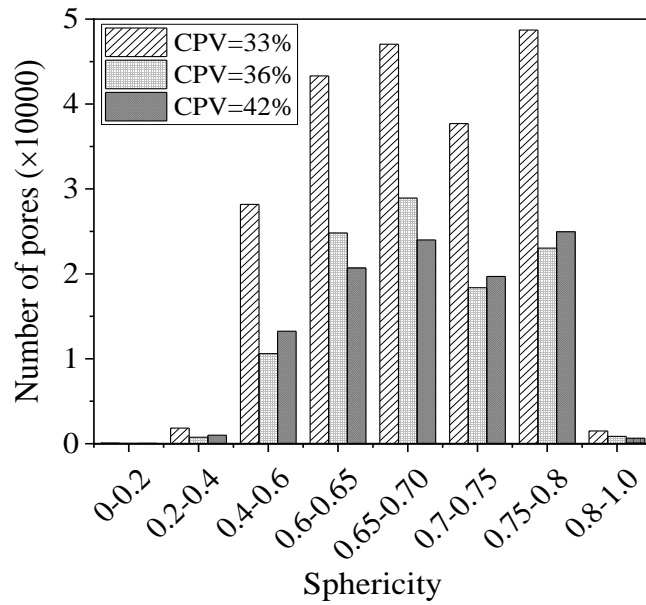
(a) Variation of CPV
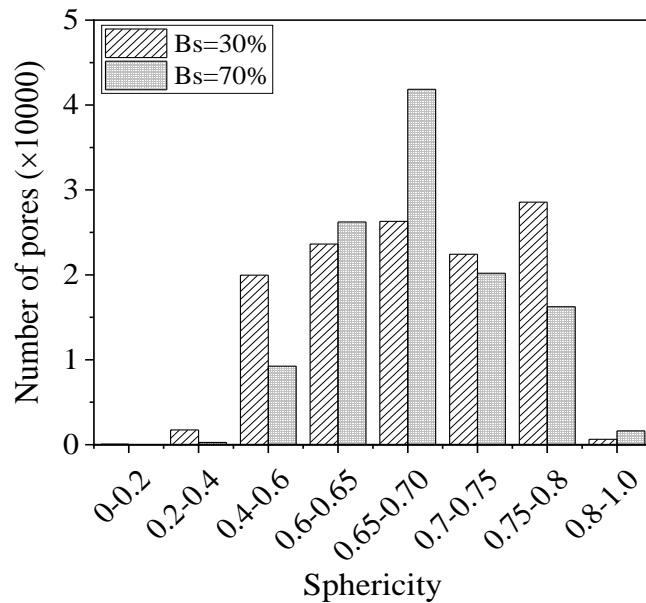
(b) Variation of Bs

Fig. 4.12 Sphericity distribution of macropores in different RACs

Table 4.3 X-ray CT results of RACs

Mix	RAC-50%-33%	RAC-50%-36%	RAC-30%-39%	RAC-70%-39%	RAC-50%-42%
Mean pore diameter (μm)	302	307	289	331	275
Macroporosity (%)	3.73%	3.21%	1.66%	2.13%	1.30%
Total pore number	208355	107429	123328	115670	104296
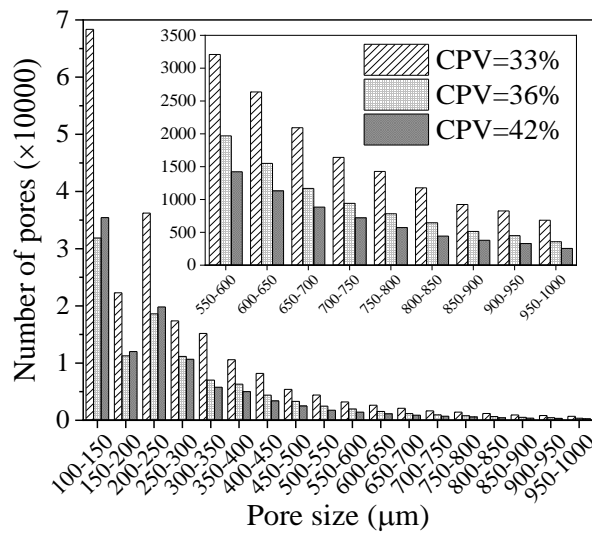
(a) Variation of CPV
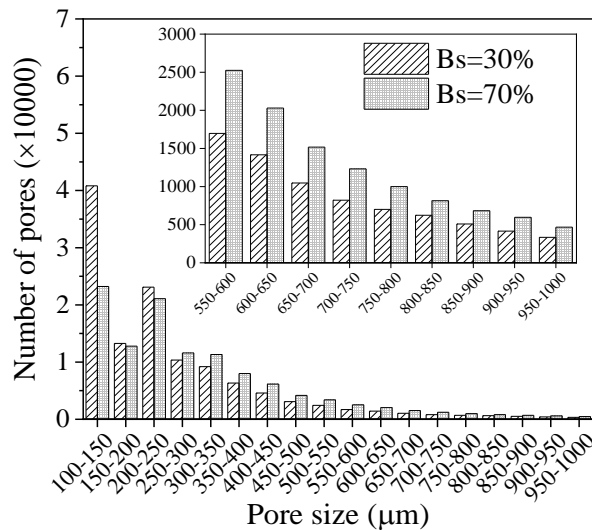
(b) Variation of Bs

Fig. 4.13 Size distribution of macropores in different RACs

(a) RAC-50%-33%   (b) RAC-50%-42%

(c) RAC-30%-39%   (d) RAC-70%-39%
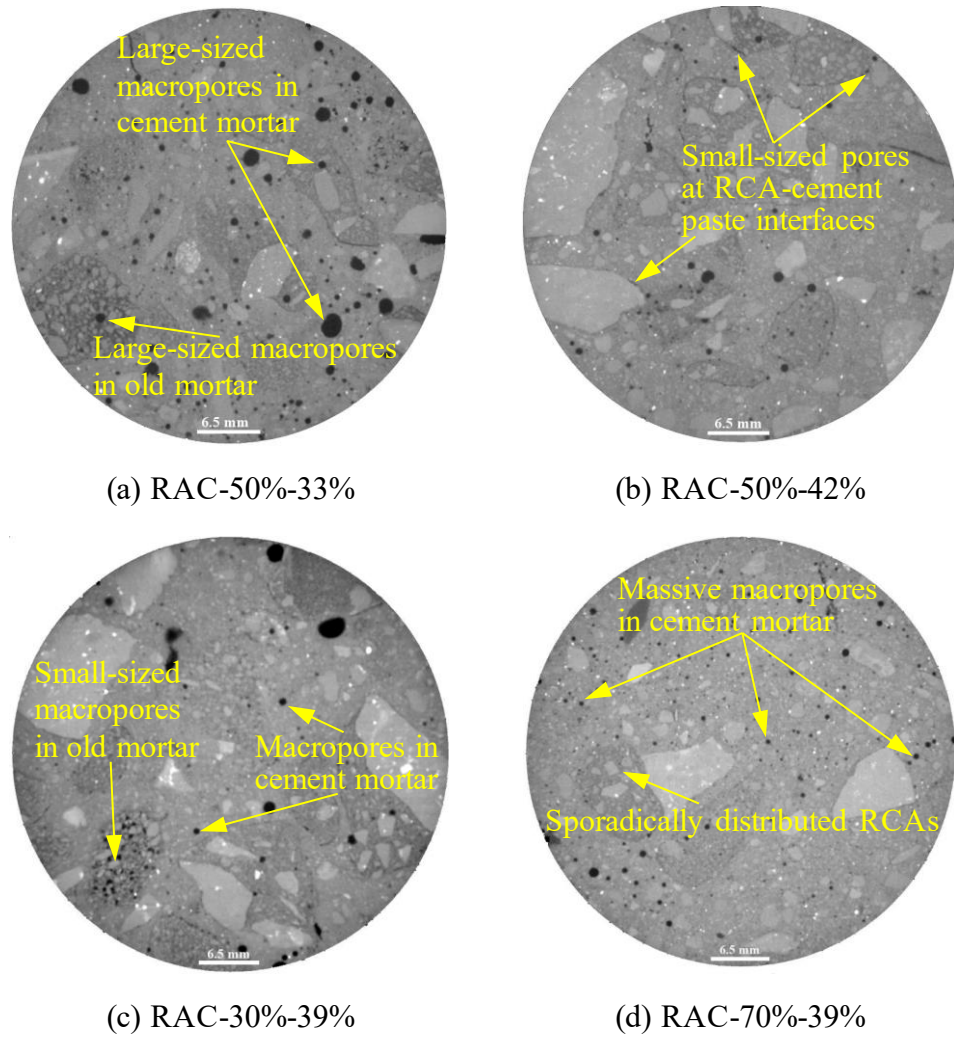
Fig. 4.14 Spatial distribution of macropores in different RACs

4.4 Summary

This chapter investigated the effects of cement paste volume and sand-to-aggregate volume ratio on the properties of fresh and hardened RAC with particle packing optimisation. The workability, mechanical properties and microstructures of RACs were evaluated. The following conclusions can be drawn based on the test results and discussion.

- The slump of fresh RAC increases in a growing rate with the cement paste volume. This is mainly attributed to the enhanced lubrication effect of cement paste on aggregates as the cement paste film thickness increases. Increasing the sand-to-aggregate volume ratio decreases the thickness of cement paste film coated on RCAs, which weakens their lubrication effect and

subsequently decreases the slump of RAC. The slump for RAC decreases by 78% as the sand-to-aggregate volume ratio increases from 30% to 70%.

- The compressive strength and Young's modulus of RAC first increase with the cement paste volume in the RAC, followed by reductions as the cement paste volume further increases. The former is mainly attributed to the refinement in macropore structure by decreasing its porosity and macropore number in RAC, while the latter is caused by the increased porosity and thickness of interfacial transition zones due to the excessive cement paste volume. Nonetheless, the flexural strength of RAC is insensitive to the variation of cement paste volume.

- The incorporation of optimum sand-to-aggregate volume ratio improves the packing density of total aggregates, and consequently enhances the compressive strength and Young's modulus of RAC. However, an excessive sand-to-aggregate volume ratio causes poorer packing status of the granular skeleton and increases the macroporosity and mean pore size of cement mortar around RCAs, which decreases the compressive strength and Young's modulus of RAC. Nonetheless, the flexural strength of RAC is marginally influenced by the sand-to-aggregate volume ratio.

- Using less cement and sand in RAC can be an effective strategy to maximise the reusing construction and demolition wastes and enhance the sustainability of concrete. An excessive cement paste volume or sand-to-aggregate volume ratio negatively affects the microstructures of RAC and degrades their mechanical properties. Thus, the cement paste volume and sand-to-aggregate volume ratio need to be properly controlled in the design of RAC.

CHAPTER 5

ROLE OF RECYCLED CONCRETE POWDER AS SAND REPLACEMENT IN THE PROPERTIES OF CEMENT MORTAR

5.1 Introduction

Rational utilisation of recycled concrete powder (RCP) is crucial for the fully recycling construction and demotion wastes in the construction industry. Existing studies have demonstrated that the use of RCP as a cement replacement has a negative impact on the microstructures and properties of cementitious materials due to its low reactivity. Furthermore, the high porosity and water absorption of RCP particles also negatively influence the properties of mortar. However, replacing sand with RCP presents an opportunity to improve the particle packing density and optimise the pore structure, which can lead to an enhancement in the properties. Few investigations have been conducted to fully understand the role of RCP as sand replacement in affecting the properties of mortar. Moreover, using RCP as a replacement for sand can also contribute to a more sustainable use of resources by reducing the demand for natural sand, which aligns with the overall sustainability goal of this research. Therefore, this chapter presents an experimental investigation on the properties of cement mortar containing RCP as sand replacement. Two types of model RCP with designated water-to-cement (W/C) ratios in the laboratory, including recycled cement paste powder (RCPP) and recycled cement mortar powder (RCMP), were intendedly prepared to better simulate the RCP obtained from the various waste concrete sources. The characteristics of RCP, including particle density, particle size distribution, mineralogical composition and micro-morphology were first studied. The physical, mechanical and drying shrinkage properties of mortars were subsequently examined. Moreover, the crystalline phases and microstructures of RCP mortars were also characterised by using the X-ray diffraction (XRD), mercury intrusion porosimeter (MIP), and scanning electron microscope (SEM). The improvements in microstructure of mortars owing to the filling effect of RCP and the hydration reaction promoted by RCP were quantified by measuring the particle packing density and hydration heat

evolution, respectively. The findings of this chapter can unveil the role of RCP in affecting the particle packing density and pore structure of RCP mortar, which is beneficial to the development of high-performance concrete prepared with RCP.

5.2 Experimental programme

5.2.1 Materials

Ordinary Portland cement (OPC) with a strength class of 42.5 N following Chinese standard GB 175-2007 (Standards China, 2007) and river sand with a medium grade as per Chinese standard GB/T 14684-2011 (Standards China, 2011) were adopted in this study. Most RCP particles are made of cement paste and mortar after separating recycled coarse aggregates (Coleman *et al.*, 2005) and have a complex composition due to various parent materials. In this study, two types of RCP were modelled by hydrated cement paste or mortar prepared with different designated water-to-cement (W/C) ratios and cement paste contents to properly reflect the quality of parent concrete materials. Similar method is also adopted by Maimouni *et al.* (2018), Zhan *et al.* (2020), and Shen *et al.* (2022) in the literature. The first is the recycled cement paste powder (RCPP) prepared with different W/C ratios, *i.e.* 0.4, 0.5 and 0.6. The second one is the recycled cement mortar powder (RCMP) with a fixed W/C ratio and aggregate-to-cement (A/C) ratio of 0.5 and 3, respectively. Specifically, RCPP is used to simulate the RCP that has a higher proportion of cement paste compared to the RCMP. In this study, RCP was prepared in the laboratory by crushing and grinding the hardened cement paste and mortar samples, preserved for at least 90 days inside the sealed containers at room temperature. Afterwards, the RCP with a grain size smaller than 150 μm was collected through mechanical sieving and then stored in air-tight containers after oven-drying. The RCP was collected without performing a secondary milling process. By using these two types of RCP, this study is able to more accurately reflect the influences of different components in RCP on the properties of cement-based materials, thereby providing more comprehensive and applicable insights for the industry.

5.2.2 Raw materials properties

The specific densities of sand and RCP were determined using a pycnometer as per BS 812-2: 1995 (BSI, 1999) and were given in Table 5.1. It can be found that the specific density of RCP is lower than that of sand, particular for the RCPP particles. The specific density of RCPP decreases as the original W/C ratio increases.

The particle size distributions of OPC and RCP were determined using the laser particle size analyser Bettersize 2000. The gradation of sand was determined by using mechanical sieving. Fig. 5.1 shows the particle size distributions of OPC, sand and RCP. The median diameters of OPC and RCP are listed in Table 5.1. It can be found that the particle size of RCP is larger than that of OPC but is much smaller than that of sand. Moreover, the RCPP prepared with various W/C ratios shows similar particle size, as evidenced by the D_{50} results, which are slightly smaller than RCMP.

Table 5.1 Specific densities and median diameters of OPC, sand and RCP

Materials	OPC	Sand	RCPP-W4	RCPP-W5	RCPP-W6	RCMP-W5
Specific density	3.10	2.57	2.42	2.36	2.32	2.52
D_{50} (μm)	21.418	N/A	31.427	34.629	31.533	42.823
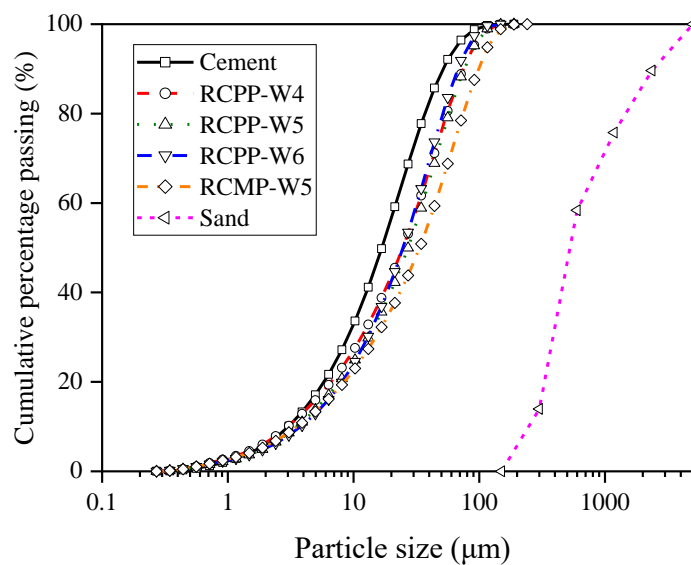
Fig. 5.1 Particle size distributions of cement, sand and RCP

The mineralogical compositions of sand and RCP were determined using X-ray diffraction (XRD) and Thermogravimetric analysis (TGA). For the XRD test, the sand and RCP were scanned with CuKα radiation ($\lambda = 1.54$Å) from 5° to 70° in 2θ with step of 0.02° and 2s/step. In the TGA, 40 mg RCP was heated up from 30°C to 1000°C at 10°C/min in N_2 atmosphere. Fig. 5.2 and Fig. 5.3 show XRD and TGA results of RCP, respectively. As shown in Fig. 5.2, the common hydration products of cement, such as portlandite, calcite and ettringite, are observed in RCP. Moreover, the presence of a belite peak indicates there is still a certain amount of unhydrated cement particles in RCP. As shown in Fig. 5.3, there are three major endothermic peaks on the DTG curves in temperature ranges of 30-200°C, 400-500°C and 600-800°C. The first peak represents the sequential dehydration of C-S-H gel and ettringite. The second peak corresponds to the dehydroxylation of $Ca(OH)_2$ crystals, and the third peak represents the decomposition of $CaCO_3$ formed by the carbonisation of the C-S-H gel and $Ca(OH)_2$ (Sun *et al.*, 2020). These endothermic peaks and mass loss of RCPP particles are higher than other RCP, demonstrating a higher content of hydration products in RCPP particles.
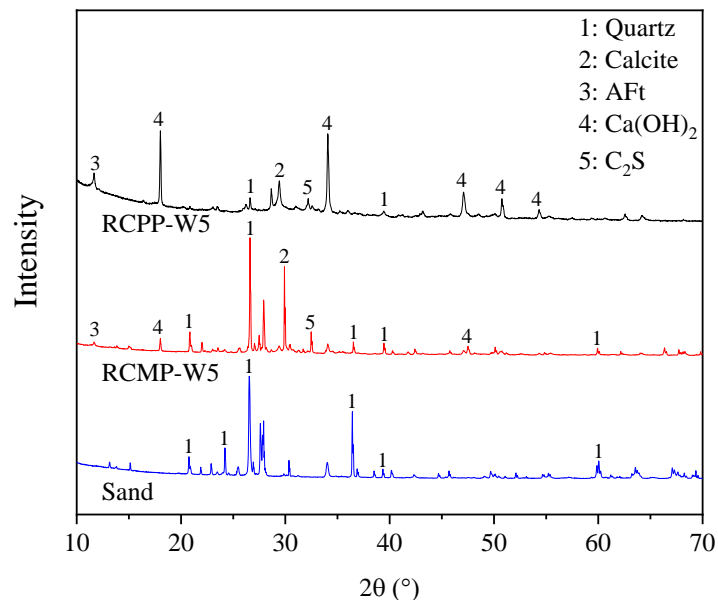
Fig. 5.2 XRD results of sand and RCP
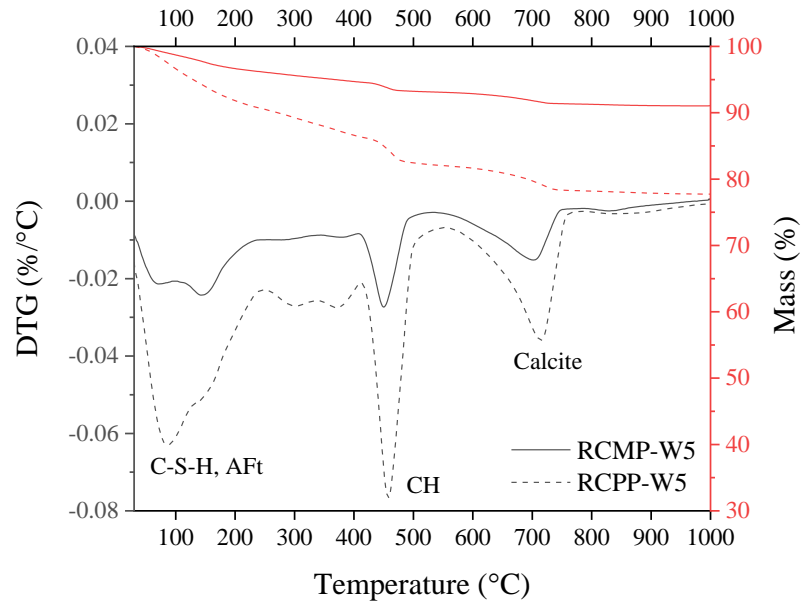
Fig. 5.3 TGA results of RCP

The micro-morphology of sand and RCP was examined by Scanning Electron microscope (SEM), as shown in Fig. 5.4. The RCPP and RCMP particles exhibit a more irregular shape and rougher surface than the sand. Massive capillary pores and microcracks exist in the RCP grains. Moreover, it can be observed that these RCP particles are usually coated with clustered hydrates, which is also confirmed by the mineralogical analysis.
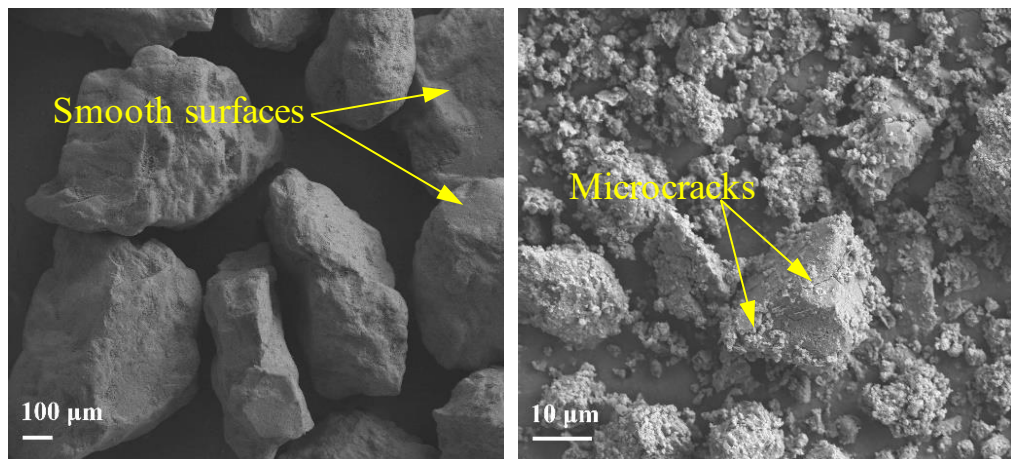
(a) Sand   (b) RCPP-W4
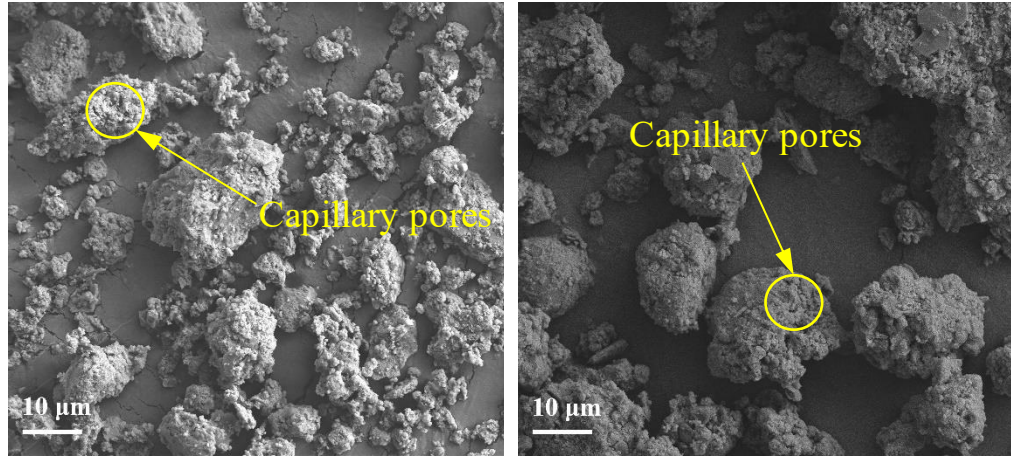
(c) RCPP-W5
(d) RCPP-W6
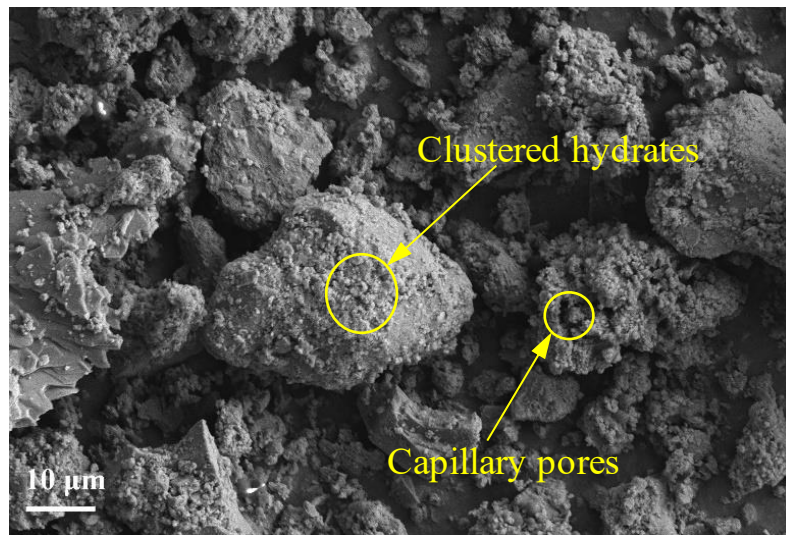
(e) RCMP-W5

Fig. 5.4 Micro-morphology of sand and RCP

The reactivity of OPC and RCP was examined using isothermal calorimeter, as shown in Fig. 5.5. As seen in Figs. 5.5(a) and 5.5(b), the exothermic peak and cumulative hydration heat of the RCP are much lower than those of the OPC, particular for the RCMP particles. For instance, the cumulative hydration heat of RCMP is approximate 7% of that of OPC. It indicates that the RCP has low reactivity, although there are unhydrated cement particles.
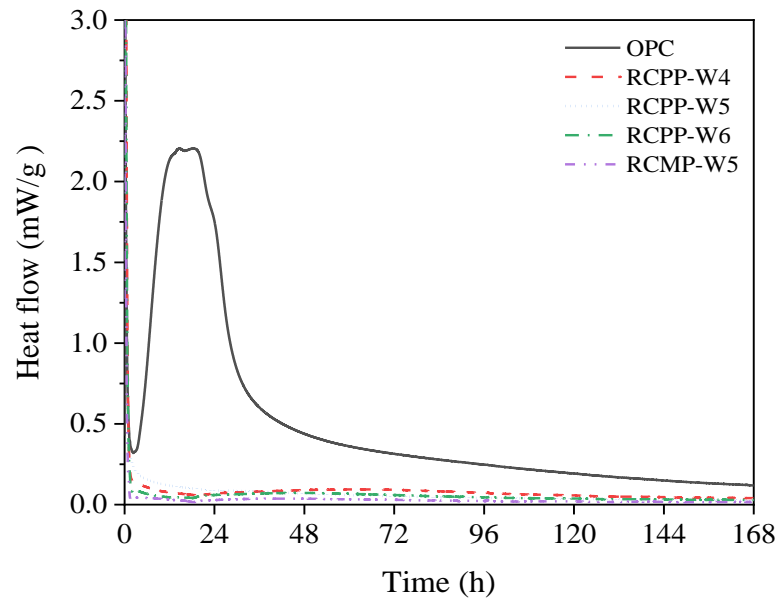
(a)
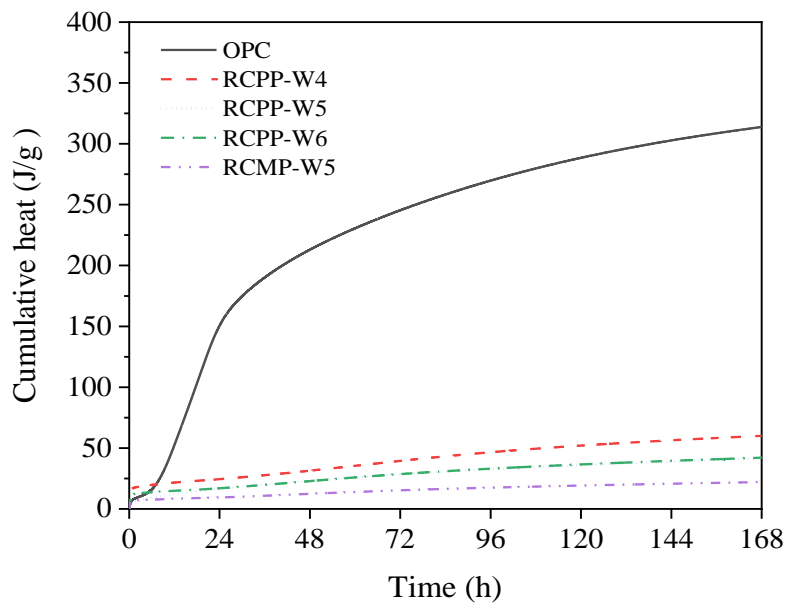
(b)

Fig. 5.5 (a) Heat flow and (b) cumulative heat release of raw materials

5.2.3 Mix formulations

Table 5.2 shows the mix proportions of mortars with or without RCP. Total 13 mix formulations were designed to investigate the influences of RCP type and replacement ratio on the properties of mortars. In addition to the reference mix, two series of mortars with RCPP or RCMP were prepared. Three different sand replacement ratios of 10%, 20% and 30% were considered for the RCP mortars.

The aggregate-to-cement ratio was fixed at 3 for all the mortars. The reference mortar without RCP was labelled as RFF, and other mixtures were named with the RCP type, original W/C ratio, and the replacement ratio. For example, mix RCPP-W5-10% represents the mixture with 10% RCP particles sourced from the hardened cement paste prepared with a W/C ratio of 0.5. The mixing water was determined to ensure mortars achieving a similar consistency of 175±10 mm based on the flowability test according to BS EN 1015-3: 1999 (BSI, 2007) with the purpose to control similar effective W/C ratio (Li *et al.*, 2019; Liang *et al.*, 2021).

Table 5.2 Mix proportions of mortars with RCP

Mix	Water	Cement	RCP	Sand
	(kg/m^3)	(kg/m^3)	(kg/m^3)	(kg/m^3)
REF	270	450	0	1350
RCPP-W4-10%	293		135	1215
RCPP-W4-20%	338	450	270	1080
RCPP-W4-30%	360		405	945
RCPP-W5-10%	300		135	1215
RCPP-W5-20%	333	450	270	1080
RCPP-W5-30%	367		405	945
RCPP-W6-10%	306		135	1215
RCPP-W6-20%	342	450	270	1080
RCPP-W6-30%	396		405	945
RCMP-W5-10%	285		135	1215
RCMP-W5-20%	307	450	270	1080
RCMP-W5-30%	334		405	945

Notes: "RCPP" and "RCMP" stand for the recycled cement paste powder and recycled cement mortar powder, respectively; and "W4", "W5", and "W6" refer to the original W/C ratio of 0.4, 0.5, 0.6, respectively; and "10%", "20%", and "30%" denote the replacement ratio of RCP, respectively.

5.2.4 Preparation of RCP mortar

The mortar samples were prepared by blending sand (or sand mixed with RCP),

OPC and water in a planetary mixer. Afterwards, the fresh mortars were poured into the moulds to cast the $25 \times 25 \times 280$ mm^3, $40 \times 40 \times 160$ mm^3 prisms and cylinders with 75 mm in diameter and 150 mm in height for the drying shrinkage and mechanical properties measurements. The samples were demoulded after curing for 24 h. Then, they were stored in a curing chamber under a constant temperature of 20°C and relative humidity of 95% until the testing age.

5.2.5 Test methods

5.2.5.1 Physical, mechanical properties and drying shrinkage

The bulk density of RCP mortars was tested according to ASTM C642-06 (ASTM Committee, 2006). Flexural and compressive strengths of mortars were evaluated as per BS EN 1015-11: 2019 (BSI, 2019a) at the curing ages of 7, 28 and 56 days. Three specimens per batch were tested, and the average strength value was recorded. The Young's modulus of mortars was determined per BS EN 12390-13: 2013 (BSI, 2019b).

The prismatic specimens with a gauge length of 250 mm were used to measure the drying shrinkage of mortars per ASTM C596-18 (ASTM Committee, 2018). The demoulded mortar samples were placed into a water tank at 20 ± 1 °C for 2 days. Afterwards, the initial lengths of the samples were recorded, and the samples were moved to an environmental chamber with a temperature of 20 ± 3 °C and relative humidity 50 ± 4%. The length changes of the specimens were recorded to calculate the average drying shrinkage of mortars at different drying ages.

5.2.5.2 Hydration heat, crystalline phase, pore structure and morphology

Hydration heat of cement with or without 10% RCP was measured using an isothermal calorimeter according to ASTM C1702–17 (ASTM Committee, 2017) to study the impact of adding RCP on the promotion of hydration (Scrivener *et al.*, 2016). Moreover, the Class F fly ash (FA) per Chinese standard GB/T 1596-2017 (Standards China, 2017) and S95 ground granulated blast-furnace slag (GGBS) following Chinese standard GB/T 18046-2008 (Standards China, 2008) were also employed as the sand replacement to compare the reactivity of RCP with them. All the samples were tested continuously for up to 7 days at a constant temperature of 20°C. The heat flow and cumulative hydration heat were

normalised per unit mass of raw materials or binder. The crystalline phases of mortars were investigated by scanning the grounded mortar powders with CuKα radiation (λ = 1.54Å) from 5° to 70° in 2θ with step of 0.02° and 2s/step.

The pore structures of the mortars at the age of 56 days were characterised using a mercury intrusion porosimeter (MIP) with a maximum pressure of 228 MPa. Small cube samples with 10-20 mm were sectioned from the specimens. Their hydration was terminated by the anhydrous ethanol exchange and then dried in a vacuum atmosphere at 60°C until constant mass. Moreover, the morphologies of mortars prepared with various types and amounts of RCP were also observed using SEM.

5.2.5.3 Particle packing density

The compressible packing model (CPM) has been adopted to optimise the particle packing statuses in various types of concrete mixtures, such as the ultra-high performance concrete (Soliman & Tagnit-Hamou, 2017b) and the recycled aggregate concrete (Amario *et al.*, 2017). In this study, the CPM was adopted to optimise the amount of RCP in combination with sand to achieve the highest particle packing density. The particle packing density of mortars with various amounts of RCP has been determined by using CPM to unveil the role of RCP in affecting the particle packing density. This model considers the interaction among all the grains and the type of compaction applied. Three parameters were pre-determined before the CPM could be applied: the particle size of each grain class (d_i), the experimentally obtained packing density of each grain class (β_i), and the mutual volume fraction of each grain class (y_i) (Bala *et al.*, 2020). The CPM considers the calculation of virtual packing density for each grain class (γ_i) using Equation (5.1). The loosening effect coefficient (a_{ij}) and the wall effect coefficient (b_{ij}) were obtained by using Equations (5.2) and (5.3), respectively. Each OPC and RCP was considered a separate grain class, represented by its diameter D_{50} (Campos *et al.*, 2020). The sand was also considered a grain class with an equivalent mono-sized particle size equal to its arithmetic mean diameter (Jiang *et al.*, 2021). The packing densities of OPC and RCP were determined using the wet packing density method (Chu *et al.*, 2021). The packing density of sand was determined per BS 812–2:1995 (BSI, 1999). The experimentally determined packing densities of OPC, RCPP-W5, RCMP-W5 and sand were

0.522, 0.420, 0.499 and 0.618, respectively. RCP shows lower packing densities than sand, which is caused by the irregular shape and rough surface of RCP, as seen in their morphologies. Based on the mix proportion, the actual packing density of a granular mixture (ϕ) could be obtained by performing the back-analysis in Equation (5.4), where the compaction energy applied to the solid mixture was considered via the compaction index (K). In this study, the compaction index K of 9 was adopted, which corresponds to vibration and compression (Roquier, 2016).

$$\gamma_i = \frac{\beta_i}{1 - \sum_{j=1}^{i-1} y_j \left(1 - \beta_i + \beta_i b_{ij} \left(1 - \frac{1}{\beta_j}\right)\right) - \sum_{j=i+1}^{n} y_j \left(1 - a_{ij} \frac{\beta_i}{\beta_j}\right)} \tag{5.1}$$

$$a_{ij} = \sqrt{1 - \left(1 - \frac{d_j}{d_i}\right)^{1.02}} \tag{5.2}$$

$$b_{ij} = 1 - \left(1 - \frac{d_i}{d_j}\right)^{1.5} \tag{5.3}$$

$$K = \sum_{i=1}^{n} K_i = \sum_{i=1}^{n} \frac{\frac{y_i}{\beta_i}}{\frac{1}{\phi} - \frac{1}{\gamma_i}} \tag{5.4}$$

5.3 Experimental results and discussion

5.3.1 Water demand of standard consistency
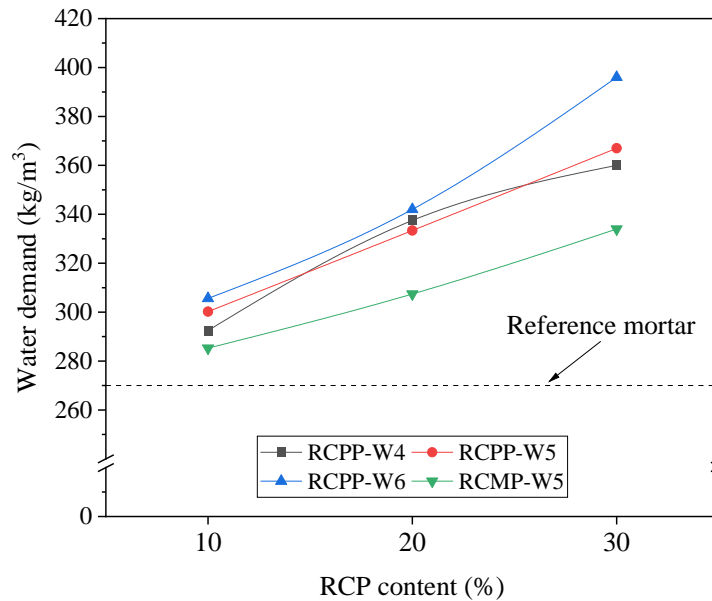
Fig. 5.6 Water demand of RCP mortars

Fig. 5.6 shows the water demand for the mortars containing different types and amounts of RCP to achieve similar consistency. Generally, the water demand for RCP mortars are higher than that of the reference mortar to maintain the same consistency and increase with the RCP content. This can be attributed to the irregular shape, rough surface, high porosity and fineness of the RCP as seen in their morphologies and particle size distributions. For example, the water demands for mortars RCPP-W4 and RCPP-W6 increase by 22.9% and 29.4% as the RCP replacement increases from 10% to 30%, respectively. The water demands for mortars with various RCPP vary marginally when the RCP replacement ratio is limited by 20%. It indicates that the water demands for mortars are insensitive to the original W/C ratios of RCP at a low replacement ratio. However, the mortar RCPP-W6-30% requires 10% higher water demand than the mortar RCPP-W4-30%, as the disturbed particle packing increases the demand on water for filling up the voids in the granular skeleton (Chu *et al.*, 2021). Moreover, the water demands for mortars with RCMP are lower than those with RCPP at the same replacement level, which can be naturally ascribed to the coarser particle size of RCMP as seen by their D_{50} results in Table 5.1.

5.3.2 dry bulk density
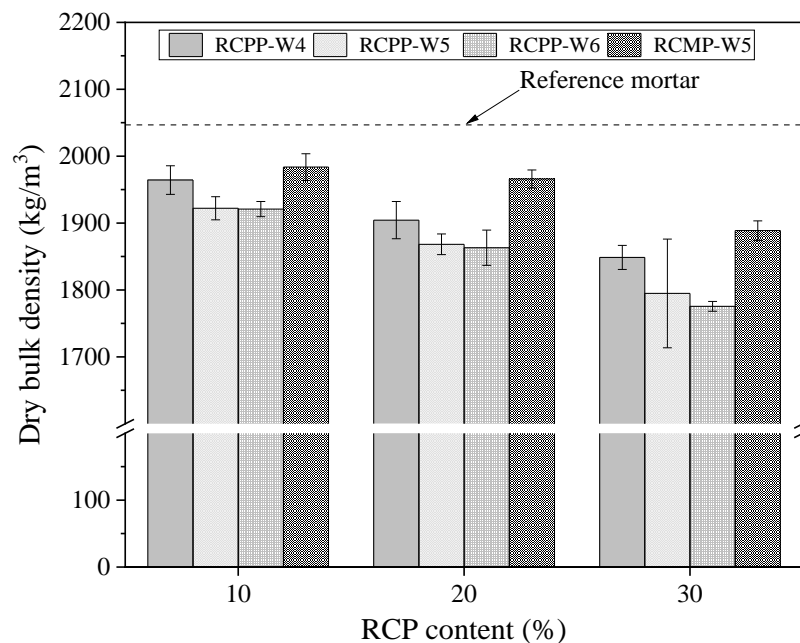
Fig. 5.7 Dry bulk density of RCP mortars

Fig. 5.7 shows the dry bulk densities of the RCP mortars against the RCP content. It is readily seen that the dry bulk densities of the mortars with RCPPs and RCMP are lower than that of the reference mortar. For example, replacing sand with 30% RCPP-W6 or RCMP-W5 decreases the dry bulk densities of mortars by 13.2% and 7.7%, respectively. It also shows that the dry bulk density of mortars generally decreases as the RCP content increases, which can be attributed to the lower densities of RCP compared to sand. The dry bulk densities of RCPP mortars are slightly lower than those of RCMP mortars. For instance, the dry bulk density of RCMP mortar is around 5% higher than that of mortar RCPP-W5 at a 30% replacement level. The use of RCPP with a higher original W/C ratio tends to slightly decrease the density of mortar with the same amount of sand replaced by RCPP. For instance, the dry bulk density of mortar RCPP-W6-30% is around 4% lower than that of mortar RCPP-W4-30%. It indicates that the variation of the original W/C ratio of the RCPP has a marginal impact on the dry bulk densities of mortars.

5.3.3 Compressive strength
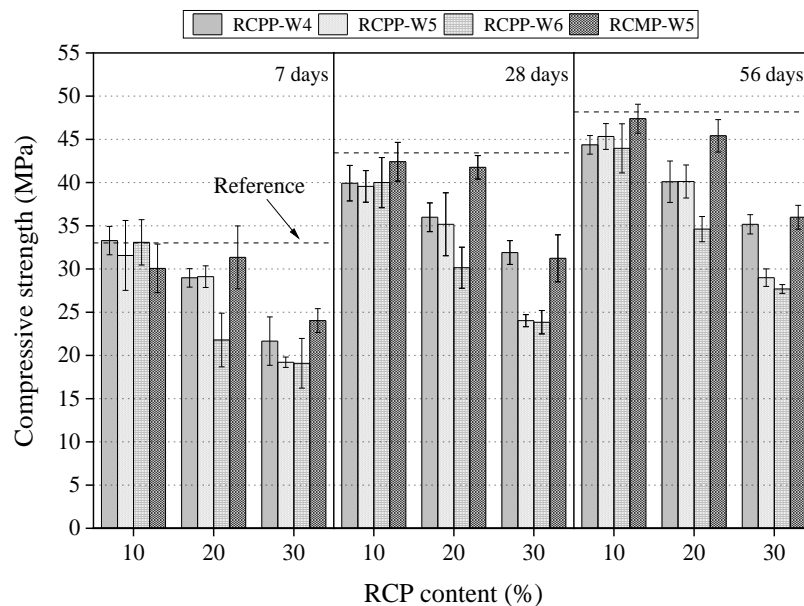
Fig. 5.8 Compressive strength of RCP mortars

Fig. 5.8 shows the compressive strengths of the mortars prepared with various types and amounts of RCP. In general, replacing sand with up to 10% RCPP or 20% RCMP has a negligible effect on the compressive strengths of mortars at

various curing ages. The use of RCP can contribute to the compressive strength development of RCP mortars through optimising their pore structures, which also compensates for the negative effects induced by the porous feature of RCP particles. Specifically, incorporating RCP can improve the packing density of mortars by filling the larger voids. Moreover, the slightly enhanced hydration reaction by adding RCP promotes the formation of hydration products, contributing to the pore structure refinement and strength development. Nevertheless, the excessive amount of RCP decreases the compressive strength as this tends to increase the total porosity of the RCP mortars due to the combined action from the decreased packing density and the high porousness of RCP particles. The RCMP mortars generally exhibit higher compressive strengths than the RCPP mortars at various curing ages, which is caused by the lower porosity of RCMP mortars. However, the 7-day compressive strengths of RCPP mortars are slightly higher than that of RCMP mortar at 10% replacement level, which is mainly attributed to the higher hydration rate in mortars with RCPP. Furthermore, the use of RCPP with a higher original W/C ratio decreases the compressive strengths of mortars with 20% or 30% RCPP, which is related to the increased porosity of RCPP prepared with a higher W/C ratio.

5.3.4 Flexural strength
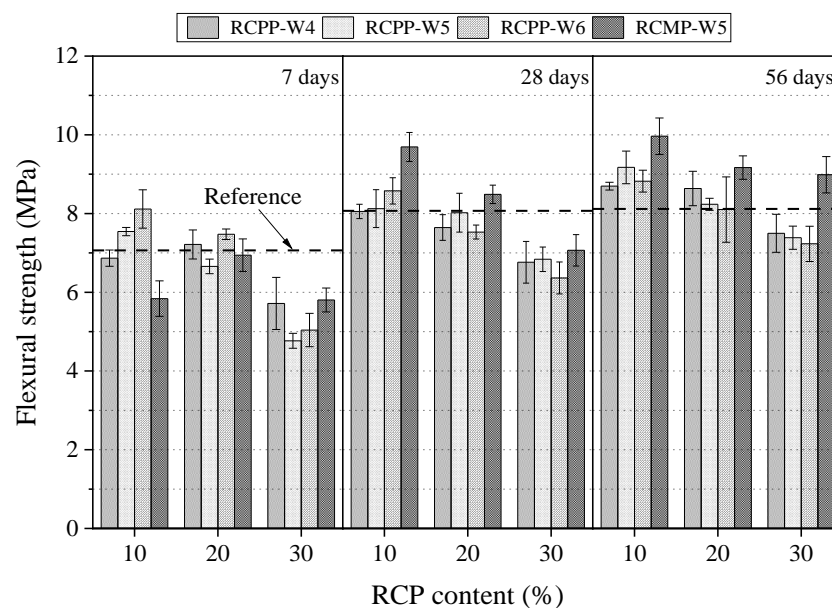
Fig. 5.9. Flexural strength of RCP mortars

Fig. 5.9 shows the flexural strengths of the mortars prepared with different types and amounts of RCP. In general, replacing sand with up to 10% RCPP or 20% of RCMP has a positive or minimal negative effect on the flexural strengths of mortars at various curing ages. Similarly, this is mainly attributed to the combined action of improved packing density and enhanced hydration reaction by adding RCP. Furthermore, the rough surface of RCP can enhance the interlocking between cement matrix and RCP, leading to a positive effect on the flexural strength (Saba & Assaad, 2021). As the RCP content increases, the flexural strengths of mortars generally decrease. For instance, the 56-day flexural strength of RCPP-W5-30% is 19.5% lower than that of RCPP-W5-10%. It indicates that the excessive amount of RCP increases the total porosity of the RCP mortars, which subsequently decreases their flexural strengths. Compared to the impact on the compressive strength, this increased porosity has a lower negative effect on RCP mortars' flexural strength, which is also consistent with findings reported by Xiao *et al.* (2018). For instance, the reduction of 56-day flexural strengths of RCPP mortars is limited by up to 11% at 30% replacement, which is lower than that of 56-day compressive strengths of RCPP mortars at the same replacement. The RCMP mortars generally exhibit higher flexural strengths than the RCPP mortars at various curing ages, which is caused by the lower porosity of RCMP mortars. For example, replacing sand with 30% RCMP increases the 56-day flexural strength of mortar by 10.7%. However, the 7-day flexural strength of RCMP mortar is around 20% lower than that of the RCPP mortars at 10% replacement, which is attributed to the lower hydration rate in RCMP mortar. Moreover, the variation of the original W/C ratio of RCPP has a marginal effect on the flexural strengths of mortars with the same amount of RCP. It indicates that the flexural strengths of mortars are insensitive to the variation of RCP porosity, which may depend more on the properties of cement paste and interfaces.

5.3.5 Young's modulus
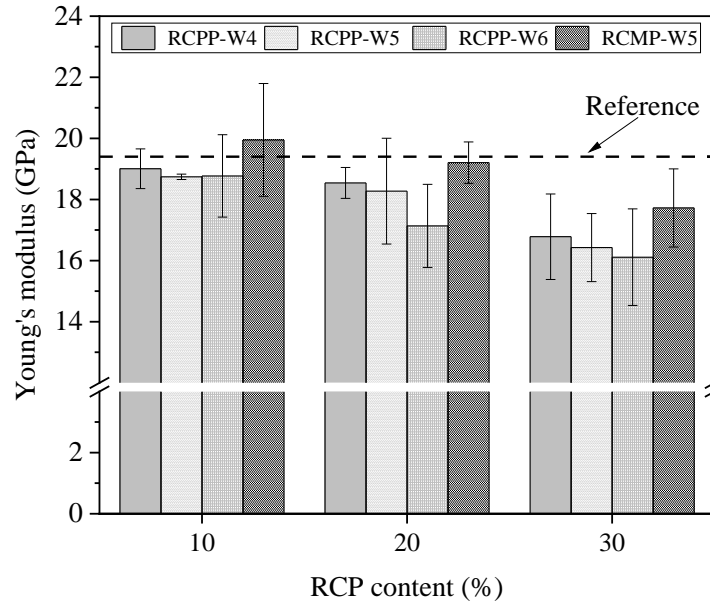
Fig. 5.10 Young's modulus of RCP mortars

Fig. 5.10 shows the 56-day Young's modulus of the mortars with various types and amounts of RCP. Similar to compressive strength, replacing sand with up to 10% RCPP or 20% RCMP has a negligible effect on Young's modulus of mortars. For instance, Young's moduli of RCPP-W6-10% and RCMP-W5-20% are slightly lower than the reference mortar. Again, this is mainly attributed to the reductions in the fraction of large voids and the total porosity with RCP incorporation in mortars. An excessive amount of RCP decreases Young's moduli of mortars. For instance, Young's moduli of RCPP-W4-30% and RCMP-W5-30% are around 12% lower than RCPP-W4-10% and RCMP-W5-10%, respectively. This is mainly due to the increased volume fraction of capillary pores and the total porosity. Besides, the higher hydration heat induced by the addition of excessive RCP tends to intensify the crack density of RCP mortars, and thereby impairing their Young's moduli (Zhang *et al.*, 2020). These also explain that the Young's moduli of RCPP mortars are lower than those of the RCMP mortars at various replacement ratios as seen in Fig. 5.10. Moreover, the use of RCPP with a higher original W/C ratio slightly decreases Young's moduli of mortars with the same amount of RCP. For instance, Young's moduli of mortars RCPP-W6-20% and RCPP-W6-30% are around 5% lower than those of RCPP-W4-20% and RCPP-W4-30%. It indicates that Young's moduli of mortars are also

insensitive to the variation of the original W/C ratio of the RCP. As concluded by the previous studies, this may be dominated by the particle packing density (Klein *et al.*, 2020; Jiang *et al.*, 2021).

5.3.6 Drying shrinkage

Fig. 5.11 shows the drying shrinkage of the mortars prepared with various types and amounts of RCP. In general, the drying shrinkages of RCP mortars mainly occur in the first week after casting. The drying shrinkages of RCP mortars are all larger than that of the reference mortar and increase with the RCP replacement level. For instance, replacing sand by 10%, 20% or 30% RCPP-W6 increases the 56-day drying shrinkage of mortars by 53%, 84% and 110%, respectively. This is attributed to the increased amount of mesopores in the RCP mortars (Collins & Sanjayan, 2000), which is confirmed by the pore structure analysis. Increasing the RCP content induces higher mesopore volume, and thereby generating higher shrinkage driving force due to the increased capillary pressure by the water meniscus (Garci Juenger & Jennings, 2002; Liu *et al.*, 2019). Moreover, the reductions in Young's modulus of RCP mortars decrease the restraint provided by the granular skeleton, which also increases the drying shrinkage (Mao *et al.*, 2021). Hence, it is also evident that the drying shrinkages of the RCMP mortars are smaller than those of RCPP mortars. For instance, the 56-day drying shrinkage of the RCMP mortar is around 30% lower than that of the mortar with RCPP-W6. Moreover, using 10-20% RCPP with a higher original W/C ratio tends to increase the drying shrinkages of mortars with the same amount of RCP. However, the drying shrinkages of mortars with various RCPP vary marginally at 30% replacement, indicating that the drying shrinkages of mortars are insensitive to the original W/C ratios of RCP.
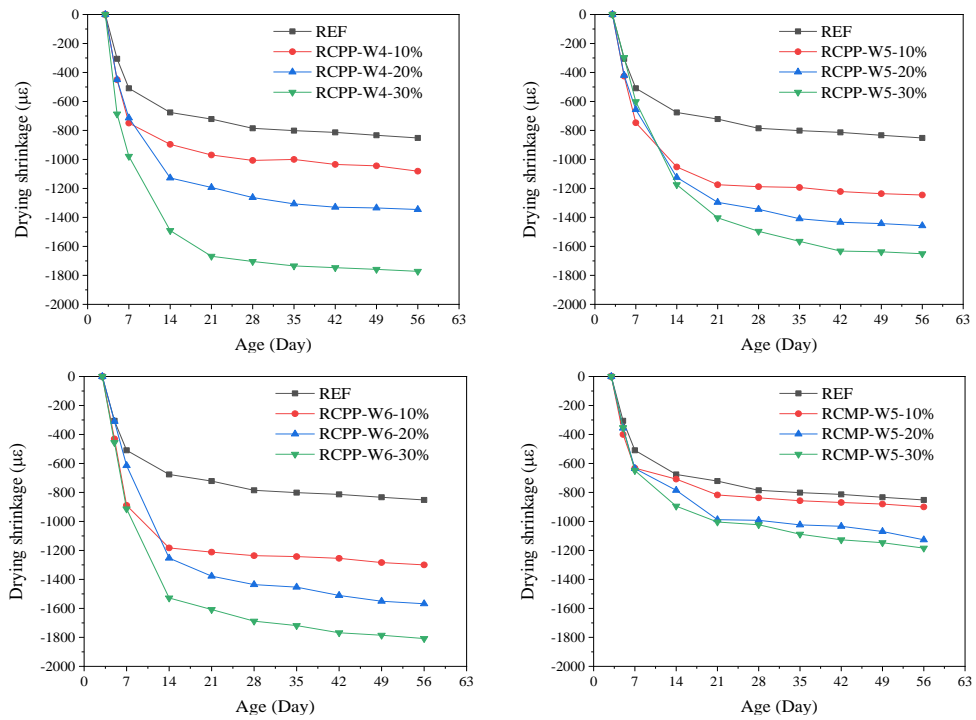
Fig. 5.11 Drying shrinkage of RCP mortars

5.3.7 Microstructural analysis

5.3.7.1 XRD analysis

Fig. 5.12 shows the XRD patterns of the mortars with or without RCP at the age of 7 days. It is evident that the incorporation of RCP as sand replacement has no impact on the change of the mineral compositions in the cement mortars. Moreover, the peak intensities of main hydration products are slightly increased after incorporating various replacement ratios and types of RCP. Specifically, the peak intensity of portlandite slightly increases with the RCPP replacement ratio. However, increasing the RCMP replacement ratio has no obvious impact on the change of mineral composition for the RCMP mortar. This is in line with the hydration heat results, and proves that the RCP particles have a low reactivity. It can also be found that the peak intensity of feldspar decreases with the RCP replacement ratio, which is associated with the decreased amount of river sand in the RCP mortars (Noda, 2005). Moreover, the change of original W/C ratios of RCP has a marginal impact on the peak intensities of main hydration products in the RCP mortars.
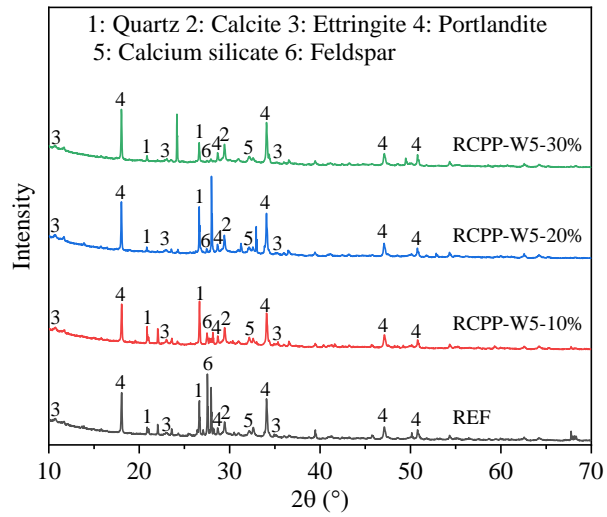
(a)
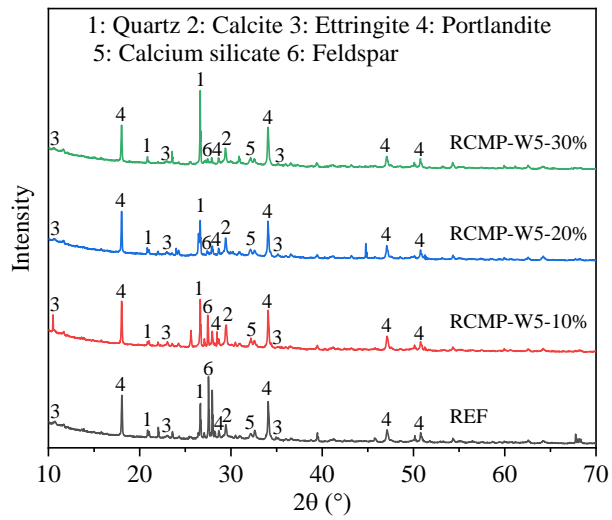
(b)
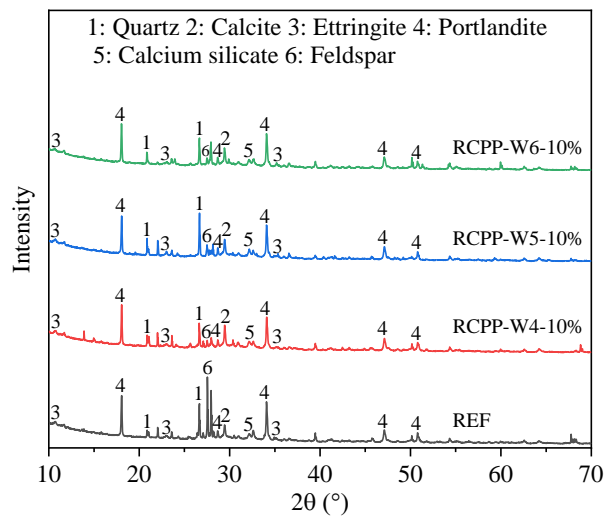
(c)

Fig. 5.12 XRD patterns of RCP mortars at 7-day curing age

5.3.7.2 SEM analysis

Fig. 5.13 depicts the morphology of the mortars prepared with various types and amounts of RCP. As seen in Fig. 5.13(a), there are massive microcracks and pores/voids inside the reference mortar (Tabatabaei *et al.*, 2020). Specifically, some microcracks exist along the rim of aggregates, which may subsequently decrease the effective bonding between cement paste and sand (Shao *et al.*, 2022). Moreover, the localised cluster of capillary pores can be found inside the reference mortar (Dong *et al.*, 2017), mainly due to the poorer particle packing status (Liu *et al.*, 2021). Differently, the mixtures RCPP-W5-10% and RCMP-W5-20% have more even and smoother texture. It indicates that adding 10% RCPP or 20% RCMP leads to a more compact microstructure with fewer microcracks (Chen *et al.*, 2021), as seen in Figs. 5.13(b) and 5.13(c). This is resulted from the combined action from the slightly enhanced hydration and filling effect of RCP particles. It reveals that the use of RCP can ameliorate the microcracking in mortars, which improves the mechanical properties of mortars. Excessive RCP potentially leads to a loose microstructure with large amounts of pores/voids and microcracks inside the matrix when comparing Figs. 5.13(b) with 5.13(d). Moreover, the massive RCP particles tend to bring about the agglomeration problem (Campos *et al.*, 2020), thereby generating more pores inside the RCP mortars, as seen in Fig. 5.13(d).
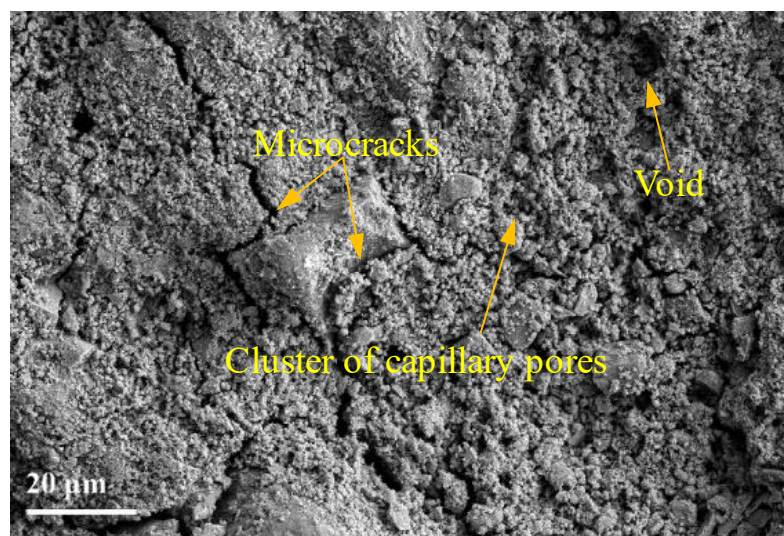
(a) REF
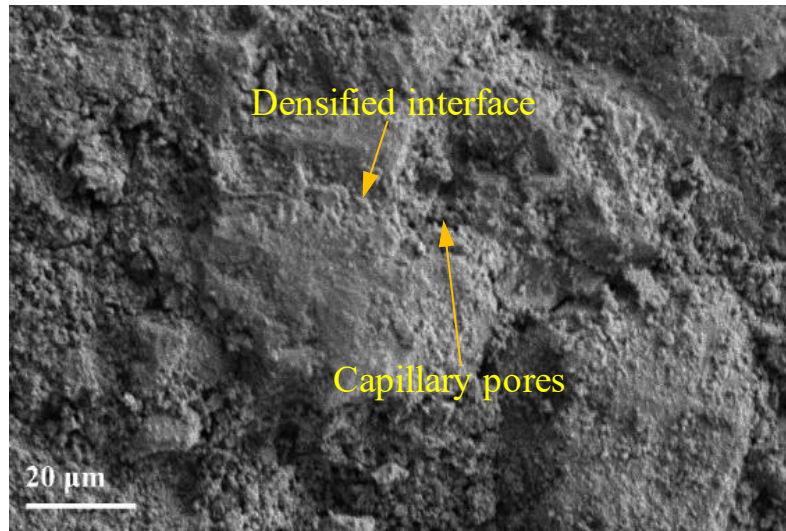
(b) RCPP-W5-10%
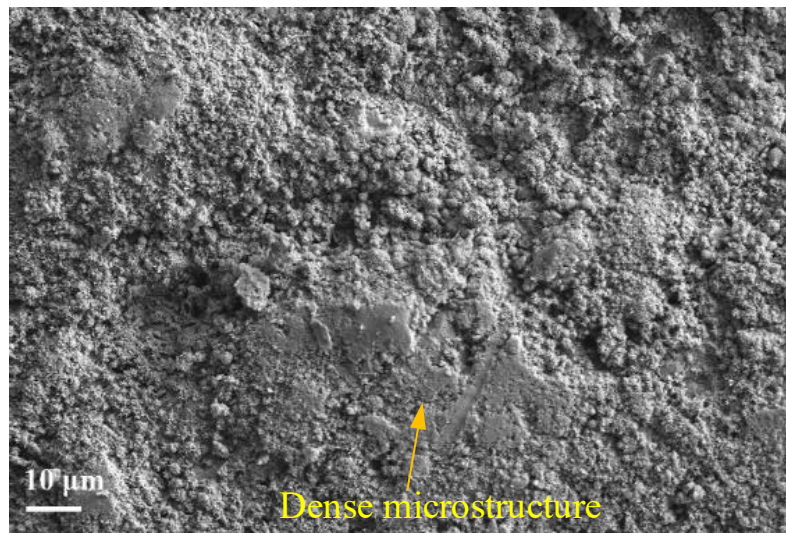
(c) RCMP-W5-20%
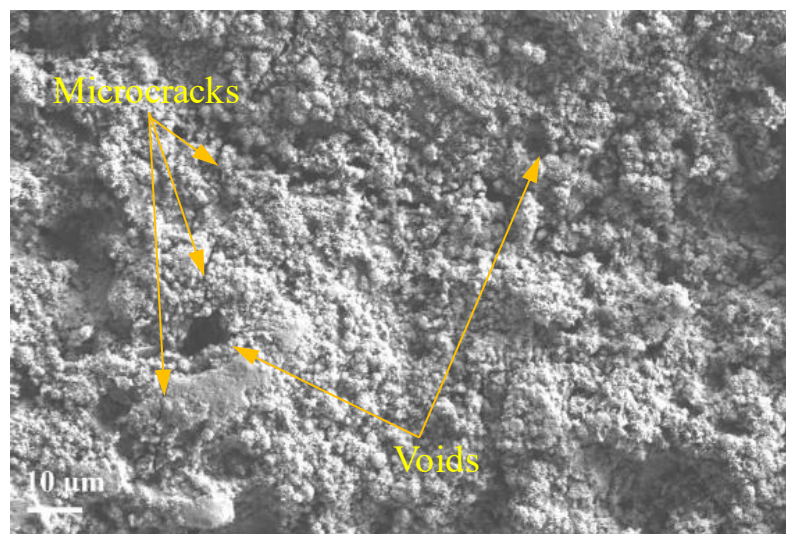
(d) RCMP-W5-30%

Fig. 5.13 Morphology of RCP mortars

5.3.7.3 MIP analysis

Fig. 5.14 shows the pore size distribution and the cumulative pore volume curves of the mortars with various types and amounts of RCP. The pores can be classified based on their sizes, including air voids with a size larger than 10 μm, large capillary pores with a size between 50 nm and 10 μm, medium capillary pores with a size between 10 and 50 nm, and gel pores with a size smaller than 10 nm (Dong *et al.*, 2017). Compared with the large capillary pores and air voids, medium capillary pores and gel pores generally have a negligible effect on the compressive strength but have a considerable influence on matrix shrinkage (Pang *et al.*, 2009; Sun *et al.*, 2020). Table 5.3 summarises the volume fractions of four types of pores in mortars with or without RCP. It shows that the reference mortar possesses a large volume fraction of large capillary pores and air voids. However, the addition of 10% RCPP or 10-20% RCMP tends to decrease the volume fractions of these macropores. For instance, adding 20% RCMP-W5 decreases the volume fractions of large capillary pores and air voids from 18.71% and 1.48% for the reference mortar to 16.17% and 1.02%, respectively. The RCP particles can fill the voids and improve the packing density of mortars, thereby lowering the large voids. Specifically, the addition of RCPP or RCMP can effectively decrease the volume of large capillary pores with a diameter between 1 μm and 10 μm, whereas it increases the volume of pores with a diameter ranging from 50 nm to 1 μm. This suggests that the use of RCP as sand replacement can refine the large capillary pores through reducing their size and volume fraction. Meanwhile, the volume fraction of medium capillary pores or gel pores increases with the addition of RCPP or RCMP, especially for the medium capillary pores. It is clear that the increment in volume of pores with a diameter ranged from 20 nm to 50 nm occurs in the RCP mortars. For instance, the volume fraction of medium capillary pores in the reference mortar is 2.89%, and it is increased to 3.78% and 3.68% for the mortar RCPP-W5-10% and RCMP-W5-20%, respectively. This increase would induce a larger shrinkage driving force inside the RCP mortars, leading to their larger drying shrinkages.

Replacing sand by up to 10% RCPP or 20% RCMP leads to a lower porosity in RCP mortars than the reference mortar through reducing the volume fraction of large capillary pores and air voids. For instance, the total porosity is reduced

from 23.31% in the reference mortar to 20.86% and 21.12% by adding 10% RCPP-W5 and 20% RCMP-W5, respectively. Besides the filling effect of RCP, the slightly enhanced hydration reaction also contributes to the densification of their microstructures. Hence, incorporating a proper amount of RCP as a sand replacement can contribute to the refinement of pore structure by decreasing the volume fraction of large capillary pores, air voids and the total porosity. The marginal or slightly positive effect of adding RCP on the mechanical properties of mortars is closely related to the improvement in the pore structure. An excessive amount of RCPP or RCMP causes a higher porosity in mortars due to the increased volume fraction of capillary pores. It can be found that adding 30% RCPP or RCMP shifts the uplift peak in the pore size between 10 nm and 1 μm towards the larger pore size. It indicates that the higher replacement of sand by RCP can disturb the particle packing state, generating more coarse pores inside the mortars. Moreover, the volume fraction of large capillary pores, air voids and the total porosity of RCPP mortars are larger than those of RCMP mortars at the same replacement level, which also helps to explain the better mechanical properties of the RCMP mortars than the RCPP mortars.
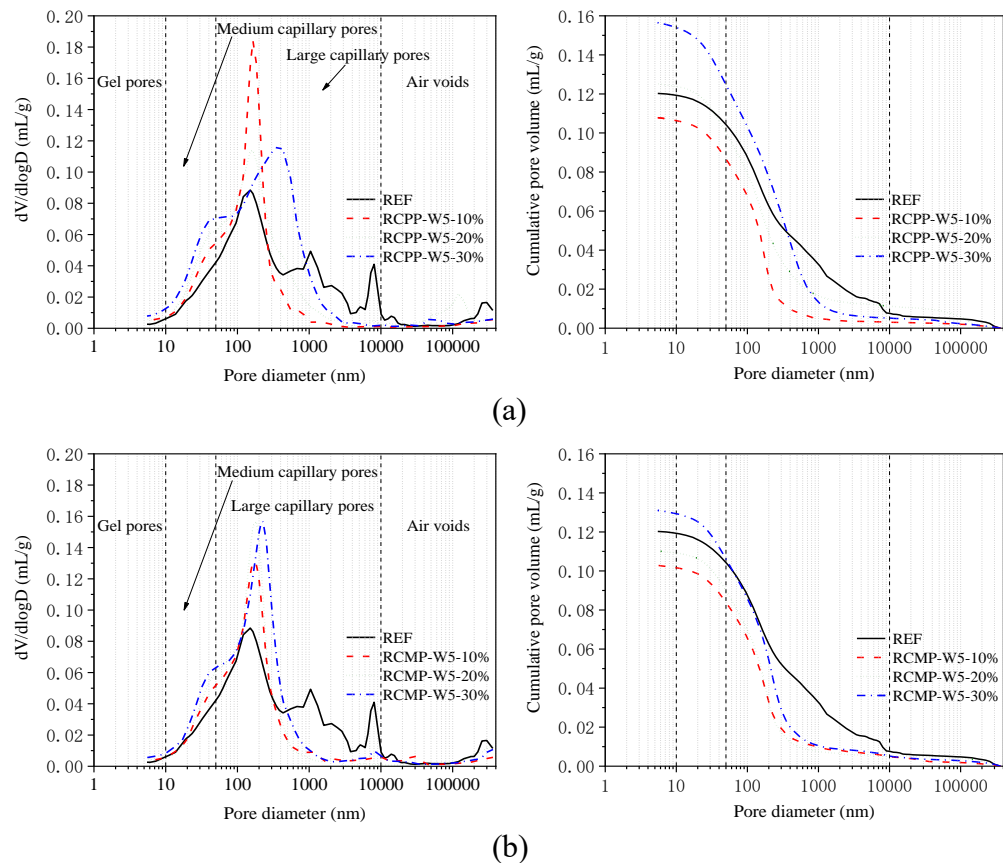
Fig. 5.14 Pore size distributions of mortars with (a) RCPP; and (b) RCMP

Table 5.3 Pore size distributions of mortars with or without RCP

Mix	Gel pores (%)	Medium capillary pores (%)	Large capillary pores (%)	Air voids (%)	Total porosity (%)	Median pore diameter (nm)
REF	0.24	2.89	18.71	1.48	23.31	216.64
RCPP-W5-10%	0.35	3.78	16.13	0.60	20.86	141.04
RCPP-W5-20%	0.31	4.44	16.64	2.10	23.49	149.46
RCPP-W5-30%	0.52	5.04	20.68	0.90	27.15	196.01
RCMP-W5-10%	0.30	3.46	15.45	1.00	20.21	144.47
RCMP-W5-20%	0.25	3.68	16.17	1.02	21.12	143.74
RCMP-W5-30%	0.39	4.41	19.27	0.99	25.06	165.69

5.3.8 Particle packing density
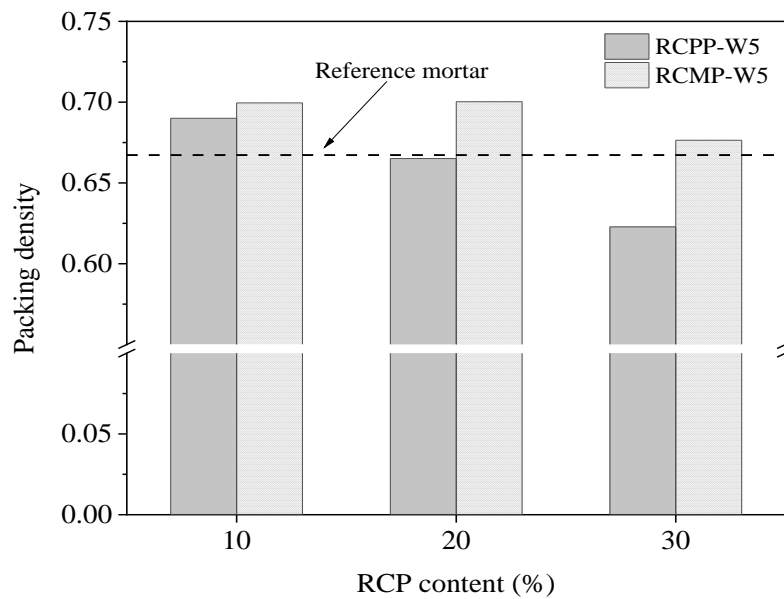
Fig. 5.15 Packing density of RCP mortars

115

Fig. 5.15 shows the packing density of mortars with various amounts and types of RCP. It can be found that the packing density of the mortars with 10% RCPP or 10-30% RCMP is larger than that of the reference mortar. It indicates that the addition of RCP can increase the particle packing density of RCP mortars, which is beneficial to the formation of a densely packing system (Fan *et al.*, 2020). This is achieved by filling larger voids with the smaller particles of RCP. As discussed in the pore structure, adding a maximum 10% RCPP or 20% RCMP decreases the volume fraction of large capillary pores and air voids, leading to reduced porosity in RCP mortars. An excessive amount of RCP would exceed the volume of voids created by the large-size aggregate skeleton, which decreases the particle packing density in mortars. Consequently, adding RCPP from 10% to 30% or RCMP from 20% to 30% decreases the packing density of RCP mortars, as seen in Fig. 5.15. The loosened packing state of the granular skeleton generates a higher amount of coarse capillary pores, which subsequently increases the porosity in RCP mortars, as seen in Figs. 5.14(a) and 5.14(b). The mortar RCMP-W5-30% exhibits a higher porosity than the reference mortar, even though its particle packing density is slightly higher than that of the reference mortar, as seen in Figs. 5.13(b) and 5.14. This discrepancy indicates that the particle packing density does not solely dominate the porosity in RCP mortar. The high amount of RCP can increase the porosity in RCP mortar induced by the porousness of RCP particles regardless of the particle packing density. Moreover, it also shows that the RCMP particles exhibit a better filling effect than the RCPP particles as the packing density of RCMP mortar is higher than that of RCPP mortar with the same amount of RCP. This is in line with the pore structure results in the previous section, which explains that the RCMP mortar exhibits a lower volume fraction of macropores and the total porosity than the RCPP mortar. Therefore, the proper addition of RCP as sand replacement can enhance the particle packing density due to its filling effect, which subsequently densifies the pore structure of RCP mortar. It reveals the importance of particle packing optimisation in the development of high-performance RCP mortar.

5.3.9 Hydration reaction
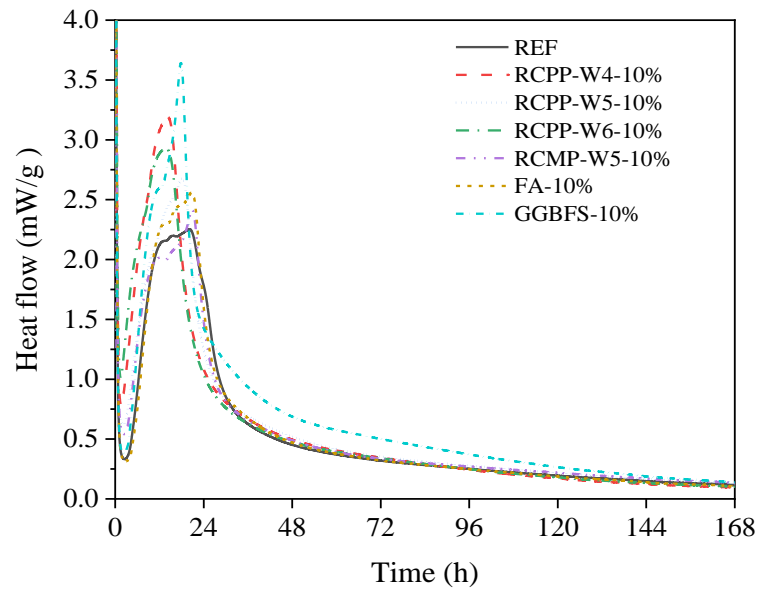
(a)
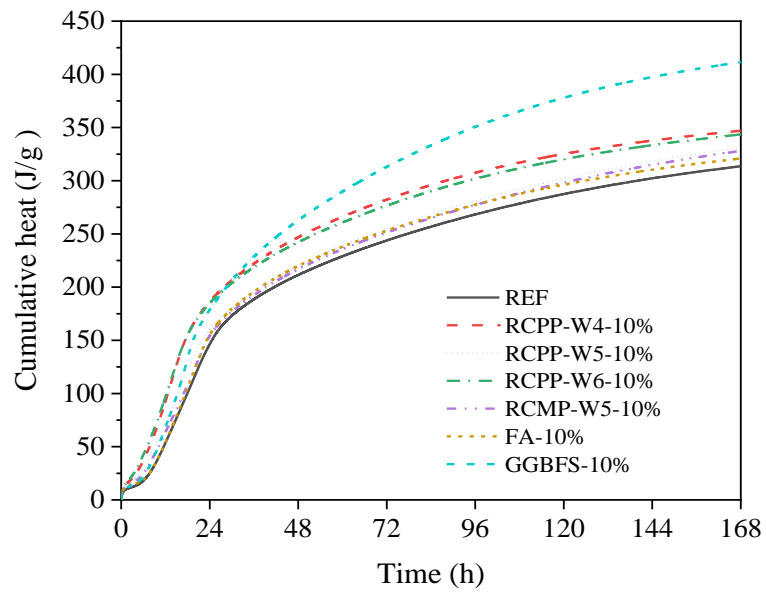
(b)

Fig. 5.16 Hydration heat of RCP mortars: (a) heat flow and (b) cumulative heat release

Fig. 5.16(a) shows that the exothermic peak rates of the RCP mortars are higher than that of the reference mortar. Specifically, the exothermic peak rates of the mortars with 10% RCPP-W4, RCPP-W5, RCPP-W6, RCMP-W5 are 41.5%, 19.6%, 30.4% and 7.6% higher than that of the reference mortar, respectively. Moreover, the exothermic peak for the reference mortar occurs at about 20 h, whereas the mortars with 10% RCPP-W4, RCPP-W5, RCPP-W6 advance it to

14 h, 18 h and 13 h, respectively. This demonstrates that the addition of RCP accelerates the early hydration of mortars. Fig. 5.16(b) also shows that the addition of RCP increases the cumulative hydration heats of mortars by a certain degree. The cumulative hydration heats of the mortars with 10% RCPP-W4, RCPP-W5, RCPP-W6, RCMP-W5 are 10.9%, 5.8%, 9.7% and 4.7% higher than that of the reference mortar, respectively. The cumulative hydration heats of all the RCP mortars are higher than that of the mortar with 10% FA, but are lower than that of the mortar with 10% GGBS. Again, this finding confirms that the addition of RCP as the sand replacement can slightly promote the hydration reaction in cement mortar. Moreover, the RCMP mortar exhibits a lower exothermic peak rate and cumulative hydration heat than the RCPP mortars, which is mainly caused by the lower reactivity of RCMP particles. However, there is no general relationship between the variation of the original W/C ratio of RCPP and the hydration rate of mortars with the same replacement of sand by RCPP.

5.4 Summary

This paper investigated the role of RCP as sand replacement in the properties of cement mortar. The physical properties, mechanical properties and microstructures of cement mortar with various amounts of RCP were evaluated. The following conclusions can be drawn based on the experimental results and discussion.

- The water demands for RCP mortars are higher than that of the reference mortar to maintain similar consistency. The water demand for RCP mortar increases by up to 29.4% as the RCP replacement increases from 10% to 30%. The dry bulk densities of RCP mortars decrease as the RCP replacement ratio increases. Replacing sand with 30% RCP decreases the dry bulk density of mortar by up to 13.2%. These can be attributed to the irregular shape, rough surface, high porosity and fineness of the RCP used in the mortars.

- Replacing sand by up to 10% RCPP with various original W/C ratios or 20% RCMP has a negligible negative effect on the compressive strength and

Young's moduli of mortars, whereas leading to a positive effect on the flexural strength. This is mainly attributed to a refinement of microstructure by decreasing the volume fraction of large capillary pores, air voids and the total porosity.

- The addition of RCP as sand replacement increases the drying shrinkage of mortars, particularly for those with RCPP. Replacing sand with 30% RCP increases the 56-day drying shrinkage of mortar by up to 110%. This is mainly caused by the increased volume fraction of mesopores in RCP mortars.

- Replacing sand by 10% RCPP or 20% RCMP maximises the particle packing density by filling the larger voids with the smaller particles, densifying the granular skeleton inside RCP mortars. Moreover, adding RCP as the sand replacement advances the exothermic peaks and increases the hydration heats of mortars by a certain degree. The cumulative hydration heat of mortar is increased by 4.7%-10.9% by adding 10% RCP. It indicates that the RCP slightly promotes the hydration reaction in cement mortar.

- Using RCP as the sand replacement can be an effective strategy to maximise the recycling and reusing C&D wastes and enhance the sustainability of mortars. An appropriate replacement of sand by RCP optimises the pore size distribution and reduces the total porosity of cement mortars by enhancing the particle packing density and slightly promoting the hydration reaction. Thus, it is recommended to adopt the particle packing method to design the high-performance RAC with RCP as sand replacement.

CHAPTER 6

LIFE CYCLE ASSESSMENT OF PACKING-OPTIMISED RECYCLED AGGREGATE CONCRETE

6.1 Introduction

Using packing-optimised recycled aggregate concrete (RAC) and replacing natural sands with recycled concrete powder (RCP) show the merit of improving the sustainability of concrete production. However, their environmental benefits have not been quantitatively demonstrated in the literature. Therefore, this chapter first presents a life cycle assessment (LCA) on the environmental impacts of optimising the packing status of RCAs in concrete. Moreover, the environmental benefits of using RCP as sand replacement in mortar are also quantified. The findings of this chapter can advance the use of particle packing optimisation in the concrete mix design from the perspective of environmental protection.

6.2 Methodology

Life cycle assessment (LCA) is a technique employed to evaluate the environmental impacts of products by tracing the resources used in production, such as energy and materials, and noting any wastes created or environmental releases (like emissions) across the entire life cycle of a product. By compiling this information, the environmental impact of different products can be examined and potential strategies to reduce ecological detriment can be proposed (Marinković *et al.*, 2010). According to ISO 14040 (ISO, 2006a) and ISO 14044 (ISO, 2006b), LCA is conducted via four steps: (1) goal and scope definition, (2) life cycle inventory analysis, (3) life cycle impact assessment, and (4) results interpretation. First of all, the goal and scope of this study and the resulting system boundaries are defined. Afterwards, the life cycle inventory analysis is performed to quantify all the data related to the materials and energy inputs and outputs to the environment in the system. For the life cycle impact assessment, the environmental impacts of the system phases are assigned to different impact categories. In the interpretation phase, the impacts of optimising the packing

status of RCAs and using RCP as sand replacement on the concrete environmental performance are analysed and evaluated with the purpose of drawing conclusions or make recommendations.

6.2.1 Goal and scope

Mix proportioning design significantly influences the environmental performance of concretes as it is related to the emissions associated with the raw materials used in concrete production, along with their energy consumption. In this study, the purpose of this LCA study is to evaluate the environmental benefits of adopting packing-optimised RAC and using RCP as sand replacement. Moreover, a comparative analysis is also performed for NAC and RAC to highlight the effect of particle packing optimisation on enhancing sustainability of RAC.

6.2.2 Function unit

The functional unit considered is the preparation of 1 m^3 of ready-mixed NAC and RAC, considering the same 28-day compressive strength and Young's modulus as demonstrated in Chapter 3. Moreover, Chapter 5 has demonstrated the replacing sand with up to 20% RCP has a negligible effect on the mechanical properties. Therefore, the packing-optimised RAC with 20% RCP as sand replacement is chosen for comparison with that without RCP. The mix proportions of concretes considered in this study are shown in Table 6.1. The mixtures are named with the concrete type (*i.e.,* NAC or RAC), the concrete design method (*i.e.,* TM or PPM), and the RCP replacement ratio. For example, mix RAC-PPM-RCP20 represents the packing-optimised RAC mixture with 20% RCP as sand replacement.

Table 6.1 Mix proportions of NACs and RACs

Mixture ID	Water (kg/m³)	Cement (kg/m³)	NCAs or RCAs (kg/m³)			River sand (kg/m³)	RCP (kg/m³)
			Size class (mm)				
			5-10	10-16	16-20		
NAC-TM	230	548	539		539	545	-
NAC-PPM	230	548	385	118	476	646	-
RAC-PPM	230	548	300	198	206	808	-
RAC-PPM-RCP20	230	548	300	198	206	646	162

Notes: (1) TM denotes the traditional concrete design method as per JGJ55-2011 (Standards China, 2011) and (2) PPM denotes the concrete design based on particle packing optimisation.

6.2.3 System boundaries

The cradle-to-gate system boundary for NAC/RAC production is graphically illustrated in Fig. 6.1. The steps considered in this system boundary are: (a) production/extraction of the raw materials, (b) transportation, and (c) concrete production as per the functional unit.
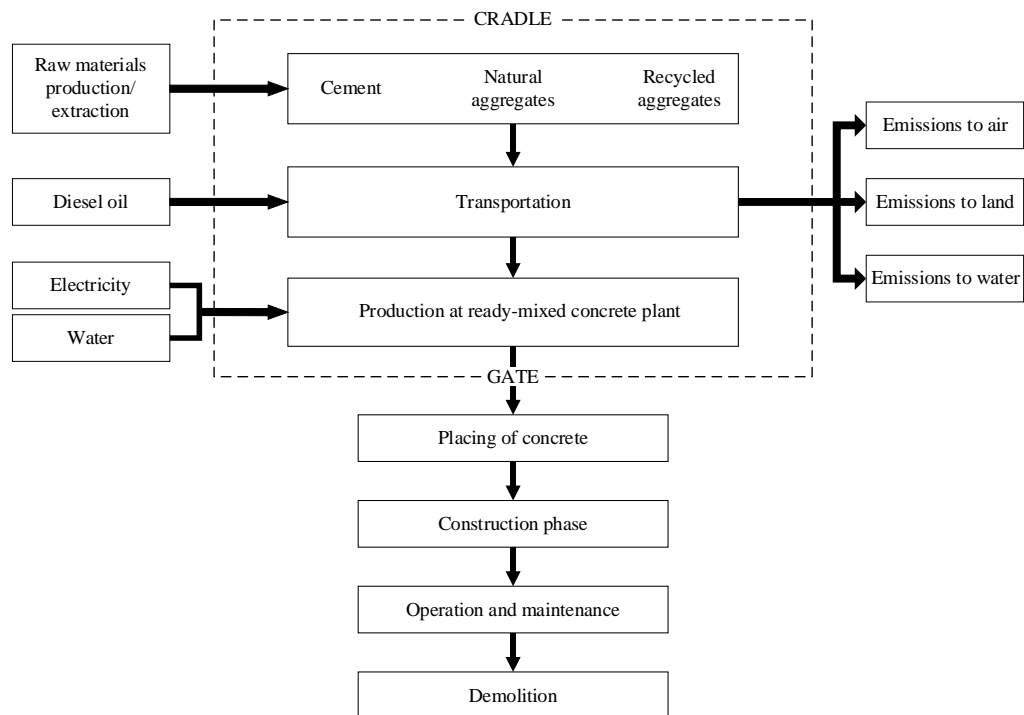
Fig. 6.1 System boundary of the concrete production

6.2.4 Life cycle inventory

Life cycle inventory (LCI) analysis is conducted to quantify all the amount and type of resources used and the amount of emissions created across all stages of a product's life, by means of a mass and energy balance (La Rosa *et al.*, 2013). The Ecoinvent database is the most integrated LCI database available, containing over 18 thousand verified datasets that have been rigorously tested for precision and thoroughness. Therefore, all the background LCI data for the inputs of raw materials, fuel and energy and the outputs of emissions to the air, water and land within the system boundary refer to the Ecoinvent 3.8 database.

The LCI data for raw materials processing of cement, river sand, and limestone aggregates are directly collected from the Ecoinvent 3.8, and their environmental impacts have been summarised in Table 6.2, and the corresponding processes are depicted in Figs. 6.2, 6.3 and 6.4, respectively. The transportation distance for delivering all raw materials is assumed to be 50 km.

The LCI data for the production of RCAs refers to Pradhan *et al.* (2019) as this data is not available in the Ecoinvent database. For the production of RCAs, the waste concretes are sorted from the Construction and Demolition (C&D) wastes and then fed to the recycling facilities with a wheel loader. After passing through the conveyor belt to the impact crusher, the waste concretes are finally sent to the jaw crusher. Vibrating screens are then employed in order to separate the RCAs into different sizes. During the recycling process, water sprinklers are used close to the crushers. The excavator is used to collect the thoroughly prepared RCAs and store them in open piles. More specifically, the production of one-ton RCAs needs 3.6 MJ diesel fuel for sorting and feeding the waste concrete, 4.32 MJ diesel fuel for storing the RCAs, 2.15 kWh electricity for crushing and screening, and 5 kg water for dust controlling by water sprinklers. The environmental impacts of additional processing for NCAs and RCAs used in the packing-optimised concretes are also considered, and this process of producing 1 ton natural or recycled aggregates consumes about 1.1 kWh electricity mainly for the additional sieving (Hossain *et al.*, 2016). Moreover, the RCP is a by-product from the C&D wastes recycling plant, normally deemed as a solid waste for landfilling. However, the RCP herein is considered as a potential sand replacement in the sustainable concrete production and the environmental impacts of recycling process for RCP are considered. These recycling processes empirically consume electricity of about 0.02 kWh per kg RCP, which is mainly for the additional sorting and sieving processes (Chen *et al.*, 2022). The LCI data considered for the diesel fuel, electricity and water used in the recycling of the RCAs and RCP into packing-optimised RAC production are directly collected from the Ecoinvent 3.8, and the environmental impacts of producing 1 kg of the RCAs or RCP have been summarised in Table 6.2, and each process of recycling RCAs and RCP is shown in Fig. 6.5.

Table 6.2 Data sources of LCA

Life cycle phase	Data source
Cement	Ecoinvent 3.8 database, Cement, Portland {RoW}
River sand	Ecoinvent 3.8 database, Sand {RoW}
Limestone aggregates	Ecoinvent 3.8 database, Gravel, crushed {RoW}
Diesel fuel	Ecoinvent 3.8 database, Diesel, burned in building machine {GLO}
Electricity	Ecoinvent 3.8 database, Electricity, medium voltage {GLO}
Water	Ecoinvent 3.8 database, Tap water {RoW}
Transportation	Ecoinvent 3.8 database, Transport, freight, lorry 7.5-16 metric ton, EURO3 {RoW}|
Recycled concrete aggregate	Pradhan *et al.* (2019)
Recycled concrete powder	Chen *et al.* (2022)
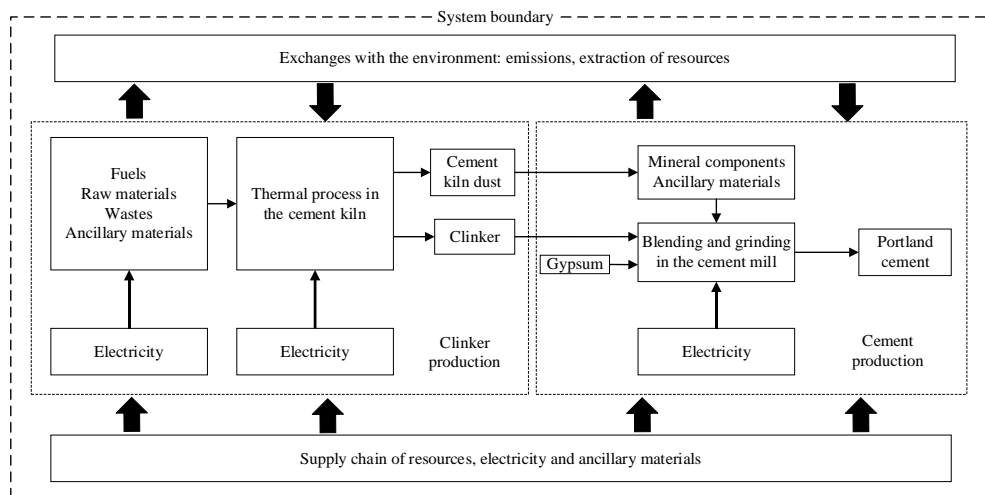
Fig. 6.2 Cement production process (Boesch & Hellweg, 2010)
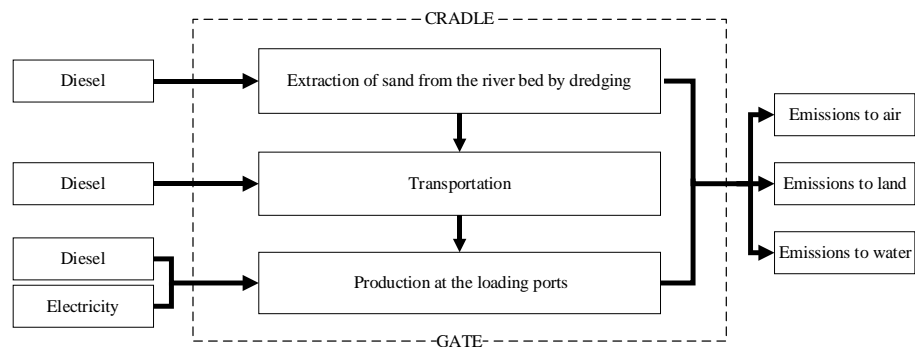
Fig. 6.3 River sand production process
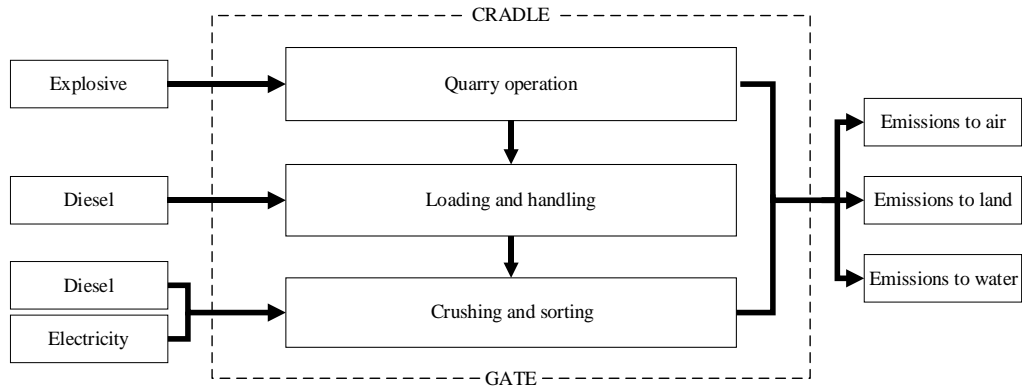
Fig. 6.4 Limestone aggregate production process
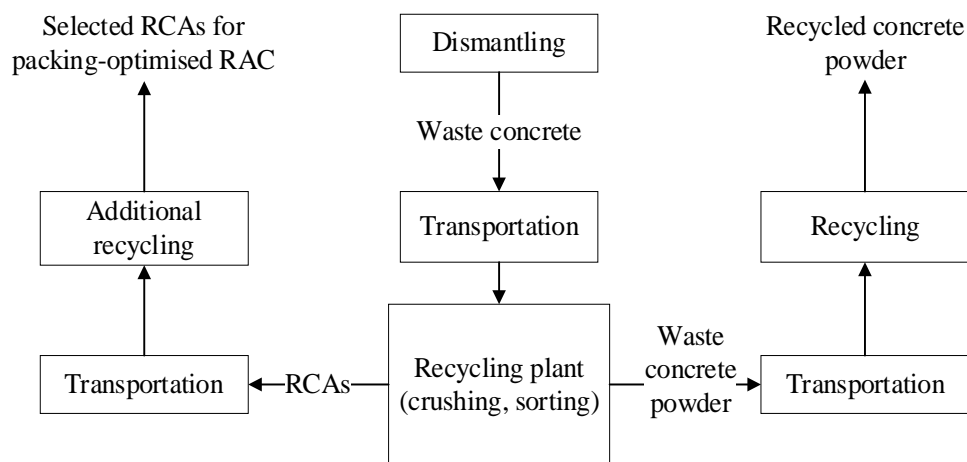
Fig. 6.5 RCAs and RCP production process

6.2.5 Life cycle impact assessment

Life cycle impact assessment (LCIA) tends to evaluate the magnitude and significance of all the environmental impacts obtained in the LCI analysis by aggregating the LCI results into an indicator result, whereas the optimal normalization, weighting and grouping are applied (Hossain *et al.*, 2016). In this study, a midpoint-oriented and hierarchist approach as defined by ReCiPe method is implemented in the LCIA to minimise the spatial uncertainty due to lack of the specific region data (Gursel & Ostertag, 2017). The environmental impact indicators being considered include global warming, stratospheric ozone depletion, terrestrial acidification, freshwater eutrophication, and land use. Non-renewable energy consumption is another environmental impact considered in this study, which is based on the cumulative energy demand method. The LCIA calculation is performed by using SimaPro 9.3.

Table 6.3 Environmental impact of each 1 kg of raw material production (ReCiPe and cumulative energy demand methods)

Impact category	Unit	Cement	River sand	Limestone aggregates	Recycled concrete aggregate	Recycled concrete powder
Global warming	kg CO_2-eq	0.849	0.005	0.012	0.004	0.002
Stratospheric ozone depletion	10^{-8} kg CFC11-eq	8.29	0.27	0.56	0.11	0.04
Terrestrial acidification	10^{-5} kg SO_2-eq	139.19	2.59	4.90	1.55	0.72
Freshwater eutrophication	10^{-7} kg P-eq	1041.86	8.13	71.3	7.34	3.92
Land use	10^{-4} m^2a crop-eq	127.36	145.08	6.34	0.50	0.25
Non-renewable, fossil	MJ	3.62	0.07	0.15	0.04	0.02

6.3 Interpretation of results

6.3.1 Environmental assessment of packing-optimised RAC

The quantified environmental impacts of concretes in various impact categories are summarised in Table 6.3 and normalised with respect to those of the reference mix NAC-TM, as presented in Fig. 6.6. The mix NAC-PPM shows a better environmental performance than the mix NAC-TM in terms of global warming, stratospheric ozone depletion, terrestrial acidification, freshwater eutrophication, and non-renewable energy. The application of PPM in concrete mix design increases the sand volume for maximising the packing density, which facilitates the reduction of concrete environmental impacts on those categories by decreasing the volume of limestone aggregates with the relatively higher impacts as seen in Table 6.2.

Moreover, the incorporation of RCAs as coarse aggregate replacement can further decrease most of environmental impacts of packing-optimised concrete considered in this study. More specifically, the global warming, stratospheric ozone depletion, terrestrial acidification, freshwater eutrophication, and non-renewable energy of the mix RAC-PPM are around 2%, 8%, 5%, 9% and 5% lower than those of the mix NAC-PPM. This is mainly attributed to the fact that the environmental impacts of natural aggregates are higher than those of the RCAs in terms of these impacts as seen in Table 6.2, which is consistent with the findings reported by Xing *et al.* (2022). Nonetheless, it can be found that these environmental benefits of fully replacing NCAs with RCAs in concrete are not remarkable, although the use of RCAs can mitigate the demand for natural aggregates in concrete production. The main reason for that is the significantly greater environmental impacts of cement on the global warming, stratospheric ozone depletion, terrestrial acidification, freshwater eutrophication, and non-renewable energy in comparison with those of other life cycle phases as seen in Fig. 6.7.

However, Fig. 6.6 also shows that the mixes NAC-PPM and RAC-PPM exhibit a higher impact on the land use than the mix NAC-TM. The land use of mixes NAC-PPM and RAC-PPM is about 9% and 19% higher than that of mix NAC-TM, respectively. This is associated with the large amount of land use required for the river sand extraction. As seen in Table 6.2, the environmental impact of

river sand on the land use is the highest among all the raw materials, reaching about 14% higher than that of cement. Moreover, packing-optimised concretes generally need more fine aggregates to fill the voids among the coarse aggregates to improve the packing density. As a result, the higher sand volume required for the packing-optimised concrete can lead to a greater impact on the land use as seen in Fig. 6.7, particularly for the mix RAC-PPM. Hence, the utilisation of particle packing method for high-performance RAC design could achieve the desired properties as NAC but increase its environmental burden in terms of land use.

Table 6.4 Environmental impacts of concretes

Impact category	Unit	NAC-TM	NAC-PPM	RAC-PPM
Global warming	kg CO_2-eq	499.1	498.4	488.5
Stratospheric ozone depletion	10^{-5} kg CFC11-eq	5.94	5.91	5.46
Terrestrial acidification	10^{-1} kg SO_2-eq	8.98	8.95	8.55
Freshwater eutrophication	10^{-2} kg P-eq	6.92	6.85	6.23
Land use	m^2a crop-eq	16.39	17.79	19.50
Non-renewable, fossil	MJ	2459.0	2451.9	2327.1
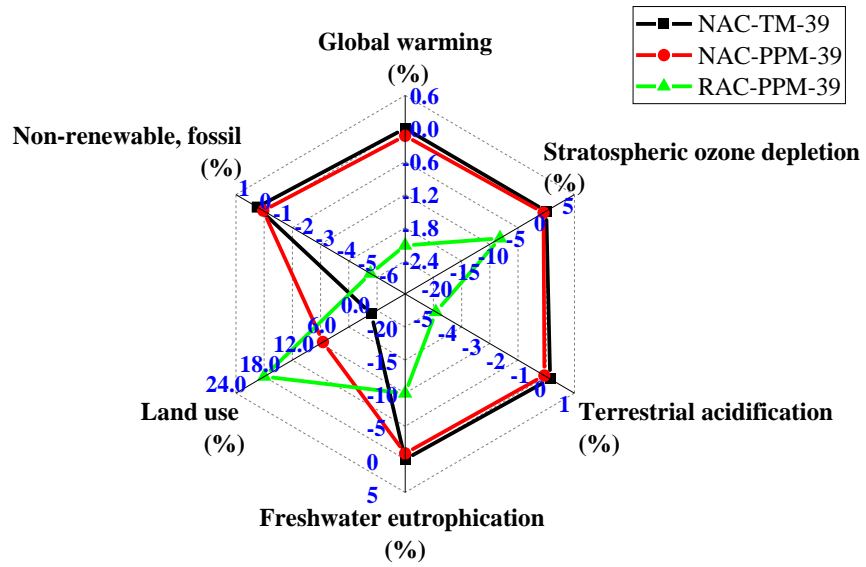
Fig. 6.6 Comparison of environmental impacts of concretes
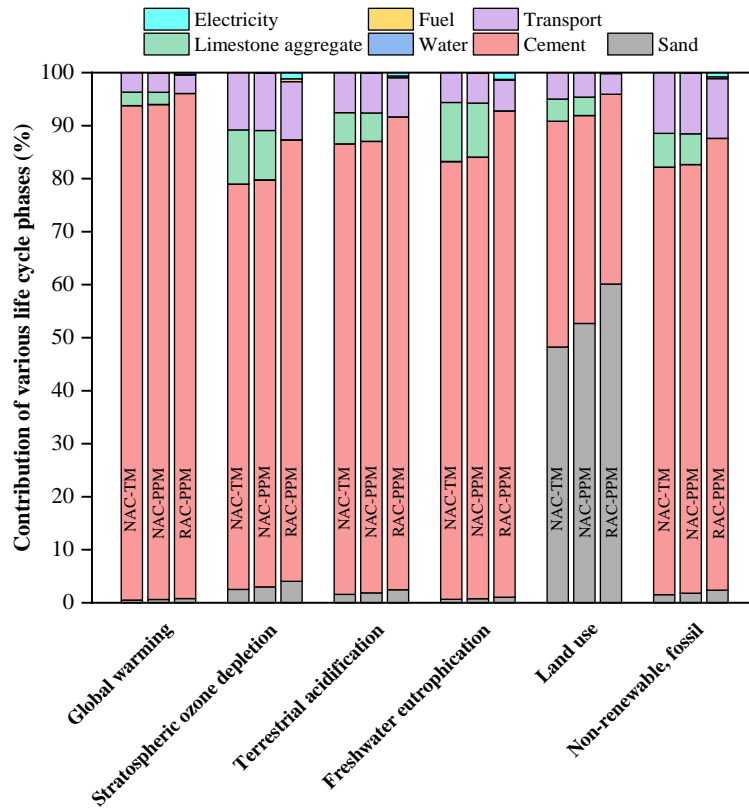
Fig. 6.7 Contribution of each life cycle phases to different impact categories for traditional and packing-optimised concretes

6.3.2 Environmental assessment of using RCP as sand replacement

The quantified environmental impacts of packing-optimised RAC with RCP as sand replacement in various impact categories are summarised in Table 6.4 and

normalised with respect to those of the reference mix RAC-PPM, as presented in Fig. 6.8. This demonstrates that the addition of RCP as sand replacement can decrease all the considered environmental impacts of packing-optimised RAC to improve its sustainability. More specifically, the global warming, stratospheric ozone depletion, terrestrial acidification, freshwater eutrophication, and non-renewable energy of the mix RAC-PPM-RCP20 are slightly lower than those of the mix RAC-PPM. While the use of RCP does not substantially reduce the environmental impacts related to the mentioned indicators, this finding underlines the dominant influence of cement in the considered life cycle phases, as shown in Fig. 6.9. These marginal impacts are mainly attributed to the reduced need for river sand extraction. As seen in Table 6.2, these environmental impacts of river sand are higher than those of RCP. Notably, the land use of river sand (145.08 m^2a crop-eq) is much higher than that of RCP (0.25 m^2a crop-eq). The life cycle phase of river sand contributes the largest part on the land use of packing-optimised concretes as seen in Fig. 6.9. This is associated with the large amount of land use required for the river sand extraction. It is evident that replacing 20% river sand with RCP could decrease the land use of packing-optimised RAC by 12%. Therefore, the adoption of RCP as sand replacement is a promising strategy to mitigate the environmental burden of land use brought about by the design of RAC with particle packing optimisation.

Table 6.5 Environmental impacts of packing-optimised RAC with or without RCP as sand replacement

Impact category	Unit	RAC-PPM	RAC-PPM-RCP20
Global warming	kg CO_2-eq	488.5	487.9
Stratospheric ozone depletion	10^{-5} kg CFC11-eq	5.46	5.42
Terrestrial acidification	10^{-1} kg SO_2-eq	8.55	8.52
Freshwater eutrophication	10^{-2} kg P-eq	6.23	6.22
Land use	m^2a crop-eq	19.50	17.16
Non-renewable, fossil	MJ	2327.1	2318.5
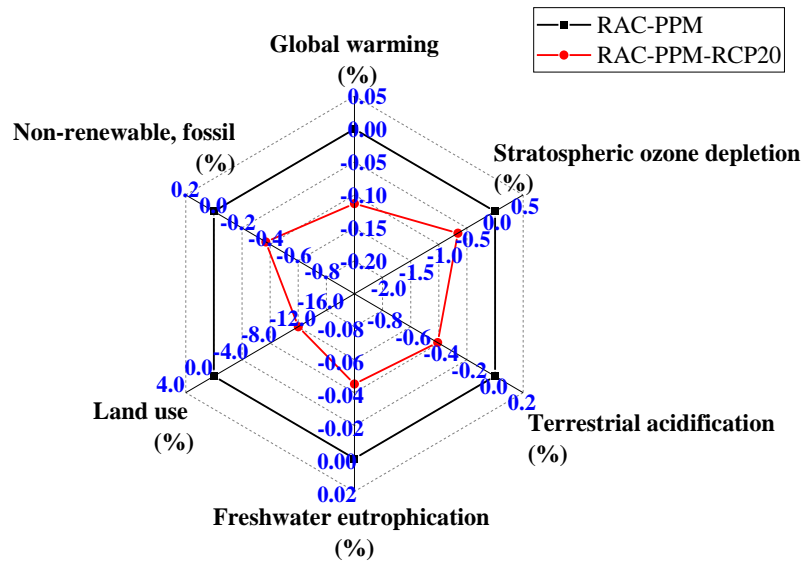
Fig. 6.8 Comparison of environmental impacts of packing-optimised RAC with or without RCP as sand replacement
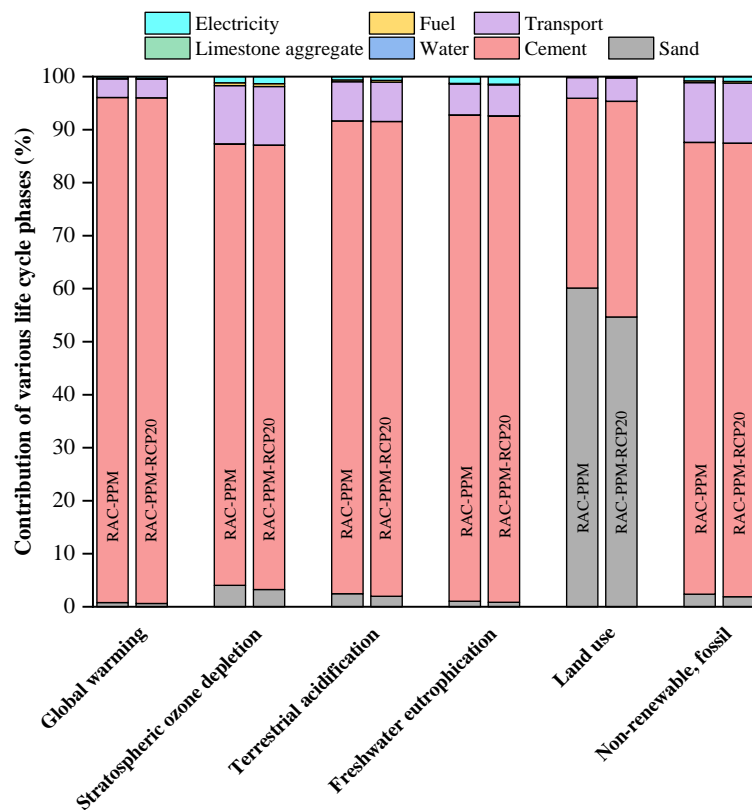
Fig. 6.9 Contribution of each life cycle phases to different impact categories for packing-optimised RAC with or without RCP as sand replacement

6.3 Summary

This chapter investigated the environmental benefits of adopting packing-optimised RAC and using RCP as sand replacement. The environmental impacts of global warming, stratospheric ozone depletion, terrestrial acidification, freshwater eutrophication, land use, and non-renewable energy consumption were evaluated. Based on the results and discussion, the following conclusions can be drawn.

- The strategy of optimising the packing status of aggregates and the incorporation of RCAs as the replacement of limestone aggregates can slightly decrease most environmental impacts of concrete production, including the global warming, stratospheric ozone depletion, terrestrial acidification, freshwater eutrophication, and non-renewable energy consumption. However, the adoption of the particle packing method for high-performance RAC design increases its environmental burden of land use, which is associated with the large amount of land use required for the river sand extraction.

- Using RCP as the sand replacement can decrease all the considered environmental impacts of packing-optimised RAC, particularly for the land use. Replacing 20% river sand with RCP can decrease the land use of packing-optimised RAC by 12%. Therefore, it is a promising strategy to incorporate a proper amount of RCP as sand replacement to enhance the sustainability of packing-optimised RAC without compromising its mechanical properties.

CHAPTER 7
CONCLUSIONS AND RECOMMENDATIONS

This chapter presents the main conclusions drawn from the experimental results and discussion of the current study. In addition, recommendations for future studies on the packing-optimised recycled aggregate concrete (RAC) and the scientific utilisation of recycled concrete powder (RCP) in concrete are also provided.

7.1 Conclusions

This study first focused on investigating the effects of aggregate packing enhancement on the workability and mechanical properties of concretes with or without recycled concrete aggregates (RCAs). The microstructure of RAC was also characterised, with a focus on its macropore structure, which helped to understand the role of aggregate packing enhancement in improving the RAC properties. Subsequently, the influences of cement paste volume (CPV) and sand-to-aggregate volume ratio (Bs) on the properties of packing-optimised RAC were further investigated. The interfacial transition zones (ITZs) and the pore structure inside RAC were analysed to explain their impacts on the macroscopic performance. Moreover, this study examined the role of RCP as sand replacement in the physical, mechanical, and drying shrinkage properties of mortars by using two different types of model RCP prepared with designated water-to-cement (W/C) ratios in the laboratory. Their macroscopic results were then linked to the microstructural study on the crystalline phases and pore structure of the RCP mortars. The particle packing density and hydration reaction degree were also quantified and analysed to comprehensively explain the impacts of RCP as sand replacement on the properties and microstructures of mortar. Lastly, the environmental benefits of adopting packing-optimised RAC and using RCP as sand replacement were evaluated by performing a life cycle assessment (LCA) with regard to the environmental categories of global warming, stratospheric ozone depletion, terrestrial acidification, freshwater eutrophication, land use, and non-renewable energy consumption. Based on the

test results and the discussion, the following conclusions can be drawn.

- The slump of fresh RAC can be improved by optimising the aggregate packing density, and it increases at a growing rate with the CPV. This is mainly attributed to the enhanced lubrication effect of cement paste on aggregates. However, increasing the Bs can decrease the thickness of cement paste film coated on RCAs, which weakens their lubrication effect and subsequently decreases the RAC slump.

- Aggregate packing enhancement can increase the compressive strength and Young's modulus of concretes through creating dense and stable aggregate skeletons inside concretes. In addition, the refinement of pore structure through decreasing the number of macro pores in the packing-optimised RAC also contributes to the enhancement in its compressive strength and Young's modulus.

- The compressive strength and Young's modulus of RAC first increase with the CPV in the RAC, followed by reductions as the CPV further increases. The former is mainly attributed to the refinement in macropore structure by decreasing its porosity and macropore number in RAC, while the latter is caused by the increased porosity and thickness of ITZs due to the excessive CPV.

- The incorporation of an optimum Bs improves the packing density of total aggregates, and consequently enhances the compressive strength and Young's modulus of RAC. However, an excessive Bs causes poorer packing status of the granular skeleton and increases the macroporosity and mean pore size of cement mortar around RCAs, which decreases the compressive strength and Young's modulus of RAC.

- The water demands for RCP mortars are higher than that of the reference mortar to maintain similar consistency. The water demand for RCP mortar increases by up to 29.4% as the RCP replacement increases from 10% to 30%. The dry bulk densities of RCP mortars decrease as the RCP replacement ratio increases. Replacing sand with 30% RCP decreases the dry bulk density of mortar by up to 13.2%. These can be attributed to the irregular shape, rough surface, high porosity, and fineness of the RCP used in the mortars.

- Replacing sand with up to 10-20% RCP has a negligible negative effect on the compressive strength and Young's moduli of mortars, whereas leading to a positive effect on the flexural strength. This is mainly attributed to a refinement of microstructure by decreasing the volume fraction of large capillary pores, air voids, and the total porosity. Moreover, the addition of RCP can increase the volume fraction of mesopores, thereby leading to a higher drying shrinkage of mortars. Replacing sand with 30% RCP increases the 56-day drying shrinkage of mortar by up to 110%.

- Proper use of RCP as sand replacement can enhance the particle packing density by filling the larger voids with the smaller particles, densifying the granular skeleton inside RCP mortars. This also slightly promotes the hydration reaction in mortars by advancing their exothermic peaks and increasing their hydration heats.

- The adoption of packing-optimised RAC can decrease the most considered environmental impacts in terms of global warming, stratospheric ozone depletion, terrestrial acidification, freshwater eutrophication, and non-renewable energy consumption, but it increases the environmental burden of land use. Nevertheless, using RCP as sand replacement decreases all the environmental impacts of packing-optimised RAC, particularly for the land use. Replacing 20% river sand with RCP can decrease the land use of packing-optimised RAC by 12%.

7.2 Recommendations for future research

This study has demonstrated the significance of particle packing optimisation in the mix design of high-performance RAC and the effectiveness of using RCP as a potential sand alternative to improve the packing density and pore structure. However, this study also has the following limitations. Firstly, this study only focused on the improvement of concrete mix design to mitigate the drawbacks of using RCAs. Secondly, this study only considered the properties of packing-optimised RAC limited to the workability, mechanical properties, and microstructure. Thirdly, this study did not consider the structural performance of packing-optimised RAC. Fourthly, the present study only considered the use of

RCP with a particle size larger than cement particles. The understanding of the impact of RCP particle size on the concrete properties and microstructures was limited. Lastly, the present study primarily dove into the potential of using RCAs and RCP for construction, yet the exploration of the practical challenges associated with implementing these strategies remained limited. Therefore, future research is recommended to be conducted in the following aspects.

- It is worth investigating the synergistic effects of using particle packing optimisation and various RCA pre-treatments (*e.g.*, accelerated carbonation and cement slurry coating) on enhancing the properties of RAC.

- It is a promising strategy to incorporate fibre reinforcement for enhancing the mechanical properties and ductility of packing-optimised RAC. More studies are needed to investigate the effect of fibre incorporation on the properties of packing-optimised RAC.

- It is recommended to study the durability of packing-optimised RAC, including freeze-thaw performance, carbonation resistance, and alkali-silica reaction, since these properties are crucial for the service life of RAC.

- Future research can be conducted to investigate the structural behaviour of packing-optimised RAC under various loading conditions such as static and dynamic loadings.

- A comprehensive study is needed to investigate the effects of various particle sizes of RCP as sand replacement on the properties and microstructures of packing-optimised RAC, since it might significantly influence the particle packing density and the hydration reaction.

- Future research endeavours can be prioritised in evaluating the economic viability of using RCAs and RCP compared to traditional materials, formulating tailored quality control standards, and navigating potential regulatory challenges to facilitate the sustainable adoption of these recycled materials for construction.

REFERENCES

Abbas, A., Fathifazl, G., Isgor, O. B., Razaqpur, A. G., Fournier, B., & Foo, S. (2009). Durability of recycled aggregate concrete designed with equivalent mortar volume method. *Cement and Concrete Composites*, *31*(8), 555–563.

Aïm, R. B., & Goff, P. L. (1968). Effet de paroi dans les empilements désordonnés de sphères et application à la porosité de mélanges binaires. *Powder Technology*, *1*(5), 281–290.

Aiqin, W., Chengzhi, Z., & Ningsheng, Z. (1999). Theoretic analysis of the influence of the particle size distribution of cement system on the property of cement. *Cement and Concrete Research*, *29*(11), 1721–1726.

Amario, M., Rangel, C. S., Pepe, M., & Toledo Filho, R. D. (2017). Optimization of normal and high strength recycled aggregate concrete mixtures by using packing model. *Cement and Concrete Composites*, *84*, 83–92.

Andreasen, A. H. M., & Andersen, J. (1930). Ueber die Beziehung zwischen Kornabstufung und Zwischenraum in Produkten aus losen Körnern (mit einigen Experimenten). *Kolloid-Zeitschrift*, *50*(3), 217–228.

ASTM Committee. (2006). *ASTM C642-06: Standard Test Method for Density, Absorption, and Voids in Hardened Concrete*.

ASTM Committee. (2017). *ASTM C1702-17: Standard Test Method for Measurement of Heat of Hydration of Hydraulic Cementitious Materials Using Isothermal Conduction Calorimetry*.

ASTM Committee. (2018). *ASTM C596-18: Standard Test Method for Drying Shrinkage of Mortar Containing Hydraulic Cement*.

Bairagi, N. K., Ravande, K., & Pareek, V. K. (1993). Behaviour of concrete with different proportions of natural and recycled aggregates. *Resources, Conservation and Recycling*, *9*(1–2), 109–126.

Bala, M., Zentar, R., & Boustingorry, P. (2020). Parameter determination of the Compressible Packing Model (CPM) for concrete application. *Powder Technology*, *367*, 56–66.

Bao, Z., & Lu, W. (2020). Developing efficient circularity for construction and demolition waste management in fast emerging economies: Lessons learned from Shenzhen, China. *Science of the Total Environment*, *724*, 138264.

Behera, M., Bhattacharyya, S. K., Minocha, A. K., Deoliya, R., & Maiti, S. (2014). Recycled aggregate from C&D waste & its use in concrete - A breakthrough towards sustainability in construction sector: A review. *Construction and Building Materials*, *68*, 501–516.

Blengini, G. A. (2009). Life cycle of buildings, demolition and recycling potential: A case study in Turin, Italy. *Building and Environment*, *44*(2), 319–330.

Blengini, G. A., & Garbarino, E. (2010). Resources and waste management in Turin (Italy): The role of recycled aggregates in the sustainable supply mix. *Journal of Cleaner Production*, *18*(10–11), 1021–1030.

Blengini, G. A., Garbarino, E., Šolar, S., Shields, D. J., Hámor, T., Vinai, R., & Agioutantis, Z. (2012). Life Cycle Assessment guidelines for the sustainable production and recycling of aggregates: The Sustainable Aggregates Resource Management project (SARMa). *Journal of Cleaner Production*, *27*(2012), 177–181.

Boesch, M. E., & Hellweg, S. (2010). Identifying improvement potentials in cement production with life cycle assessment. *Environmental Science and Technology*, *44*(23), 9143–9149.

Braga, A. M., Silvestre, J. D., & de Brito, J. (2017). Compared environmental and economic impact from cradle to gate of concrete with natural and recycled coarse aggregates. *Journal of Cleaner Production*, *162*(2017), 529–543.

Braga, M., De Brito, J., & Veiga, R. (2014). Reduction of the cement content in mortars made with fine concrete aggregates. *Materials and Structures*, *47*(1–2), 171–182.

BSI. (1999). *BS 812-2:1995: Testing aggregates. Methods of determination of density*.

BSI. (2007). *BS EN 1015-3:1999: Methods of test for mortar for masonry. Part 3: Determination of consistence of fresh mortar (by flow table).*

BSI. (2009a). *BS EN 12350-2:2009: Testing fresh concrete, Part 2: Slump-test.*

BSI. (2009b). *BS EN 12390-3:2009: Testing hardened concrete. Compressive strength of test specimens.*

BSI. (2009c). *BS EN 12390-5:2009: Testing hardened concrete. Part 5: Flexural strength of test specimens.*

BSI. (2019a). *BS EN 1015-11:2019: Methods of test for mortar for masonry-Part 11: Determination of flexural and compressive strength of hardened mortar.*

BSI. (2019b). *BS EN 12390-13:2013: Testing hardened concrete. Part 13: Determination of secant modulus of elasticity in compression.*

Campos, H. F., Klein, N. S., & Marques Filho, J. (2020). Proposed mix design method for sustainable high-strength concrete using particle packing optimization. *Journal of Cleaner Production*, *265*, 121907.

Campos, H. F., Klein, N. S., Marques Filho, J., & Bianchini, M. (2020). Low-cement high-strength concrete with partial replacement of Portland cement with stone powder and silica fume designed by particle packing optimization. *Journal of Cleaner Production*, *261*, 121228.

Chateau, X., Ovarlez, G., & Trung, K. L. (2008). Homogenization approach to the behavior of suspensions of noncolloidal particles in yield stress fluids. *Journal of Rheology*, *52*(2), 489–506.

Chen, J. J., Li, B. H., Ng, P. L., & Kwan, A. K. H. (2021). Adding granite polishing waste to reduce sand and cement contents and improve performance of mortar. *Journal of Cleaner Production*, *279*.

Chen, X., Zhang, D., Cheng, S., Xu, X., Zhao, C., Wang, X., Wu, Q., & Bai, X. (2022). Sustainable reuse of ceramic waste powder as a supplementary cementitious material in recycled aggregate concrete: Mechanical properties, durability and microstructure assessment. *Journal of Building Engineering*, *52*, 104418.

Chidiac, S. E., Moutassem, F., & Mahmoodzadeh, F. (2013). Compressive strength model for concrete. *Magazine of Concrete Research*, *65*(9), 557–572.

Cho, G.-C., Dodds, J., & Santamarina, J. C. (2006). Particle Shape Effects on Packing Density, Stiffness, and Strength: Natural and Crushed Sands. *Journal of Geotechnical and Geoenvironmental Engineering*, *132*(5), 591–602.

Choi, M., Roussel, N., Kim, Y., & Kim, J. (2013). Lubrication layer properties during concrete pumping. *Cement and Concrete Research*, *45*(1), 69–78.

Chu, S. H. (2019). Effect of paste volume on fresh and hardened properties of concrete. *Construction and Building Materials*, *218*, 284–294.

Chu, S. H., Chen, J. J., Li, L. G., Ng, P. L., & Kwan, A. K. H. (2021). Roles of packing density and slurry film thickness in synergistic effects of metakaolin and silica fume. *Powder Technology*, *387*, 575–583.

Coleman, N. J., Lee, W. E., & Slipper, I. J. (2005). Interactions of aqueous Cu^{2+}, Zn^{2+} and Pb^{2+} ions with crushed concrete fines. *Journal of Hazardous Materials*, *121*(1–3), 203–213.

Collins, F., & Sanjayan, J. G. (2000). Effect of pore size distribution on drying shrinkage of alkali-activated slag concrete. *Cement and Concrete Research*, *30*(9), 1401–1406.

De Oliveira, M. B., & Vazquez, E. (1996). The influence of retained moisture in aggregates from recycling on the properties of new hardened concrete. *Waste Management*, *16*(1–3), 113–117.

Ding, T., Xiao, J., & Tam, V. W. Y. (2016). A closed-loop life cycle assessment of recycled aggregate concrete utilization in China. *Waste Management*, *56*, 367–375.

Dingqiang, F., Rui, Y., Zhonghe, S., Chunfeng, W., Jinnan, W., & Qiqi, S. (2020). A novel approach for developing a green Ultra-High Performance Concrete (UHPC) with advanced particles packing meso-structure. *Construction and Building Materials*, *265*, 120339.

Dong, H., Gao, P., & Ye, G. (2017). Characterization and comparison of capillary pore structures of digital cement pastes. *Materials and Structures*, *50*(2).

Duan, Z. H., & Poon, C. S. (2014). Properties of recycled aggregate concrete made with recycled aggregates with different amounts of old adhered mortars. *Materials and Design*, *58*, 19–29.

Duan, Z., Hou, S., Xiao, J., & Li, B. (2020). Study on the essential properties of recycled powders from construction and demolition waste. *Journal of Cleaner Production*, *253*.

Duan, Z., Singh, A., Xiao, J., & Hou, S. (2020). Combined use of recycled powder and recycled coarse aggregate derived from construction and demolition waste in self-compacting concrete. *Construction and Building Materials*, *254*, 119323.

Estanqueiro, B., Dinis Silvestre, J., de Brito, J., & Duarte Pinheiro, M. (2016). Environmental life cycle assessment of coarse natural and recycled aggregates for concrete. *European Journal of Environmental and Civil Engineering*, *22*(4), 429–449.

Farris, R. J. (1968). Prediction of the Viscosity of Multimodal Suspensions from Unimodal Viscosity Data. *Transactions of the Society of Rheology*, *12*(2), 281–301.

Fuller, W. B., & Thompson, S. E. (1907). The Laws of Proportioning Concrete. *American Society of Civil Engineers*, *33*, 223–298.

Funk, J. E., & Dinger, D. R. (1994). Predictive Process Control of Crowded Particulate Suspensions. *Predictive Process Control of Crowded Particulate Suspensions*. Springer US.

Furnas, C. C. (1931). Grading aggregates I: Mathematical Relations for Beds of Broken Solids of Maximum Density. *Industrial & Engineering Chemistry*, *23*(9), 1052–1058.

Gálvez-Martos, J. L., Styles, D., Schoenberger, H., & Zeschmar-Lahl, B. (2018). Construction and demolition waste best management practice in Europe.

Resources, Conservation and Recycling, *136*, 166–178.

Gao, Y., De Schutter, G., Ye, G., Tan, Z., & Wu, K. (2014). The ITZ microstructure, thickness and porosity in blended cementitious composite: Effects of curing age, water to binder ratio and aggregate content. *Composites Part B: Engineering*, *60*, 1–13.

Garci Juenger, M. C., & Jennings, H. M. (2002). Examining the relationship between the microstructure of calcium silicate hydrate and drying shrinkage of cement pastes. *Cement and Concrete Research*, *32*(2), 289–296.

Ghasemi, Y., Emborg, M., & Cwirzen, A. (2018). Estimation of specific surface area of particles based on size distribution curve. *Magazine of Concrete Research*, *70*(10), 533–540.

Gokce, A., Nagataki, S., Saeki, T., & Hisada, M. (2011). Identification of frost-susceptible recycled concrete aggregates for durability of concrete. *Construction and Building Materials*, *25*(5), 2426–2431.

Gómez-Soberón, J. M. V. (2002). Porosity of recycled concrete with substitution of recycled concrete aggregate. *Cement and Concrete Research*, *32*(8), 1301–1311.

Gong, F., Zhang, D., Sicat, E., & Ueda, T. (2014). Empirical Estimation of Pore Size Distribution in Cement, Mortar, and Concrete. *Journal of Materials in Civil Engineering*, *26*(7), 04014023.

Gursel, A. P., & Ostertag, C. (2017). Comparative life-cycle impact assessment of concrete manufacturing in Singapore. *International Journal of Life Cycle Assessment*, *22*(2), 237–255.

Hafid, H., Ovarlez, G., Toussaint, F., Jezequel, P. H., & Roussel, N. (2016). Effect of particle morphological parameters on sand grains packing properties and rheology of model mortars. *Cement and Concrete Research*, *80*, 44–51.

Hanzic, L., & Ho, J. C. M. (2017). Multi-sized fillers to improve strength and flowability of concrete. *Advances in Cement Research*, *29*(3), 112–124.

Helal, K., Istaitiyeh, H., Zaher, A., Yehia, S., & Abusharkh, A. (2015). Strength

and Durability Evaluation of Recycled Aggregate Concrete. *International Journal of Concrete Structures and Materials*, *9*(2), 219–239.

Hossain, M. U., Poon, C. S., Lo, I. M. C., & Cheng, J. C. P. (2016). Comparative environmental evaluation of aggregate production from recycled waste materials and virgin sources by LCA. *Resources, Conservation and Recycling*, *109*, 67–77.

Ismail, S., & Ramli, M. (2013). Engineering properties of treated recycled concrete aggregate (RCA) for structural applications. *Construction and Building Materials*, *44*, 464–476.

ISO. (2006a). *ISO 14040：Environmental Management – Life Cycle Assessment – Principles and Framework*.

ISO. (2006b). *ISO 14044：Environmental Management – Life Cycle Assessment – Requirements and Guidelines*.

Jiang, Y., Liu, S., Li, B., He, J., & Hernandez, A. G. (2022). Effects of aggregate packing optimization and cement paste volume on the properties of natural and recycled aggregate concrete. *Structural Concrete*, *23*, 2260–2273.

Jiménez, C., Barra, M., Josa, A., & Valls, S. (2015). LCA of recycled and conventional concretes designed using the Equivalent Mortar Volume and classic methods. *Construction and Building Materials*, *84*, 245–252.

Kaliyavaradhan, S. K., Ling, T. C., & Mo, K. H. (2020). Valorization of waste powders from cement-concrete life cycle: A pathway to circular future. *Journal of Cleaner Production*, *268*.

Katz, A. (2004). Treatments for the Improvement of Recycled Aggregate. *Journal of Materials in Civil Engineering*, *16*(6), 597–603.

Kazmi, S. M. S., Munir, M. J., Wu, Y. F., Patnaikuni, I., Zhou, Y., & Xing, F. (2019). Influence of different treatment methods on the mechanical behavior of recycled aggregate concrete: A comparative study. *Cement and Concrete Composites*, *104*, 103398.

Kim, Y. J. (2017). Quality properties of self-consolidating concrete mixed with waste concrete powder. *Construction and Building Materials*, *135*, 177–

185.

Kim, Y. J., & Choi, Y. W. (2012). Utilization of waste concrete powder as a substitution material for cement. *Construction and Building Materials*, *30*, 500–504.

Kisku, N., Joshi, H., Ansari, M., Panda, S. K., Nayak, S., & Dutta, S. C. (2017). A critical review and assessment for usage of recycled aggregate as sustainable construction material. *Construction and Building Materials*, *131*, 721–740.

Kleijer, A. L., Lasvaux, S., Citherlet, S., & Viviani, M. (2017). Product-specific Life Cycle Assessment of ready mix concrete: Comparison between a recycled and an ordinary concrete. *Resources, Conservation and Recycling*, *122*, 210–218.

Klein, N. S., Lenz, L. A., & Mazer, W. (2020). Influence of the granular skeleton packing density on the static elastic modulus of conventional concretes. *Construction and Building Materials*, *242*, 118086.

Knoeri, C., Sanyé-Mengual, E., & Althaus, H. J. (2013). Comparative LCA of recycled and conventional concrete for structural applications. *International Journal of Life Cycle Assessment*, *18*(5), 909–918.

Kolias, S., & Georgiou, C. (2005). The effect of paste volume and of water content on the strength and water absorption of concrete. *Cement and Concrete Composites*, *27*(2), 211–216.

Kou, S. C., & Poon, C. S. (2010). Properties of concrete prepared with PVA-impregnated recycled concrete aggregates. *Cement and Concrete Composites*, *32*(8), 649–654.

Kou, S. C., & Poon, C. S. (2013). Long-term mechanical and durability properties of recycled aggregate concrete prepared with the incorporation of fly ash. *Cement and Concrete Composites*, *37*(1), 12–19.

Kou, S. C., & Poon, C. S. (2015). Effect of the quality of parent concrete on the properties of high performance recycled aggregate concrete. *Construction and Building Materials*, *77*, 501–508.

Kou, S. C., Poon, C. S., & Chan, D. (2007). Influence of Fly Ash as Cement Replacement on the Properties of Recycled Aggregate Concrete. *Journal of Materials in Civil Engineering*, *19*(9), 709–717.

Kurda, R., Silvestre, J. D., & de Brito, J. (2018). Life cycle assessment of concrete made with high volume of recycled concrete aggregates and fly ash. *Resources, Conservation and Recycling*, *139*, 407–417.

Kwan, A. K.H., & Li, L. G. (2012). Combined effects of water film thickness and paste film thickness on rheology of mortar. *Materials and Structures*, *45*(9), 1359–1374.

Kwan, Albert K.H., & Li, L. G. (2014). Combined effects of water film, paste film and mortar film thicknesses on fresh properties of concrete. *Construction and Building Materials*, *50*, 598–608.

La Rosa, A. D., Cozzo, G., Latteri, A., Recca, A., Björklund, A., Parrinello, E., & Cicala, G. (2013). Life cycle assessment of a novel hybrid glass-hemp/thermoset composite. *Journal of Cleaner Production*, *44*, 69–76.

Larrard, F. de. (1999). Concrete mixture proportioning: A scientific approach. In *Modern Concrete Technology* (Vol. 9).

Li, J., & Yang, E. H. (2017). Macroscopic and microstructural properties of engineered cementitious composites incorporating recycled concrete fines. *Cement and Concrete Composites*, *78*, 33–42.

Li, L. G., & Kwan, A. K. H. (2014). Packing density of concrete mix under dry and wet conditions. *Powder Technology*, *253*, 514–521.

Li, L. G., Lin, C. J., Chen, G. M., Kwan, A. K. H., & Jiang, T. (2017). Effects of packing on compressive behaviour of recycled aggregate concrete. *Construction and Building Materials*, *157*, 757–777.

Li, L., Xuan, D., Chu, S. H., Lu, J. X., & Poon, C. S. (2021). Efficiency and mechanism of nano-silica pre-spraying treatment in performance enhancement of recycled aggregate concrete. *Construction and Building Materials*, *301*, 124093.

Li, L., Zhan, B. J., Lu, J., & Poon, C. S. (2019). Systematic evaluation of the

effect of replacing river sand by different particle size ranges of fine recycled concrete aggregates (FRCA) in cement mortars. *Construction and Building Materials*, *209*, 147–155.

Li, S., Gao, J., Li, Q., & Zhao, X. (2021). Investigation of using recycled powder from the preparation of recycled aggregate as a supplementary cementitious material. *Construction and Building Materials*, *267*, 120976.

Li, Z., Bian, Y., Zhao, J., Wang, Y., & Yuan, Z. (2022). Recycled concrete fine powder (RFP) as cement partial replacement: Influences on the physical properties, hydration characteristics, and microstructure of blended cement. *Journal of Building Engineering*, *62*, 105326.

Liang, K., Hou, Y., Sun, J., Li, X., Bai, J., Tian, W., & Liu, Y. (2021). Theoretical analysis of water absorption kinetics of recycled aggregates immersed in water. *Construction and Building Materials*, *302*, 124156.

Liao, G., & Yao, W. (2022). Upcycling of waste concrete powder into a functionalized host for nano-TiO_2 photocatalyst: Binding mechanism and enhanced photocatalytic efficiency. *Journal of Cleaner Production*, *366*, 132918.

Lin, W. T. (2020). Effects of sand/aggregate ratio on strength, durability, and microstructure of self-compacting concrete. *Construction and Building Materials*, *242*, 118046.

Liu, G., Florea, M. V. A., & Brouwers, H. J. H. (2019). Performance evaluation of sustainable high strength mortars incorporating high volume waste glass as binder. *Construction and Building Materials*, *202*, 574–588.

Liu, Q., Xiao, J., & Sun, Z. (2011). Experimental study on the failure mechanism of recycled concrete. *Cement and Concrete Research*, *41*(10), 1050–1057.

Liu, S., Minne, P., Lulić, M., Li, J., & Gruyaert, E. (2021). Implementation and validation of Dewar's particle packing model for recycled concrete aggregates. *Construction and Building Materials*, *294*.

Liu, X., Liu, L., Lyu, K., Li, T., Zhao, P., Liu, R., Zuo, J., Fu, F., & Shah, S. P. (2022). Enhanced early hydration and mechanical properties of cement-

based materials with recycled concrete powder modified by nano-silica. *Journal of Building Engineering*, *50*.

Liu, Y., Lu, C., Zhang, H., & Li, J. (2016). Experimental study on chemical activation of recycled powder as a cementitious material in mine paste backfilling. *Environmental Engineering Research*, *21*(4), 341–349.

Maimouni, H., Remond, S., Huchet, F., Richard, P., Thiery, V., & Descantes, Y. (2018). Quantitative assessment of the saturation degree of model fine recycled concrete aggregates immersed in a filler or cement paste. *Construction and Building Materials*, *175*(2018), 496–507.

Majidi, B., Azari, K., Alamdari, H., Fafard, M., & Ziegler, D. (2014). Simulation of vibrated bulk density of anode-grade coke particles using discrete element method. *Powder Technology*, *261*, 154–160.

Mao, Y., Liu, J., & Shi, C. (2021). Autogenous shrinkage and drying shrinkage of recycled aggregate concrete: A review. *Journal of Cleaner Production*, *295*, 126435.

Marinković, S., Radonjanin, V., Malešev, M., & Ignjatović, I. (2010). Comparative environmental assessment of natural and recycled aggregate concrete. *Waste Management*, *30*(11), 2255–2264.

Mefteh, H., Kebaïli, O., Oucief, H., Berredjem, L., & Arabi, N. (2013). Influence of moisture conditioning of recycled aggregates on the properties of fresh and hardened concrete. *Journal of Cleaner Production*, *54*, 282–288.

Mehdipour, I., & Khayat, K. H. (2017). Effect of particle-size distribution and specific surface area of different binder systems on packing density and flow characteristics of cement paste. *Cement and Concrete Composites*, *78*, 120–131.

Mohammed, T. U., & Rahman, M. N. (2016). Effect of types of aggregate and sand-to-aggregate volume ratio on UPV in concrete. *Construction and Building Materials*, *125*, 832–841.

Moini, M., Flores-Vivian, I., Amirjanov, A., & Sobolev, K. (2015). The optimization of aggregate blends for sustainable low cement concrete.

Construction and Building Materials, *93*, 627–634.

Mostofinejad, D., & Reisi, M. (2012). A new DEM-based method to predict packing density of coarse aggregates considering their grading and shapes. *Construction and Building Materials*, *35*, 414–420.

Nanthagopalan, P., & Santhanam, M. (2012). An empirical approach for the optimisation of aggregate combinations for self-compacting concrete. *Materials and Structures*, *45*(8), 1167–1179.

Noda, A. (2005). Texture and petrology of modern river, beach and shelf sands in a volcanic back-arc setting, northeastern Japan. *Island Arc*, *14*(4), 687–707.

Noor, M. A., & Uomoto, T. (2004). Rheology of high flowing mortar and concrete. *Materials and Structures*, *37*(272), 513–521.

Oksri-Nelfia, L., Mahieux, P. Y., Amiri, O., Turcry, P., & Lux, J. (2016). Reuse of recycled crushed concrete fines as mineral addition in cementitious materials. *Materials and Structures*, *49*(8), 3239–3251.

Ortiz, O., Castells, F., & Sonnemann, G. (2009). Sustainability in the construction industry: A review of recent developments based on LCA. *Construction and Building Materials*, *23*(1), 28–39.

Padmini, A. K., Ramamurthy, K., & Mathews, M. S. (2009). Influence of parent concrete on the properties of recycled aggregate concrete. *Construction and Building Materials*, *23*(2), 829–836.

Pang, G.-S., Chae, S.-T., & Chang, S.-P. (2009). Predicting Model for Pore Structure of Concrete Including Interface Transition Zone between Aggregate and Cement Paste. *International Journal of Concrete Structures and Materials*, *3*(2), 81–90.

Piasta, W., & Zarzycki, B. (2017). The effect of cement paste volume and w/c ratio on shrinkage strain, water absorption and compressive strength of high performance concrete. *Construction and Building Materials*, *140*, 395–402.

Pickel, D., Tighe, S., & West, J. S. (2017). Assessing benefits of pre-soaked recycled concrete aggregate on variably cured concrete. *Construction and*

Building Materials, *141*, 245–252.

Poon, C. S., Kou, S. C., & Lam, L. (2002). Use of recycled aggregates in molded concrete bricks and blocks. *Construction and Building Materials*, *16*(5), 281–289.

Poon, C. S., Kou, S. C., & Lam, L. (2007). Influence of recycled aggregate on slump and bleeding of fresh concrete. *Materials and Structures*, *40*(9), 981–988.

Poon, C. S., Shui, Z. H., Lam, L., Fok, H., & Kou, S. C. (2004). Influence of moisture states of natural and recycled aggregates on the slump and compressive strength of concrete. *Cement and Concrete Research*, *34*(1), 31–36.

Powers, T. C. (1968). *The properties of fresh concrete*. John Wiley and Sons.

Pradhan, S., Tiwari, B. R., Kumar, S., & Barai, S. V. (2019). Comparative LCA of recycled and natural aggregate concrete using Particle Packing Method and conventional method of design mix. *Journal of Cleaner Production*, *228*, 679–691.

Qian, D., Yu, R., Shui, Z., Sun, Y., Jiang, C., Zhou, F., Ding, M., Tong, X., & He, Y. (2020). A novel development of green ultra-high performance concrete (UHPC) based on appropriate application of recycled cementitious material. *Journal of Cleaner Production*, *261*, 121231.

Qiu, J., Zhou, Y., Guan, X., & Zhu, M. (2021). The influence of fly ash content on ITZ microstructure of coal gangue concrete. *Construction and Building Materials*, *298*, 123562.

Rangaraju, P. R., Olek, J., & Diamond, S. (2010). An investigation into the influence of inter-aggregate spacing and the extent of the ITZ on properties of Portland cement concretes. *Cement and Concrete Research*, *40*(11), 1601–1608.

Reisi, M., Mostofinejad, D., & Ramezanianpour, A. A. (2018). Computer simulation-based method to predict packing density of aggregates mixture. *Advanced Powder Technology*, *29*(2), 386–398.

Ren, P., Li, B., Yu, J.-G., & Ling, T.-C. (2020). Utilization of recycled concrete fines and powders to produce alkali-activated slag concrete blocks. *Journal of Cleaner Production*, *267*, 122115.

Roquier, G. (2016). The 4-parameter Compressible Packing Model (CPM) including a new theory about wall effect and loosening effect for spheres. *Powder Technology*, *302*, 247–253.

Ryu, H. S., Kim, D. M., Shin, S. H., Lim, S. M., & Park, W. J. (2018). Evaluation on the Surface Modification of Recycled Fine Aggregates in Aqueous H2SiF6 Solution. *International Journal of Concrete Structures and Materials*, *12*(1).

Saba, M., & Assaad, J. J. (2021). Effect of recycled fine aggregates on performance of geopolymer masonry mortars. *Construction and Building Materials*, *279*, 122461.

Schwartzentruber, L. D. A., Le Roy, R., & Cordin, J. (2006). Rheological behaviour of fresh cement pastes formulated from a Self Compacting Concrete (SCC). *Cement and Concrete Research*, *36*(7), 1203–1213.

Scrivener, K., Snellings, R., & Lothenbach, B. (2016). A Practical Guide to Microstructural Analysis of Cementitious Materials. In K. Scrivener, R. Snellings, & B. Lothenbach (Eds.), *A Practical Guide to Microstructural Analysis of Cementitious Materials*. CRC Press.

Shao, J., Zhu, H., Zhao, B., Haruna, S. I., Xue, G., Jiang, W., Wu, K., & Yang, J. (2022). Combined effect of recycled tire rubber and carbon nanotubes on the mechanical properties and microstructure of concrete. *Construction and Building Materials*, *322*, 126493.

Shen, P., Zhang, Y., Jiang, Y., Zhan, B., Lu, J., Zhang, S., Xuan, D., & Poon, C. S. (2022). Phase assemblance evolution during wet carbonation of recycled concrete fines. *Cement and Concrete Research*, *154*, 106733.

Shen, S., & Yu, H. (2011). Characterize packing of aggregate particles for paving materials: Particle size impact. *Construction and Building Materials*, *25*(3), 1362–1368.

Shen, W., Wu, M., Zhang, B., Xu, G., Cai, J., Xiong, X., & Zhao, D. (2021). Coarse aggregate effectiveness in concrete: Quantitative models study on paste thickness, mortar thickness and compressive strength. *Construction and Building Materials*, *289*, 123171.

Sidiq, A., Gravina, R. J., Setunge, S., & Giustozzi, F. (2019). Microstructural analysis of healing efficiency in highly durable concrete. *Construction and Building Materials*, *215*, 969–983.

Sidiq, A., Gravina, R. J., Setunge, S., & Giustozzi, F. (2020). High-efficiency techniques and micro-structural parameters to evaluate concrete self-healing using X-ray tomography and Mercury Intrusion Porosimetry: A review. *Construction and Building Materials*, *252*, 119030.

Silva, R. V., de Brito, J., & Dhir, R. K. (2018). Fresh-state performance of recycled aggregate concrete: A review. *Construction and Building Materials*, *178*, 19–31.

Simion, I. M., Fortuna, M. E., Bonoli, A., & Gavrilescu, M. (2013). Comparing environmental impacts of natural inert and recycled construction and demolition waste processing using LCA. *Journal of Environmental Engineering and Landscape Management*, *21*(4), 273–287.

Soliman, N. A., & Tagnit-Hamou, A. (2017a). Using glass sand as an alternative for quartz sand in UHPC. *Construction and Building Materials*, *145*, 243–252.

Soliman, N. A., & Tagnit-Hamou, A. (2017b). Using Particle Packing and Statistical Approach to Optimize Eco-Efficient Ultra-High-Performance Concrete. *ACI Materials Journal*, *114*(6), 847–858.

Standards China. (2007). *GB 175-2007: Common Portland cement (in Chinese)*.

Standards China. (2008). *GB/T 18046-2008: Ground granulated blast furnace slag used for cement and concrete (in Chinese)*.

Standards China. (2011a). *GB/T 14684-2011: Sand for construction (in Chinese)*.

Standards China. (2011b). *JGJ55-2011: Specification for mix proportion design of ordinary concrete (in Chinese)*.

Standards China. (2017). *GB/T 1596-2017: Fly ash used for cement and concrete (in Chinese)*.

Stovall, T., de Larrard, F., & Buil, M. (1986). Linear packing density model of grain mixtures. *Powder Technology*, *48*(1), 1–12.

Su, J. K., Cho, S. W., Yang, C. C., & Huang, R. (2002). Effect of sand ratio on the elastic modulus of self-compacting concrete. *Journal of Marine Science and Technology*, *10*(1), 8–13.

Sun, C., Chen, L., Xiao, J., Zuo, J., & Wu, H. (2022). Effects of eco powders from solid waste on freeze-thaw resistance of mortar. *Construction and Building Materials*, *333*, 127405.

Sun, J., Zhang, Z., & Hou, G. (2020). Utilization of fly ash microsphere powder as a mineral admixture of cement: Effects on early hydration and microstructure at different curing temperatures. *Powder Technology*, *375*, 262–270.

Tabatabaei, M., Dahi Taleghani, A., & Alem, N. (2020). Nanoengineering of cement using graphite platelets to refine inherent microstructural defects. *Composites Part B: Engineering*, *202*, 108277.

Tam, V. W. Y., Gao, X. F., & Tam, C. M. (2005). Microstructural analysis of recycled aggregate concrete produced from two-stage mixing approach. *Cement and Concrete Research*, *35*(6), 1195–1203.

Topçu, I. B., & Şengel, S. (2004). Properties of concretes produced with waste concrete aggregate. *Cement and Concrete Research*, *34*(8), 1307–1312.

Toufar, W., Born, M., & Klose, E. (1976). *Contribution of optimisation of components of different density in polydispersed particles systems*.

Van Den Heede, P., & De Belie, N. (2012). Environmental impact and life cycle assessment (LCA) of traditional and "green" concretes: Literature review and theoretical calculations. *Cement and Concrete Composites*, *34*(4), 431–442.

Vargas, P., Restrepo-Baena, O., & Tobón, J. I. (2017). Microstructural analysis of interfacial transition zone (ITZ) and its impact on the compressive

strength of lightweight concretes. *Construction and Building Materials*, *137*, 381–389.

Verian, K. P., Ashraf, W., & Cao, Y. (2018). Properties of recycled concrete aggregate and their influence in new concrete production. *Resources, Conservation and Recycling*, *133*, 30–49.

Wallevik, J. E. (2006). Relationship between the Bingham parameters and slump. *Cement and Concrete Research*, *36*(7), 1214–1221.

Wang, B., Yan, L., Fu, Q., & Kasal, B. (2021). A Comprehensive Review on Recycled Aggregate and Recycled Aggregate Concrete. *Resources, Conservation and Recycling*, *171*, 105565.

Wang, J., Zhang, J., Cao, D., Dang, H., & Ding, B. (2020). Comparison of recycled aggregate treatment methods on the performance for recycled concrete. *Construction and Building Materials*, *234*, 117366.

Wang, J., Vandevyvere, B., Vanhessche, S., Schoon, J., Boon, N., & De Belie, N. (2017). Microbial carbonate precipitation for the improvement of quality of recycled aggregates. *Journal of Cleaner Production*, *156*, 355–366.

Wang, L., Wang, J., Qian, X., Chen, P., Xu, Y., & Guo, J. (2017). An environmentally friendly method to improve the quality of recycled concrete aggregates. *Construction and Building Materials*, *144*, 432–441.

Wang, X., Yu, R., Song, Q., Shui, Z., Liu, Z., Wu, S., & Hou, D. (2019). Optimized design of ultra-high performance concrete (UHPC) with a high wet packing density. *Cement and Concrete Research*, *126*, 105921.

Wang, X., Taylor, P., Wang, K., & Morcous, G. (2015). Effects of paste-to-voids volume ratio on performance of selfconsolidating concrete mixtures. *Magazine of Concrete Research*, *67*(14), 771–785.

Weil, M., Jeske, U., & Schebek, L. (2006). Closed-loop recycling of construction and demolition waste in Germany in view of stricter environmental threshold values. *Waste Management and Research*, *24*(3), 197–206.

Wu, H., Wang, C., & Ma, Z. (2022). Drying shrinkage, mechanical and transport properties of sustainable mortar with both recycled aggregate and powder

from concrete waste. *Journal of Building Engineering*, *49*, 104048.

Wu, H., Yang, D., Xu, J., Liang, C., & Ma, Z. (2021). Water transport and resistance improvement for the cementitious composites with eco-friendly powder from various concrete wastes. *Construction and Building Materials*, *290*, 123247.

Xiao, J., Li, J., & Zhang, C. (2005). Mechanical properties of recycled aggregate concrete under uniaxial loading. *Cement and Concrete Research*, *35*(6), 1187–1194.

Xiao, J., Ma, Z., Sui, T., Akbarnezhad, A., & Duan, Z. (2018). Mechanical properties of concrete mixed with recycled powder produced from construction and demolition waste. *Journal of Cleaner Production*, *188*, 720–731.

Xing, W., Tam, V. W., Le, K. N., Hao, J. L., & Wang, J. (2022). Life cycle assessment of recycled aggregate concrete on its environmental impacts: A critical review. *Construction and Building Materials*, *317*.

Xing, W., Tam, V. W. Y., Le, K. N., Butera, A., Hao, J. L., & Wang, J. (2022). Effects of mix design and functional unit on life cycle assessment of recycled aggregate concrete: Evidence from CO2 concrete. *Construction and Building Materials*, *348*, 128712.

Xuan, D., Zhan, B., & Poon, C. S. (2016). Assessment of mechanical properties of concrete incorporating carbonated recycled concrete aggregates. *Cement and Concrete Composites*, *65*, 67–74.

Yang, K. H., Chung, H. S., & Ashour, A. F. (2008). Influence of Type and Replacement Level of Recycled Aggregates on Concrete Properties. *ACI Materials Journal*, *105*(3), 289–296.

Yu, A. B., Bridgwater, J., & Burbidge, A. (1997). On the modelling of the packing of fine particles. *Powder Technology*, *92*, 185–194.

Yurdakul, E., Taylor, P. C., Ceylan, H., & Bektas, F. (2013). Effect of Paste-to-Voids Volume Ratio on the Performance of Concrete Mixtures. *Journal of Materials in Civil Engineering*, *25*(12), 1840–1851.

Zhan, B. J., Xuan, D. X., Poon, C. S., & Scrivener, K. L. (2020). Characterization of interfacial transition zone in concrete prepared with carbonated modeled recycled concrete aggregates. *Cement and Concrete Research*, *136*, 106175.

Zhang, Y., Ju, J. W., Zhu, H., & Yan, Z. (2020). A novel multi-scale model for predicting the thermal damage of hybrid fiber-reinforced concrete. *International Journal of Damage Mechanics*, *29*(1), 19–44.

Zhao, Y., Peng, L., Zeng, W., Poon, C. sun, & Lu, Z. (2021). Improvement in properties of concrete with modified RCA by microbial induced carbonate precipitation. *Cement and Concrete Composites*, *124*, 104251.

Zhao, Z., Courard, L., Groslambert, S., Jehin, T., Leonard, A., & Xiao, J. (2020). Use of recycled concrete aggregates from precast block for the production of new building blocks: An industrial scale study. *Resources, Conservation and Recycling*, *157*, 104786.

Zhao, Z., Remond, S., Damidot, D., & Xu, W. (2015). Influence of fine recycled concrete aggregates on the properties of mortars. *Construction and Building Materials*, *81*, 179–186.